University of Kaiserslautern

GraduiertenKollegs "Mathematik und Praxis"

Modeling and Simulation of the Float Glass Process

Dipl. Math. Serban Rares POP

Supervisor: Prof. Dr. Dr. h. c. em. Helmut NEUNZERT

Kaiserslautern, January 2005

Contents

Acknowledgements

First and foremost, I would like to thank my supervisor Prof. Dr. Helmut Neunzert for the discussions and suggestions given for the fundamental processes of this thesis, and for his continuous encouragment and guidance during these three years.

This project would have never come to an end without the financial support given by the Deutsch Forschungsgemeinschaft (DFG) and the University of Kaiserslautern, for which I am very grateful.

I would like to thank my advisors from the industrial part, Dr. Ulrich Lange from the Schott Glas Company, Mainz and Dr. Norbert Siedow from the Fraunhofer ITWM, Kaiserslautern, for keeping me with my both feet on the ground and providing me with very helpful suggestions.

My work couldn't been done without the constant collaboration with my friends and colleagues, Satiananda Panda, Alexander Grm, Satish Malik and Dr. Teodor Grosan, for which I am very grateful.

Finally, and not the last, I would like to thank my family for the encouragment and devotion in all these years of hard work.

Abstract

Since its invention by Sir Allistair Pilkington in 1952, the float glass process has been used to manufacture long thin flat sheets of glass. Today, float glass is very popular due to its high quality and relatively low production costs. When producing thinner glass the main concern is to retain its optical quality, which can be deteriorated during the manufacturing process. The most important stage of this process is the floating part, hence is considered to be responsible for the loss in the optical quality. A series of investigations performed on the finite products showed the existence of many short wave patterns, which strongly affect the optical quality of the glass. Our work is concerned with finding the mechanism for wave development, taking into account all possible factors.

In this thesis, we model the floating part of the process by an theoretical study of the stability of two superposed fluids confined between two infinite plates and subjected to a large horizontal temperature gradient. Our approach is to take into account the mixed convection effects (viscous shear and buoyancy), neglecting on the other hand the thermo-capillarity effects due to the length of our domain and the presence of a small stabilizing vertical temperature gradient. Both fluids are treated as Newtonian with constant viscosity. They are immiscible, incompressible, have very different properties and have a free surface between them. The lower fluid is a liquid metal with a very small kinematic viscosity, whereas the upper fluid is less dense. The two fluids move with different velocities: the speed of the upper fluid is imposed, whereas the lower fluid moves as a result of buoyancy effects.

We examine the problem by means of small perturbation analysis, and obtain a system of two Orr-Sommerfeld equations coupled with two energy equations, and general interface and boundary conditions. We solve the system analytically in the long- and short- wave limit, by using asymptotic expansions with respect to the wave number. Moreover, we write the system in the form of a general eigenvalue problem and we solve the system numerically by using Chebyshev spectral methods for fluid dynamics. The results (both analytical and numerical) show the existence of the small-amplitude travelling waves, which move with constant velocity for wave numbers in the intermediate range. We show that the stability of the system is ensured in the long wave limit, a fact which is in agreement with the real float glass process. We analyze the stability for a wide range of wave numbers, Reynolds, Weber and Grashof number, and explain the physical implications on the dynamics of the problem. The consequences of the linear stability results are discussed.

In reality in the float glass process, the temperature strongly influences the viscosity of

both molten metal and hot glass, which will have direct consequences on the stability of the system. We investigate the linear stability of two superposed fluids with temperature dependent viscosities by considering a different model for the viscosity dependence of each fluid. Although, the temperature-viscosity relationships for glass and metal are more complex than those used in our computations, our intention is to emphasize the effects of this dependence on the stability of the system. The construction of the problem is similar to the constant viscosity case studied above and we solve our system of motion numerically using the same technique as in the previous case. It is known from the literature that in the case of one fluid, the heat, which causes viscosity to decrease along the domain, usually destabilizes the flow. For the two superposed fluids problem we investigate this behaviour and discuss the consequences of the linear stability in this new case.

The thesis contains six chapters and four appendices. A brief description of the float glass process, together with our motivation and physical implications of the problem, is presented in Chapter 1 - *Introduction*. In Chapter 2 - *Mathematical formulation* we derive the governing equations, the interface and boundary conditions and the non-dimensional system of motion, which characterize our problem. In order to perform a stability analysis on our given system of equations, it is necessary to construct the stationary, unperturbed solution, which we call "basic flow". We perturb the basic flow by small deviations and we obtain, by linearization, the equations for the perturbation. We analyze this new system for two limits: long and short wave. These procedures are presented in the Chapter 3 - *Non-constant temperature boundary conditions*. A short introduction of spectral methods in fluid dynamics, together with the collocation method using Chebyshev polynomials, applied in the long and short waves cases, is presented in Chapter 4 - *Numerical method*. The next part of our work, Chapter 5, covers the temperature dependent viscosity case, which contains the following: the general system of motion, the basic flow profiles, the viscosity models, the linearized system of motion and the numerical results for the long and short waves cases. Finally, in Chapter 6, we present some discussions and conclusions of our work.

Chapter 1

Introduction

1.1 Float Glass

As suggested by its name, float glass denotes perfectly clear, flat glass (basic product). The term *float* derives from the production method, introduced in the UK by Sir Alastair Pilkington in the late 1950's [16], by which 90 percent of today's flat glass is manufactured. Nowadays, the float glass process is a very popular production technique due to the high quality of the resulting glass and the relatively low production costs. The large sheets of glass produced each day are almost distortion and defect free.

The process is a complex one and consists of four different stages (figure 1.1). At the beginning, the raw materials are properly weighted, mixed and then introduced into a furnace where they are melted at a temperature of 1500 C. After the melting, the hot glass flows in a continuous ribbon into a bath of liquid metal (molten tin). The glass, which has a high kinematic viscosity, and the tin, which has a much smaller viscosity, do not mix and the contact surface between these two materials can be considered to be perfectly flat. The ribbon of glass has a velocity given by the speed of the rollers that stretch it. When it leaves the bath, the glass has cooled down sufficiently to pass to an annealing chamber called *lehr*. Here it is cooled until it reaches room temperature, then it is cut and shipped. Various information about the manufacturing process can be collected from specialized literature or from the internet [52, 53, 54, 55, 56]. In this section, we build an overview by combining all the important data which characterize the float glass process.

1.1.1 Stages of the process

Stage 1: Melting

High quality ingredients (mainly silica sand, soda, limestone, dolomite, oxide and magnesium), are weighted, crushed and mixed. The batch flows as a blanket on to molten

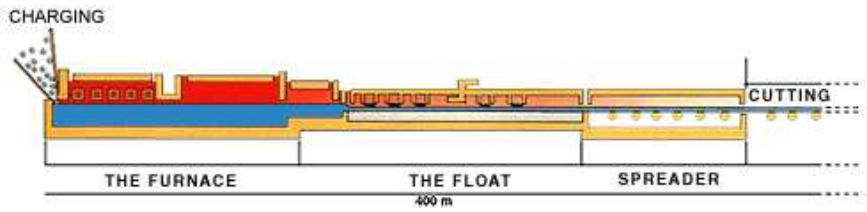

Figure 1.1: The float glass process [52]

glass in the furnace. Raw materials and compositions can be changed in order to obtain the desired properties of a specific type of glass.

Today, the flat glass manufactured with the float process has a very high optical quality. In the furnace, simultaneously but in separate zones, take place several important processes such as melting, refining, homogenizing. The result is a complex glass flow driven by high temperature gradients, which governs all the stages of the melting pre-process. The quality of the glass is directly influenced by the melting process.

The raw materials are melted in the furnace at a high temperature produced by powerful fuel-oil and gas burners. Leaving the furnace, the molten glass passes through the refiner, then through the waist area, where the glass is homogenized by stirring, and finally arrives into the working end of the melting furnace where, through channels, the glass flows into the floating bath. At this stage, the glass, free from inclusions and bubbles, flows smoothly and continuously onto molten tin.

Stage 2: Float bath

At the inlet of the float bath, molten glass pass over a refractory spout and plunges onto the flat surface of molten tin. At the beginning of the floating process, the glass has a temperature of 1100C and at the end, when is leaving the float bath as a solid ribbon, the temperature decreases to 660C. During the process a sheet of glass is formed by flotation (figure 1.2). Top rollers on either side draw out the glass mechanically to give it the required thickness and width. The ribbon thickness can vary between 2 and 20 mm, while the width can range from 3 to 5 meters. During the process, the temperature of the continuous ribbon is controlled and gradually reduced in order for the glass to become flat and parallel.

At the beginning of the process, hot glass is poured on molten tin and spreads out until its natural equilibrium thickness is reached (i.e. 7 mm). The thickness of the glass sheet is determined by the surface tensions, the densities (glass, tin) and the interface between glass and tin [16]. Moreover, this particular value of glass thickness do not depends on changes in the chemical composition of glass, metal or atmosphere. The surface tension and gravitational forces that help form glass of equilibrium thickness also work against forming thinner glass. Changes in the factors that govern the equilibrium thickness will not provide a significant reduction in thickness [17]. The force necessary to change the thickness of the glass is greater than the force available to obtain a high quality surface, therefore in order to obtain such a surface the overall thickness of the glass ribbon remain near the equilibrium value. Any attempt to change the ribbon thickness by modifying the

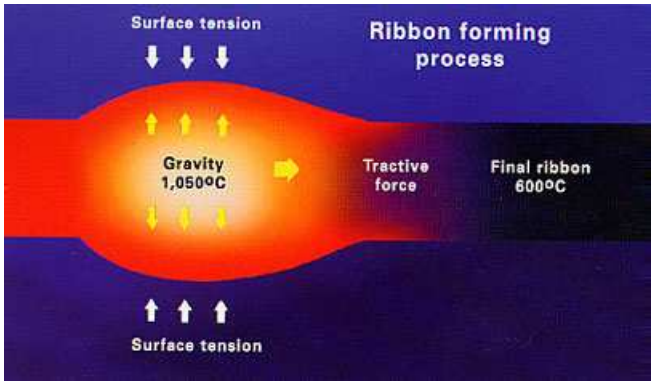

Figure 1.2: The forming of the hot glass ribbon [54]

applied tractive force (changing the speed of the rollers at the outer part of float bath) produces relatively large changes in width but small changes in thickness.

However, this can be obtain by mechanical stretching of the glass ribbon. The width and thickness of the glass ribbon at float bath inlet are controlled using pairs of driven edge rolls which define its speed. Thus, on the ribbon is applied first a low tractive force (forming the ribbon) which is different from the high tractive force (stretching process) applied by the edge rollers in the stiff section of the process [16].

The molten tin is a liquid metal with various properties which makes it perfect for this process [57]. Hence, in the liquid phase, forms a flat surface underside of the glass. Like any other liquid metal, the molten tin has a high thermal diffusivity which allows it to keep the glass hot and fluid long enough for top surface imperfections to level out. It remains liquid to a temperature below that at which glass becomes rigid enough to be cut, handle and remove. Tin is considered to be relatively inexpensive, non toxic, non reactive and its impurities can be cleaned easily from the cooled surface of the glass.

Stage 3: Coating and annealing

After it leaves the floating bath, the ribbon of glass passes to an annealing chamber called "lehr". Here, the glass is cleaned from the optical impurities (coating) and cooled down in a "stress free" controlled way (annealing).

The optical properties of the glass are dramatically changed by the coating process. This process, using advanced high temperature techniques, is applied to the cooling glass ribbon. Moreover, metal oxide coatings are applied directly to the hot glass, in the annealing lehr. Using special extractor and scrubbing units, the glass is cleansed from the reaction products.

During the cooling process, considerable stresses appear in the glass ribbon. These stresses make the cutting process very critical for the glass which can now break easily. A series of rollers carry the glass ribbon through the lehr where the temperature of the glass is reduced according to a precise cooling curve. Thus, the stresses are relieved, preventing in this manner splitting and breaking in the cutting phase. The glass comes out of the lehr at ambient temperature, ready for cutting.

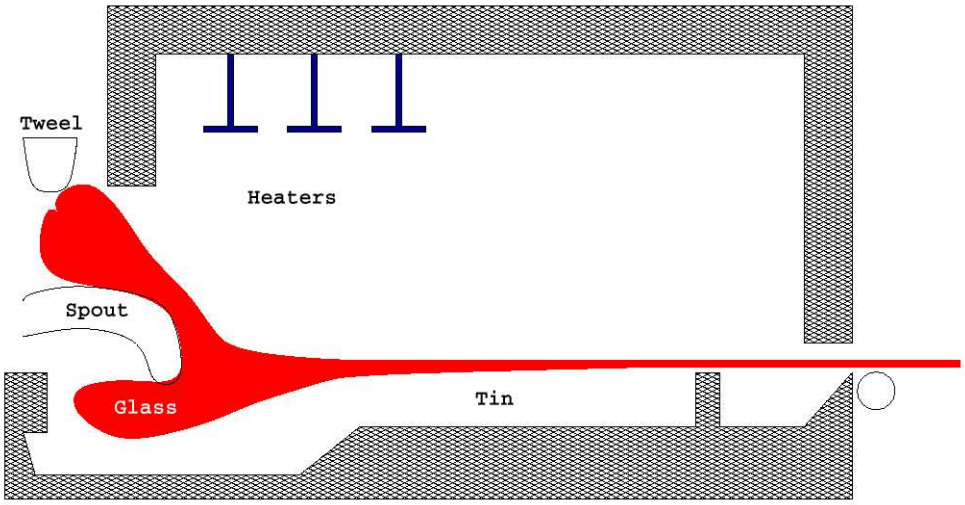

Figure 1.3: The floating bath

Stage 4: Inspection and cutting

The float glass process makes everyday, large sheets of almost perfectly flat, defect-free glass. All stages of the process are inspected in order to ensure the highest glass quality. After annealing, the glass strip is inspected by an optical laser system and cut automatically as it moves along the rollers.

1.1.2 Floating bath

Nowadays, there is an increasing demand for float glass of low thickness (notebook screens). Experiments and observations made on finite products showed a loss in the optical quality of the glass due to the presence at the glass surface of continuous patterns of small amplitude waves. As the formation of the ribbon takes place in a molten tin bath, it is considered that the flow and heat transfer induced there, are partially responsible for the development of such patterns and implicitly for the loss of optical quality. A schematic description of the floating bath is presented in figure 1.3. The floating part of the process consists in four stages [17, 18, 19, 20]:

Stage 1: The molten glass is poured onto molten tin and allowed to spread out to its equilibrium thickness. The temperature in this region, around 1500C, is high enough to allow any surface irregularities to even out by the flow and to ensure uniform thickness (7 mm).

Stage 2: The glass is cooled to 900C and the ribbon edges are gripped by pairs of edge rollers. The speed of the rollers determines the local speed and width of the ribbon. These rollers also counteract the longitudinal tractive force applied to stretch the ribbon and thus prevent the transmission of this large force to the low-viscosity glass upstream.

Stage 3: The ribbon is re-heated to a temperature around 1000C. The corresponding viscosity is low enough to allow stretching without the generation of excessive stresses, and yet high enough to prevent surface tension forces from driving the thickness back to its equilibrium value.

Stage 4: In this final stage, the ribbon is cooled and removed mechanically from the tin bath without any surface damage.

The float glass process is one of the most stable manufacturing processes in the world, by producing very long and thin sheets of glass everyday. Nevertheless, investigations performed on the finite products showed the existence of many short wave patterns, which can affect strongly the optical quality of the glass.

Our work is devoted to finding the waves development mechanism, taking into account all possible factors that can influence its appearance. We perform a linear stability analysis, using normal modes, on the two dimensional system of two superposed fluids in the presence of a large temperature gradients. The movement of the fluids is characterized by a combination of inertial and buoyancy forces, thus we are in the presence of a mixed convection problem.

1.2 Mixed convection in a liquid metal

Mixed convection flow and heat transfer occur frequently in engineering and natural situations. Therefore, it appears in many configurations with applications in food industry, crystal growth, thermal-hydraulics problem or float glass process.

Liquid metals are excellent heat transfer media. Therefore, oscillation of the temperature due to instability of the buoyant flow induces non-uniform cooling. The buoyant flow in low Prandtl fluids (i.e. the thermal diffusivity much larger than the kinematical viscosity) is usually nonlinear; the flow is dominated by inertia force (advection mechanism) because the viscosity of liquid metals is considerable low. The viscosity of the fluid may not sufficiently enough to damp any perturbations in the boundary conditions. Therefore, the flow becomes unstable at moderately low Grashof parameters (i.e. the viscous force acting on a fluid much larger than the buoyancy force). In the float glass process the ratio of the viscosities is very large.

The topic of convective instabilities for a system of two superposed fluids was treated by many authors in terms of thermo-capillarity and buoyancy effects [41, 46]. When a horizontal temperature gradient is imposed to a liquid layer constrained between two rigid walls, the problem becomes very complicated. In this case, the basic profile is not a trivial one, resulting in a complex flow and a non-linear vertical temperature profile [11]. At low Prandtl (i.e. the thermal diffusivity of the fluid is much larger than its dynamical viscosity), the energy necessary to sustain the disturbances comes from the horizontal temperature gradient which creates hydrothermal waves and stationary rolls.

1.3 Stability analysis of a given flow

The main purpose of our work is to perform a stability analysis of the float part of the process in order to find the causes for the small waves development at the surface between the glass and the metal. The existence of the homogeneous wavy patterns on the surface of glass can be explained in terms of hydrodynamical stability problems.

The traditional method used to determine the stability of a given flow is the linear stability analysis using normal modes. First, we model the full problem by prescribing the equations and conditions which characterize the flow. Further, we construct the basic flow solution of our problem subject to certain assumptions. Our interest is to model a simple case where the flow is laminar and steady. The main assumption is to take into account only the component of the velocity in the x direction (i.e. parallel with the flow), thus the flow will not vary in this direction. Moreover, for the two dimensional problem, the conservation of mass implies that all the unknown parameters are functions of z direction (i.e. perpendicular to the flow).

Having defined the flow in the stationary case, we add to this model a small perturbation. The governing equations are linearized and linear boundary and interface conditions are applied. The advantage of linearization is that the properties which holds only for linear equations and hence cannot be applied to hydrodynamic equations, becomes applicable to the perturbation equations. One example is the principle of superposition, where any perturbation can be thought as a superposition of many components (Chebyshev, Fourier) and the evolution of each mode can be studied directly from the equations. The normal mode approach can provide the wave number, growth rate, and spatial structure of the most unstable modes. The main assumption of linear stability analysis is that, if the initial perturbation contains all the modes, then the most unstable mode will grow fastest and dominate the disturbance field.

In order to investigate the stability of a given flow, linear stability analysis is first performed. However, this procedure is valid only when the disturbance amplitudes are assumed to be very small in absolute value. The nonlinear effects grow faster and become quickly important. The linear stability analysis can provide information about which modes are likely to develop faster and which parameter produces first instability in our given flow. Usually, the information gathered by performing the linear stability analysis is used for the construction of nonlinear simulations.

Long wave limit was first done by Yih for the plane Poiseuille flow, with results given for the case $\rho = 1$, where ρ is the densities ratio. Yih has shown that variation of viscosity in a fluid can cause instability for an arbitrary small Reynolds number [1]. Later, Yiantsios and Higgins have discussed in detail the influence of thickness ratio on flow stability and found that inertia can stabilize the instability caused by viscosity-stratification for small shear effects [5]. Numerical and analytical works performed by Hooper [2], Charru and Fabre [8], Joseph and Renardy [6], Smith and Davis [27], Blennerhassett [26] come to complete the study of long wave disturbances for two superposed fluids system, although without involving horizontal temperature effects and large differences in viscosity and density.

Short wave limit was first investigate by Hooper and Boyd, and they showed that small perturbations are always creating instability, especially when the thinner layer is the most viscous [3]. In this case, surface tension stabilize the flow when inertia produces destabilizing effects. Moreover, when both fluids have the same viscosity the system tends to stabilize itself. Various works analyze the stability of small amplitude waves for different kind of models (oil-water, air-water)[9, 10]. Considering the air-water model, Blennerhassett and Benney found the mechanisms by which short waves give energy to long waves increasing their unstable behaviour. In the present work, we construct a model for hot glass-molten metal characteristic of the float glass process.

The conclusion is that the very thin less viscous fluid layer stabilizes the long waves whereas the surface tension stabilizes the short waves. In this work, we explore the mixed convection effects on the stability of two superposed fluids which have different characteristics (kinematical viscosity, density). Hence, due to the presence of a small stabilizing vertical temperature gradient and to the high buoyancy movement of the molten metal, the above conclusions are not always satisfied.

Chapter 2

Mathematical formulation

Two immiscible, incompressible fluids, labeled $j = \overline{1,2}$, are confined between two planes subject to a large horizontal temperature gradient. The lower fluid is denoted by 1 and the upper fluid by 2. Also, we denote with d_1 the height of the lower fluid, and with d_2 the height of the upper fluid, which is smaller than the previous one. We assume a positive vertical temperature gradient. The fluids are moving with different velocities: the speed of the upper fluid is constant, whereas the movement of the lower fluid is caused by the thermal buoyancy effects coupled with the motion of the upper fluid (figure 2.1).

2.1 Governing Equations

The equations that govern the system of motion are the incompressible, Navier-Stokes and energy coupled with the Boussinesq approximation:

Mass

$$\nabla \cdot \mathbf{u}_j = 0 \tag{2.1}$$

Momentum

$$\bar{\rho}_j \left[\frac{\partial \mathbf{u}_j}{\partial \bar{t}} + (\mathbf{u}_j \cdot \nabla)\mathbf{u}_j \right] = -\nabla \bar{p}_j + \mu_j \Delta \mathbf{u}_j - \bar{\rho}_j \mathbf{g} \tag{2.2}$$

Energy

$$\frac{\partial T_j}{\partial \bar{t}} + (\mathbf{u}_j \cdot \nabla) T_j = \alpha_j \Delta T_j, \quad j = \overline{1,2} \tag{2.3}$$

where $\mathbf{u}_j = (\bar{u}_j, \bar{w}_j)$, $\bar{u}_j$ is the velocity in the $\bar{x}$ direction, $\bar{w}_j$ is the velocity in the $\bar{z}$ direction, $\mathbf{g} = (0, g)$, g is acceleration due to the gravity, $\bar{p}_j$ is the pressure, μ_j is the dynamic viscosity, $\bar{\rho}_j$ is the density, α_j is the thermal diffusivity and T_j is the temperature of the fluid for each phase ($j = \overline{1,2}$).

We write the above equations by components and we obtain:

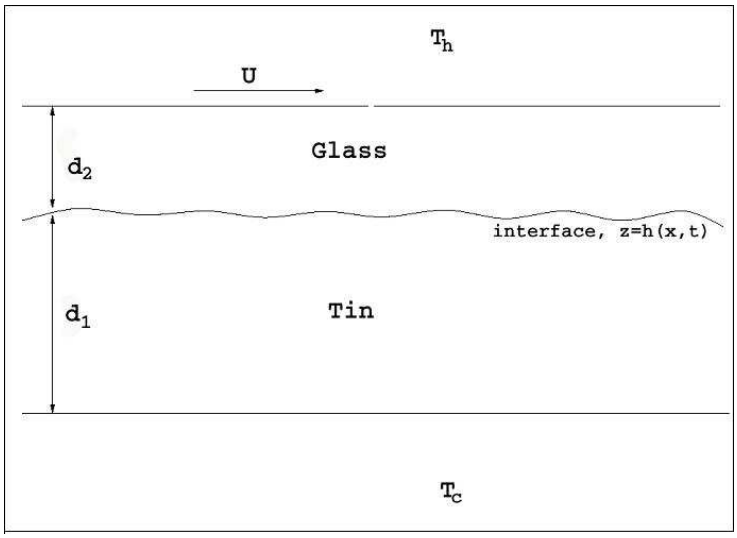

Figure 2.1: A schematic description of the problem

Mass

$$\frac{\partial \bar{u}_j}{\partial \bar{x}} + \frac{\partial \bar{w}_j}{\partial \bar{z}} = 0 \tag{2.4}$$

Momentum

$$\frac{\partial \bar{u}_j}{\partial \bar{t}} + \bar{u}_j \frac{\partial \bar{u}_j}{\partial \bar{x}} + \bar{w}_j \frac{\partial \bar{u}_j}{\partial \bar{z}} = -\frac{1}{\bar{\rho}_j} \frac{\partial \bar{p}_j}{\partial \bar{x}} + \frac{\mu_j}{\bar{\rho}_j} \left(\frac{\partial^2 \bar{u}_j}{\partial \bar{x}^2} + \frac{\partial^2 \bar{u}_j}{\partial \bar{z}^2} \right) \tag{2.5}$$

$$\frac{\partial \bar{w}_j}{\partial \bar{t}} + \bar{u}_j \frac{\partial \bar{w}_j}{\partial \bar{x}} + \bar{w}_j \frac{\partial \bar{w}_j}{\partial \bar{z}} = -\frac{1}{\bar{\rho}_j} \frac{\partial \bar{p}_j}{\partial \bar{z}} + \frac{\mu_j}{\bar{\rho}_j} \left(\frac{\partial^2 \bar{w}_j}{\partial \bar{x}^2} + \frac{\partial^2 \bar{w}_j}{\partial \bar{z}^2} \right) - g \tag{2.6}$$

Energy

$$\frac{\partial T_j}{\partial \bar{t}} + \bar{u}_j \frac{\partial T_j}{\partial \bar{x}} + \bar{w}_j \frac{\partial T_j}{\partial \bar{z}} = \alpha_j \left(\frac{\partial^2 T_j}{\partial \bar{x}^2} + \frac{\partial^2 T_j}{\partial \bar{z}^2} \right), \quad j = \overline{1,2} \tag{2.7}$$

2.1.1 Boussinesq approximation

When thermal effects are taken into account, and the buoyancy forces are comparable with the inertial and viscous forces, the Boussinesq approximation can be used. In the momentum equation (2.2), this approximation is plugged into the gravity term and characterizes the thermal expansion of each fluid,

$$\bar{\rho}_1 = \rho_1 \left[1 - \beta_1 \left(T_1 - T_{ref} \right) \right]$$

$$\bar{\rho}_2 = \rho_2 \left[1 - \beta_2 \left(T_2 - T_{ref} \right) \right] \tag{2.8}$$

where β_j is the thermal expansion coefficient and T_{ref} is a reference temperature which will be chosen subsequently.

In fluid dynamics, the Boussinesq approximation is used in the field of buoyancy-driven flow. The motion of a fluid initiated by heat results mostly from an excess of buoyancy and is not due to internal waves excited by density variations. The Boussinesq approximation states that variations of the density are sufficiently small to be neglected in the inertial acceleration, except where they appear in terms multiplied by g, the acceleration due to gravity. The essence of the Boussinesq approximation is that the difference in inertia is negligible but gravity is sufficiently strong to make the specific weight appreciably different between the two fluids [44, 46, 58].

The derivation of conditions for the validity of the Boussinesq approximations is not as straightforward as many would assume. In the literature, a variety of sets of conditions have been assumed which, if satisfied, allow the application of the Boussinesq approximations [20, 21]. The Boussinesq approximation consists of a group of assumptions which allows the use of incompressible mass continuity and linearization of the ideal gas law.

2.1.2 Interface and boundary conditions

We introduce the interface and boundary conditions which complete our system of motion. Therefore, we define the stress tensors valid for each fluid, unit vectors normal and tangential to the interface, the curvature of the interface at a given point and the jump across the interface.

The stress tensor, denoted with τ, is given by the following relation:

$$\tau = \begin{bmatrix} -\bar{p} + 2\mu\frac{\partial \bar{u}}{\partial \bar{x}} & \mu\left(\frac{\partial \bar{u}}{\partial \bar{z}} + \frac{\partial \bar{w}}{\partial \bar{x}}\right) \\ \mu\left(\frac{\partial \bar{u}}{\partial \bar{z}} + \frac{\partial \bar{w}}{\partial \bar{x}}\right) & -\bar{p} + 2\mu\frac{\partial \bar{w}}{\partial \bar{z}} \end{bmatrix}. \tag{2.9}$$

We introduce the normal vector, $\mathbf{n}$, pointing from phase 1 into phase 2, and the tangential vector $\mathbf{t}$:

$$\mathbf{n} = \left(\frac{-\bar{h}_{\bar{x}}}{(1+\bar{h}_{\bar{x}}^2)^{1/2}}, \frac{1}{(1+\bar{h}_{\bar{x}}^2)^{1/2}}\right) \tag{2.10}$$

$$\mathbf{t} = \left(\frac{1}{(1+\bar{h}_{\bar{x}}^2)^{1/2}}, \frac{\bar{h}_{\bar{x}}}{(1+\bar{h}_{\bar{x}}^2)^{1/2}}\right). \tag{2.11}$$

In the following computations, κ_j is the thermal conductivity ($j = \overline{1,2}$), σ is the surface tension and κ_S is the mean curvature of the interface, given by:

$$\kappa_S = -\frac{\bar{h}_{\bar{x}\bar{x}}}{(\bar{h}_{\bar{x}}^2+1)^{3/2}} \tag{2.12}$$

The jump of the quantity f across the interface is denoted by $[f] = f_2 - f_1$.

The system is coupled with the following conditions at the interface ($\bar{z} = \bar{h}(\bar{x}, \bar{t})$):

Kinematical condition

$$\bar{w}_j = \frac{\partial \bar{h}}{\partial \bar{t}} + \bar{u}_j \frac{\partial \bar{h}}{\partial \bar{x}}, \quad j = \overline{1,2} \tag{2.13}$$

The kinematical condition must be satisfied by any bounding surface, whether an interface or a rigid boundary due to the fact that there is no transfer of matter across the surface. The interface moves with the velocity of the flow.

The dynamical conditions are based on the following assumptions [40]:

1. The effect of surface tension as one passes through the interface is to produce a discontinuity in the normal stress proportional to the mean curvature of the boundary surface.
2. For viscous fluids the tangential stress must be continuous across the interface.
3. For viscous fluids the tangential component of the velocity must be continuous across the interface.

Dynamical conditions:

$$[\mathbf{n} \cdot \tau \cdot \mathbf{n}] = \sigma \kappa_S \tag{2.14}$$

$$[\mathbf{t} \cdot \tau \cdot \mathbf{n}] = 0 \tag{2.15}$$

In the construction of our model we assume no-slip and no-penetration of the interface.

Velocity condition:

$$[\mathbf{u} \cdot \mathbf{t}] = 0 \tag{2.16}$$

Moreover, the temperatures and the heat fluxes are equal at the interface.

Heat transfer conditions:

$$T_1 = T_2, \qquad \kappa_1 \frac{\partial T_1}{\partial \mathbf{n}} = \kappa_2 \frac{\partial T_2}{\partial \mathbf{n}} \tag{2.17}$$

The velocity and the temperature for both fluids satisfy the following boundary conditions:

$$\begin{aligned} &\bar{z} = -d_1 : \quad \bar{u}_1 = \bar{w}_1 = 0, \quad T_1 = T_c(\bar{x}) \\ &\bar{z} = d_2 : \quad \bar{u}_2 = U, \quad \bar{w}_2 = 0, T_2 = T_h(\bar{x}). \end{aligned} \tag{2.18}$$

Moreover, we prescribe the mass flow rate conditions, which characterize the mass of fluid passing through an area in the system per unit time:

$$\bar{Q}_1 = \rho_1 \int_{-d_1}^{0} \bar{u}_1 d\bar{z}, \quad \bar{Q}_2 = \rho_2 \int_{0}^{d_2} \bar{u}_2 d\bar{z}. \tag{2.19}$$

2.2 Non-dimensional system of motion

Further, it is convenient to examine the non-dimensional equations. This has the advantage of classifying various flows by the means of certain characteristic parameters.

The motion is governed by the two dimensional incompressible full Navier Stokes equations in each layer coupled with Boussinesq approximation, together with energy equation, continuity of stress and velocity across the unknown interface $\bar{z} = \bar{h}(\bar{x}, \bar{t})$ and the boundary conditions.

Our motivation is to emphasize any waves development that can occur at the interface between the fluids. These waves have small amplitude in comparison with the height of each fluid. Hence, we use as characteristic length, the height of the thinner fluid layer, which in our problem is denoted with d_2.

Moreover, due to the movement of the upper boundary, the upper fluid is moving with constant velocity. Any disturbance that can appear at the interface is produced by the buoyant movement of the lower fluid and the inertial behaviour of the upper fluid. Thus, we use U as the characteristic speed, the drag velocity of the upper layer in x direction. Moreover, viscosity and density of the lower fluid, are used in the following non-dimensionalization.

The lower fluid starts to move due to the temperature difference along the domain. In order to express the non-dimensional temperature quantities, we use the largest and the smallest temperatures of the system (T^h_{ref}, T^c_{ref}), values which are taken from the real problem. In the float glass process these temperatures correspond with inlet and outlet temperatures of the float bath. We denote with ΔT_{ref} the difference between T^h_{ref} and T^c_{ref}, (i.e. $\Delta T_{ref} = T^h_{ref} - T^c_{ref}$).

Therefore, the non-dimensionalization is performed as follows:

$$\begin{gathered}
\bar{x} = d_2 x, \quad \bar{z} = d_2 z, \quad \bar{u}_j = U u_j, \quad \bar{w}_j = U w_j, \\
\bar{h} = d_2 h, \quad \bar{\sigma} = (\mu_1 U)\,\sigma, \quad \bar{p}_j = \left(\mu_1 \tfrac{U}{d_2}\right) p_j + p^j_\infty, \quad \bar{\kappa_S} = \tfrac{\kappa_S}{d_2}, \\
\theta_j = \tfrac{T_j - T^c_{ref}}{\Delta T_{ref}}, \quad \bar{t} = \tfrac{d_2}{U} t, \quad \bar{Q}_j = Q_j \rho_1 U d_2, \quad j = \overline{1,2}
\end{gathered}$$

where $p^j_\infty = \rho_j g z$ is the hydrostatic pressure written for each fluid. In our computations, we use the following dimensionless numbers:

- Reynolds number, $Re_1 = \frac{\rho_1 U d_2}{\mu_1}$, which characterizes the relation between inertial and viscous forces,
- Grashof number, $Gr_1 = \frac{\rho_1^2 g \beta_1 \Delta T_{ref} d_2^3}{\mu_1^2}$, which approximates the ratio of buoyancy force to the viscous force acting on a fluid,
- Prandtl number, $Pr_1 = \frac{\mu_1}{\rho_1 \alpha_1}$, which is the ratio of kinematic viscosity to thermal diffusivity,

- Weber number, $We_1 = \frac{\rho_1 U^2 d_2}{\sigma}$, represents an index of the inertial force to the surface tension force acting on a fluid element.

We express all the dimensionless numbers of the second fluid with respect to the dimensionless numbers of the first fluid, by making the appropriate transformations:

$$Re_2 = \frac{\rho}{\mu} Re_1, \quad Gr_2 = \frac{\rho^2 \beta}{\mu^2} Gr_1, \quad Pr_2 = \frac{\mu}{\rho \alpha} Pr_1 \tag{2.20}$$

where

$$\rho = \frac{\rho_2}{\rho_1}, \quad \alpha = \frac{\alpha_2}{\alpha_1}, \quad \beta = \frac{\beta_2}{\beta_1}, \quad \mu = \frac{\mu_2}{\mu_1}, \quad \kappa = \frac{\kappa_2}{\kappa_1}, \quad d = \frac{d_1}{d_2}. \tag{2.21}$$

Further we drop the bars and the subscript "1" from the non-dimensional numbers for simplicity.

2.2.1 Governing equations

The non-dimensional equations which characterize our process are stated below:

Mass

$$\frac{\partial u_1}{\partial x} + \frac{\partial w_1}{\partial z} = 0 \tag{2.22}$$

$$\frac{\partial u_2}{\partial x} + \frac{\partial w_2}{\partial z} = 0 \tag{2.23}$$

Momentum

$$Re \left(\frac{\partial u_1}{\partial t} + u_1 \frac{\partial u_1}{\partial x} + w_1 \frac{\partial u_1}{\partial z} \right) = -\frac{\partial p_1}{\partial x} + \left(\frac{\partial^2 u_1}{\partial x^2} + \frac{\partial^2 u_1}{\partial z^2} \right) \tag{2.24}$$

$$\frac{\partial w_1}{\partial t} + u_1 \frac{\partial w_1}{\partial x} + w_1 \frac{\partial w_1}{\partial z} = \frac{1}{Re} \left(-\frac{\partial p_1}{\partial z} + \frac{\partial^2 w_1}{\partial x^2} + \frac{\partial^2 w_1}{\partial z^2} \right) + \frac{Gr}{Re^2} \theta_1 \tag{2.25}$$

$$\rho Re \left(\frac{\partial u_2}{\partial t} + u_2 \frac{\partial u_2}{\partial x} + w_2 \frac{\partial u_2}{\partial z} \right) = -\frac{\partial p_2}{\partial x} + \mu \left(\frac{\partial^2 u_2}{\partial x^2} + \frac{\partial^2 u_2}{\partial z^2} \right) \tag{2.26}$$

$$\frac{\partial w_2}{\partial t} + u_2 \frac{\partial w_2}{\partial x} + w_2 \frac{\partial w_2}{\partial z} = -\frac{1}{Re\rho} \frac{\partial p_2}{\partial z} + \frac{\mu}{Re\rho} \left(\frac{\partial^2 w_2}{\partial x^2} + \frac{\partial^2 w_2}{\partial z^2} \right) + \beta \frac{Gr}{Re^2} \theta_2 \tag{2.27}$$

Energy

$$\frac{\partial \theta_1}{\partial t} + u_1 \frac{\partial \theta_1}{\partial x} + w_1 \frac{\partial \theta_1}{\partial z} = \frac{1}{RePr} \left(\frac{\partial^2 \theta_1}{\partial x^2} + \frac{\partial^2 \theta_1}{\partial z^2} \right) \tag{2.28}$$

$$\frac{\partial \theta_2}{\partial t} + u_2 \frac{\partial \theta_2}{\partial x} + w_2 \frac{\partial \theta_2}{\partial z} = \frac{\alpha}{RePr} \left(\frac{\partial^2 \theta_2}{\partial x^2} + \frac{\partial^2 \theta_2}{\partial z^2} \right) \tag{2.29}$$

Further, we make some remarks about the form of the above system. In the equations (2.25) and (2.27) appears the non-dimensional term Gr/Re^2 known in literature as *the Richardson number* [25, 24]. This number represents the ratio of buoyancy to inertial forces and is considered to be the main parameter which describes mixed convection. When this parameter is much greater than unity, $Gr/Re^2 >> 1$, the buoyancy dominates and force convection effects are negligible. When $Gr/Re^2 << 1$, inertia dominates the flow and buoyancy effects can be neglected. Hence, when the parameter is of order one we are in the case of mixed convection [22, 46].

In the energy equations (2.28) and (2.29) appears the non-dimensional product between Reynolds number and Prandtl number, known in literature as *the Peclet number*. This parameter is the ratio between advection and conduction of heat in the system and also relates the inertia of the system to its capability of distributing heat by conduction [23, 22].

2.2.2 Interface and boundary conditions

The above system is coupled with the following conditions at the interface ($z = h(x,t)$):

Kinematical condition

$$w_1 = \frac{\partial h}{\partial t} + u_1 \frac{\partial h}{\partial x} \tag{2.30}$$

$$w_2 = \frac{\partial h}{\partial t} + u_2 \frac{\partial h}{\partial x} \tag{2.31}$$

Normal stress

$$\begin{aligned} &-p_2 + p_1 + \mu \left[2 \frac{\partial u_2}{\partial x} \frac{h_x^2 - 1}{h_x^2 + 1} - 2 \frac{h_x}{h_x^2 + 1} \left(\frac{\partial u_2}{\partial z} + \frac{\partial w_2}{\partial x} \right) \right] - \\ &- \left[2 \frac{\partial u_1}{\partial x} \frac{h_x^2 - 1}{h_x^2 + 1} - 2 \frac{h_x}{h_x^2 + 1} \left(\frac{\partial u_1}{\partial z} + \frac{\partial w_1}{\partial x} \right) \right] = -\frac{Re}{We} \frac{h_{xx}}{(h_x^2 + 1)^{3/2}} \end{aligned} \tag{2.32}$$

Tangential stress

$$\begin{aligned} &\mu \left[\frac{h_x^2 - 1}{h_x^2 + 1} \left(\frac{\partial u_2}{\partial z} + \frac{\partial w_2}{\partial x} \right) + 4 \frac{\partial u_2}{\partial x} \frac{h_x}{h_x^2 + 1} \right] - \\ &- \left[\frac{h_x^2 - 1}{h_x^2 + 1} \left(\frac{\partial u_1}{\partial z} + \frac{\partial w_1}{\partial x} \right) + 4 \frac{\partial u_1}{\partial x} \frac{h_x}{h_x^2 + 1} \right] = 0 \end{aligned} \tag{2.33}$$

Velocity condition

$$u_2 - u_1 + h_x (w_2 - w_1) = 0 \tag{2.34}$$

Heat transfer conditions

$$\theta_1 = \theta_2, \qquad \left(\frac{\partial \theta_1}{\partial x}\frac{\partial h}{\partial x} - \frac{\partial \theta_1}{\partial z}\right) = \kappa \left(\frac{\partial \theta_2}{\partial x}\frac{\partial h}{\partial x} - \frac{\partial \theta_2}{\partial z}\right) \tag{2.35}$$

We introduce the following *boundary conditions*, which complete our non-dimensional model:

$$\begin{array}{l} z = -d\text{:} \quad u_1 = w_1 = 0, \quad \theta_1 = (T_c(x) - T^c_{ref})/\Delta T_{ref} \\ z = 1\text{:} \quad u_2 = 1, \quad w_2 = 0, \, \theta_2 = (T_h(x) - T^c_{ref})/\Delta T_{ref}. \end{array}$$

In the right-hand side of the equation (2.32) appears the term Re/We which characterize the influence of the surface tension over the stability of the system. Moreover, this ratio shows that any stabilizing effects of the surface tension are counterbalanced by the inertial forces.

We observe that in the condition for the temperature fluxes (2.35), the derivative of temperature with respect to x appears. The literature treated the case when the basic flow temperature was function of one dimension only (i.e. z direction). Therefore, this term will vanish after linearization. In this work, we will show that this is not always the case due to the fact we consider the basic flow temperature as a function depending of both directions. This case will be treated in the next chapter . Moreover, the temperature flux condition is derived by taking into account that the interface between fluids is a *wavy surface* [28].

Chapter 3

Non-constant temperature boundary conditions

It is known from the literature [41, 42, 46], that in cases when temperature is taken into account, the linear stability analysis is performed with constant boundary conditions. In the real float glass process, the temperature along boundaries decreases gradually from the inlet to the outlet of bath. The instabilities, which can appear in the problem of two superposed, immiscible, incompressible fluids, were investigated by many authors without considering thermal combined effects.

In this work, we take into account the temperature influence over the system in order to observe if the temperature has a stabilizing effect. From the technical point of view we have the combination of two temperature gradients. The difference between the temperatures at the inlet and the outlet of the bath is high, hence we are in the presence of a large horizontal temperature gradient, which induces the buoyancy movement of the liquid metal below. In contrast, the temperature difference between the top and bottom of the bath is small and positive, hence, along the process, the hot glass is subject to a small stabilizing vertical temperature gradient (i.e. the temperature at the upper boundary is larger than the temperature at the bottom creating, thus, a stable configuration). In the following we investigate the combination of these two factors.

3.1 Basic flow

In order to apply the stability analysis using linearization we should construct a special, "simple" (unperturbed) flow which characterize the motion in its stable phase. The basic flow represents the stationary solution of the system of equations (2.1-2.3) together with interface and boundary conditions (2.13-2.19). The free surface between the fluids is perfectly flat ($\bar{h} = const.$). The component of the velocity in $\bar{z}$ direction is assumed to be zero, so from the mass equation we obtain that $\mathbf{u}_j = (\bar{u}_j(\bar{z}), 0), \quad j = \overline{1,2}$.

For each fluid, we have the following equations:

$$\frac{\partial^2 U_j}{\partial z^2} = \frac{\partial P_j}{\partial x}, \quad \frac{\partial P_j}{\partial z} = N_j \Theta_j \quad j = \overline{1,2} \tag{3.1}$$

where

$$N_1 = \frac{Gr}{Re}, \quad N_2 = \frac{\rho Gr \beta}{\mu Re}.$$

After applying some transformations, the *governing equations* for the basic flow has the form stated below:

$$\frac{\partial^3 U_j}{\partial z^3} = N_j \frac{\partial \Theta_j}{\partial x}, \quad U_j = U_j(z), \quad \Theta_j = \Theta_j(x,z) \tag{3.2}$$

$$U_j \frac{\partial \Theta_j}{\partial x} = M_j \left(\frac{\partial^2 \Theta_j}{\partial x^2} + \frac{\partial^2 \Theta_j}{\partial z^2} \right), \quad j = \overline{1,2} \tag{3.3}$$

where

$$M_1 = \frac{1}{RePr}, \quad M_2 = \frac{\alpha}{RePr}.$$

The following interface and boundary conditions complete our basic system of motion:

$$U_1(0) = U_2(0), \quad \mu U_2^{'}(0) = U_1^{'}(0), \quad \Theta_1(0) = \Theta_2(0), \quad \kappa \Theta_2^{'}(0) = \Theta_1^{'}(0) \tag{3.4}$$

$$U_1(-d) = 0, \quad U_2(1) = 1, \quad \Theta_1(-d) = \Theta_c^0 + x\Theta_c^1, \quad \Theta_2(1) = \Theta_h^0 + x\Theta_h^1 \tag{3.5}$$

Hence, making use of the first two relations we obtain:

$$U_j = U_j(z) \overset{(3.2)}{\Longrightarrow} N_j \frac{\partial \Theta_j}{\partial x} \text{ depends only on } z, \quad j = \overline{1,2}. \tag{3.6}$$

Let

$$\begin{aligned} &\frac{\partial \Theta_j}{\partial x} = f_j(z) \implies \Theta_j(x,z) = x f_j(z) + g_j(z) \implies \\ &\implies \frac{\partial^2 \Theta_j}{\partial x^2} = 0 \text{ and } \frac{\partial^2 \Theta_j}{\partial z^2} = x f_j^{''}(z) + g_j^{''}(z). \end{aligned} \tag{3.7}$$

From relation (3.3), we obtain the final relation for the basic temperature:

$$\begin{aligned} &U_j(z) f_j(z) = M_j [x f_j^{''}(z) + g_j^{''}(z)] \Longrightarrow f_j^{''}(z) = 0 \\ \implies &f_j(z) = C_{j1} z + C_{j2} \implies \frac{\partial \Theta_j}{\partial x} = C_{j1} z + C_{j2} \implies \\ \implies &\Theta_j(x,z) = x(C_{j1} z + C_{j2}) + g_j(z), \quad j = \overline{1,2}. \end{aligned} \tag{3.8}$$

Moreover, taking into account relation (3.2) and performing some integration with respect to the z direction, we have the following form for the basic velocity:

$$\frac{\partial^3 U_j}{\partial z^3} = N_j(C_{j1}z + C_{j2}) \implies$$
$$U_j(z) = \frac{N_j C_{j1}}{24}z^4 + \frac{N_j C_{j2}}{6}z^3 + \frac{C_{j3}}{2}z^2 + C_{j4}z + C_{j5} \tag{3.9}$$

Having defined the basic velocity for each fluid, from relations (3.8) and (3.9) we can now compute $g_j(z)$:

$$M_j g_j^{''}(z) = \frac{N_j C_{j1}^2}{24}z^5 + \left(\frac{N_j C_{j1}C_{j2}}{24} + \frac{N_j C_{j1}C_{j2}}{6}\right)z^4 + \left(\frac{N_j C_{j2}^2}{6} + \frac{C_{j1}C_{j3}}{2}\right)z^3 +$$
$$+\left(\frac{C_{j2}C_{j3}}{2} + C_{j1}C_{j4}\right)z^2 + (C_{j2}C_{j4} + C_{j5}C_{j1})z + C_{j2}C_{j5} \overset{\text{Integration}}{\Longrightarrow}$$

$$g_j(z) = \frac{N_j C_{j1}^2}{1008M_j}z^7 + \frac{7N_j C_{j1}C_{j2}}{720M_j}z^6 + \left(\frac{N_j C_{j2}^2}{120M_j} + \frac{C_{j1}C_{j3}}{40M_j}\right)z^5 + \left(\frac{C_{j2}C_{j3}}{24M_j} + \frac{C_{j1}C_{j4}}{12M_j}\right)z^4 +$$
$$+\frac{1}{6M_j}(C_{j2}C_{j4} + C_{j5}C_{j1})z^3 + \frac{C_{j2}C_{j5}}{2M_j}z^2 + \frac{1}{M_j}\left(C_{j6}z + C_{j7}\right).$$

Thus, the solutions of the system of motion in the basic state have the following forms:

$$\Theta_j(x,z) = (C_{j1}z + C_{j2})x + g_j(z) \tag{3.10}$$
$$U_j(x,z) = \frac{N_j C_{j1}}{24}z^4 + \frac{N_j C_{j2}}{6}z^3 + \frac{C_{j3}}{2}z^2 + C_{j4}z + C_{j5}, \quad j = \overline{1,2}. \tag{3.11}$$

The problem is determined by 7 constants for one fluid and 7 constants for the other one. Overall 14 constants which can be computed from the following relations plus the flow rate conditions:

$$z = -d: \quad U_1(-d) \overset{1}{=} 1, \quad \Theta_1(x,-d) = \Theta_c^0 \overset{2}{+} x\Theta_c^1, \text{ where } \Theta_c^0,\ \Theta_c^1 \text{consts.}$$
$$z = 0: \quad U_1(0) \overset{1}{=} U_2(0), \quad \mu\frac{\partial U_2(0)}{\partial z} \overset{1}{=} \frac{\partial U_1(0)}{\partial z}$$
$$\Theta_1(x,0) \overset{2}{=} \Theta_2(x,0), \quad \kappa\frac{\partial \Theta_2}{\partial z}(x,0) \overset{2}{=} \frac{\partial \Theta_1}{\partial z}(x,0)$$
$$z = 1: \quad U_2(1) \overset{1}{=} 0, \quad \Theta_2(x,1) = \Theta_h^0 \overset{2}{+} x\Theta_h^1, \text{ where } \Theta_h^0,\ \Theta_h^1 \text{ consts.}$$
$$Q_1 = 0, \quad Q_2 = const. \text{ given}$$

One boundary condition, that involves temperature, gives two conditions for the constants. Moreover, the system which determines the constants is a non-linear algebraic system.

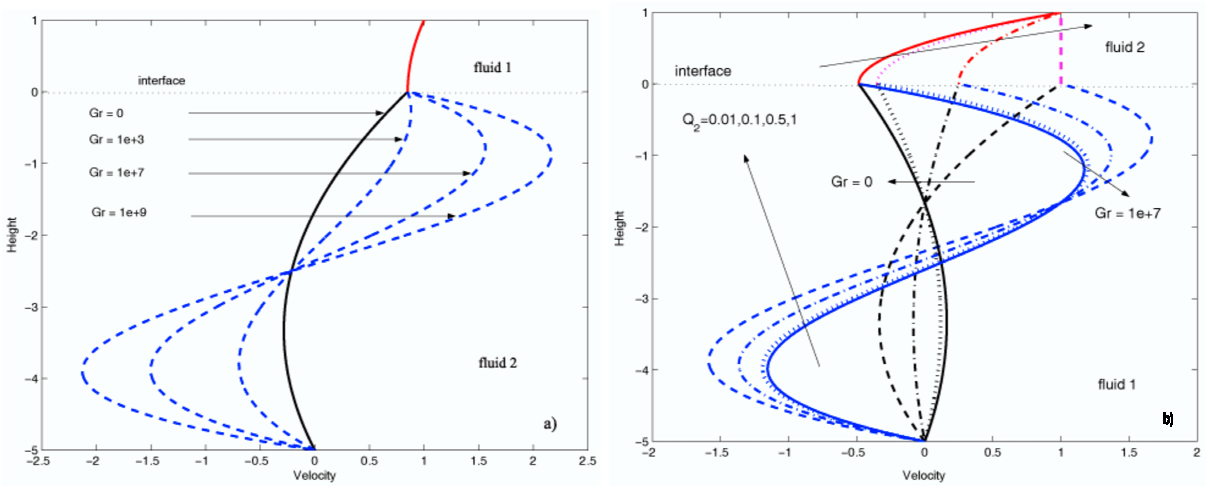

Figure 3.1: The velocity profiles for the basic flow

The velocity and temperature basic profiles must be uniquely determined, although the above system does not guarantee this fact. Moreover, it is shown later in this chapter that the perturbations of the basic flow are functions only of one direction, z. Hence, in order to apply the stability analysis without restrictions, we must consider some additional conditions which characterize entirely the basic flow when non-constant temperature boundary conditions are considered.

In more details, the basic temperature is a function depending of both directions x and z. Thus, in equations (3.36) and (3.37), the basic temperature derivative according with z dimension should cancel the x dimension from the equations, due to the fact that temperature perturbations, which are solutions of these equations, are functions depending only of z dimension. Hence, we prescribe the following condition:

$$C_{11} = C_{21} = 0. \tag{3.12}$$

The dimensional basic temperature and velocity constants are computed as follows, from the non-linear algebraic system introduced above, and are presented in the appendix D. The computations were performed by using the commercial software MATHEMATICA 5.0.

3.1.1 Basic velocity profiles

The non-dimensional basic flow velocities can be seen in the figure 3.1(a). In the case when temperature plays no role ($Gr = 0$), the profiles look identical to the profiles from the classical case for low Prandtl numbers (i.e. small kinematic viscosity). Moreover, the temperature gradient in the horizontal direction is increased and the lower fluid starts to move due to buoyancy effects. For large values of Grashof number the profiles describe exactly the recirculation of the fluid in the stable case.

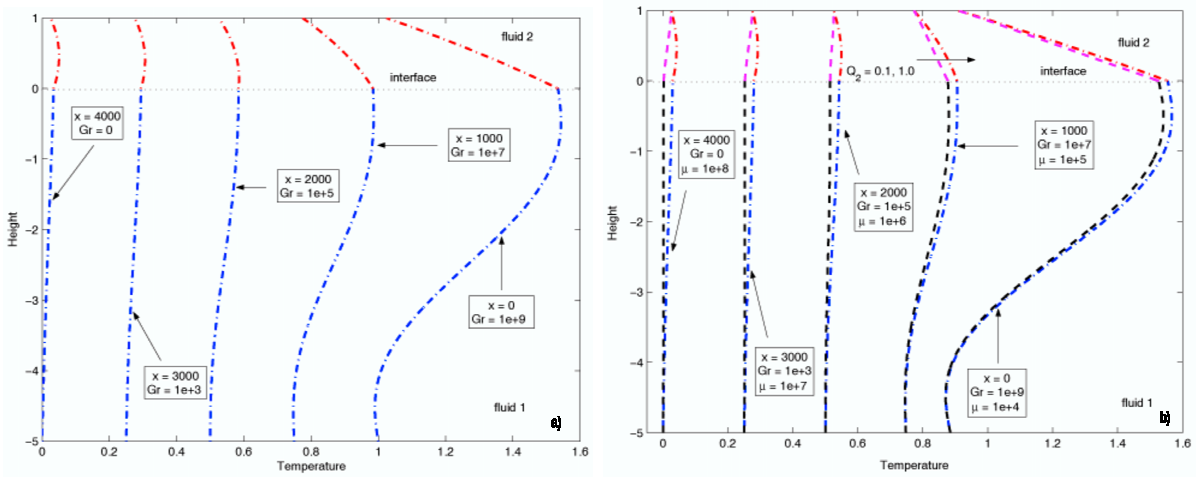

Figure 3.2: The temperature profiles for the basic flow

In our computations we used for the non-dimensional mass flow rate of the upper fluid the constant value one ($Q_2 = 1$). Nevertheless, in the industry, the mass flow rate of the floating bath depends on the manufacturing technique, therefore smaller values for the flow rate are also characteristic for the float glass process ($Q_2 = 0.1, 0.01$).

In figure 3.1(b) it is shown that for small values of the upper fluid mass flow rate and large values of the Grashof number, the velocity of the upper fluid is comparable in magnitude with the buoyant velocity of the lower fluid near interface, which is in agreement with the industrial measurements. Moreover, in the absence of the temperature gradient and for small mass flow rates, ($Gr = 0,\ Q_2 = 0.1, 0.001$), the velocity of the lower fluid changes its convexity and the upper fluid starts to move faster. These behaviours will produce strong effects over the perturbations of the system.

3.1.2 Basic temperature profiles

The non-dimensional basic temperature profiles can be seen in the figure 3.2(a), where the evolution of the temperature is represented from right to left. Hence, at the outlet of the float bath, ($x = 4000$), the temperature gradient for the basic flow plays no role ($Gr = 0$) due to the fact that we scaled with the lowest value of the temperature.

Further evolutions in the temperature profiles along the bath ($x = 3000,\ x = 2000$), influence the temperature distribution for both fluids ($Gr = 10^3,\ Gr = 10^5$) and the profiles experienced small changes. Moreover, at the inlet, we are in the presence of a large horizontal gradient that induces buoyancy movements to the lower fluid. The top temperature for the upper fluid is much lower than the temperature at the contact surface, fact which is in a perfect agreement with the float glass process.

The changes in the upper fluid mass flow rate have almost no influence over the basic temperature profile, although in the second computations we used different viscosities

ratio at each x. This is similar with the real process, where the viscosities ratio changes during the passing of the glass through the bath.

3.2 Equations for the perturbation

Linear stability with normal modes is an analytical tool used to investigate the stability of a given flow. First, we constructed an unperturbed flow, a solution of the motion system in the steady state, defined only in one direction. In order to perform linear stability, we disturb the basic flow by means of small perturbations. Next, we derive linearized equations for the perturbations. Normal modes approach assumes that the disturbances are proportional to $exp[ik(x-ct)]$.

In order to perform linear stability analysis for our problem we consider that the non-dimensional wave number, k, is real and positive. The non-dimensional wave speed, c, is complex $c = c_r + ic_i$ and is the most important parameter of our analysis. The linear stability is determined by the sign of the amplification factor kc_i. For $c_i > 0$, the perturbations will grow exponentially and the flow will evolve to instability (*unstable flow*). For $c_i < 0$, the disturbance is damped and the flow is considered to be *stable*. A special case is when $c_i = 0$; from this point the flow can evolve to stability or to instability easily. In this case the flow is said to be *neutrally stable*. We are looking for any disturbance that will grow in time, thus we apply temporal modes by choosing k real and c complex.

It is known that linear stability analysis can only determine local stability and is valid only for a short period of time before nonlinear effects become relevant. However, linear stability describe properly the evolution of the small perturbations in its early stage of development and model, qualitatively, the overall stability of the flow [43].

Using the normal-mode approach of linear stability analysis we reduce the system of non-linear partial differential equations into a system of linear ordinary differential equations where the interface and boundary conditions are changed due to the flow configuration [39]. In our case, the new system of ordinary differential equations can be written in the form of a general eigenvalue problem, where the wave speed c is the eigenvalue. Usually these problems can be solved only in very limited cases for steady flows. For more complicated flow profiles, asymptotic approximations or numerical methods are used to solve the problem.

We perturb the basic flow by an infinitesimal disturbances:

$$u_1 = U_1(z) + \epsilon\tilde{u}_1(z)e^{ik(x-ct)}, \quad u_2 = U_2(z) + \epsilon\tilde{u}_2(z)e^{ik(x-ct)} \tag{3.13}$$

$$w_1 = \epsilon\tilde{w}_1(z)e^{ik(x-ct)}, \quad w_2 = \epsilon\tilde{w}_2(z)e^{ik(x-ct)} \tag{3.14}$$

$$p_1 = P_1(x,z) + \epsilon\tilde{p}_1(z)e^{ik(x-ct)}, \quad p_2 = P_2(x,z) + \epsilon\tilde{p}_2(z)e^{ik(x-ct)} \tag{3.15}$$

$$h = \epsilon\tilde{h}e^{ik(x-ct)} \tag{3.16}$$

$$\theta_1 = \Theta_1(x,z) + \epsilon\tilde{\theta}_1(z)e^{ik(x-ct)}, \quad \theta_2 = \Theta_2(x,z) + \epsilon\tilde{\theta}_2(z)e^{ik(x-ct)} \tag{3.17}$$

where k is the wave number and c is the wave speed.

We denote with capital letters the basic flow velocities, temperatures and pressures. Taking into account that the basic flow quantities satisfy the equations of motion and collecting only the first order terms in ϵ, we obtain the linearized system of motion:

for the Lower Fluid:

Mass

$$ik\tilde{u}_1 + \frac{\partial\tilde{w}_1}{\partial z} = 0 \tag{3.18}$$

Momentum

$$Re\left(-ikc\tilde{u}_1 + ikU_1\tilde{u}_1 + \tilde{w}_1\frac{\partial U_1}{\partial z}\right) = -ik\tilde{p}_1 - k^2\tilde{u}_1 + \frac{\partial^2\tilde{u}_1}{\partial z^2} \tag{3.19}$$

$$-ikc\tilde{w}_1 + ikU_1\tilde{w}_1 = \frac{1}{Re}\left(\frac{-\partial\tilde{p}_1}{\partial z} - k^2\tilde{w}_1 + \frac{\partial^2\tilde{w}_1}{\partial z^2}\right) + \frac{Gr}{Re^2}\tilde{\theta}_1 \tag{3.20}$$

Energy

$$-ikc\tilde{\theta}_1 + ikU_1\tilde{\theta}_1 + \tilde{u}_1\frac{\partial\Theta_1}{\partial x} + \tilde{w}_1\frac{\partial\Theta_1}{\partial z} = \frac{1}{RePr}\left(\frac{\partial^2\tilde{\theta}_1}{\partial z^2} - k^2\tilde{\theta}_1\right) \tag{3.21}$$

for the Upper Fluid:

Mass

$$ik\tilde{u}_2 + \frac{\partial\tilde{w}_2}{\partial z} = 0 \tag{3.22}$$

Momentum

$$-ikc\tilde{u}_2 + ikU_2\tilde{u}_2 + \tilde{w}_2\frac{\partial U_2}{\partial z} = -i\frac{k}{\rho Re}\tilde{p}_2 + \frac{\mu}{\rho Re}\left(\frac{\partial^2\tilde{u}_2}{\partial z^2} - k^2\tilde{u}_2\right) \tag{3.23}$$

$$-ikc\tilde{w}_2 + ikU_2\tilde{w}_2 = \frac{\mu}{\rho Re}\left(-\frac{1}{\mu}\frac{\partial\tilde{p}_2}{\partial z} - k^2\tilde{w}_2 + \frac{\partial^2\tilde{w}_2}{\partial z^2}\right) + \beta\frac{Gr}{Re^2}\tilde{\theta}_2 \tag{3.24}$$

Energy

$$-ikc\tilde{\theta}_2 + ikU_2\tilde{\theta}_2 + \tilde{u}_2\frac{\partial\Theta_2}{\partial x} + \tilde{w}_2\frac{\partial\Theta_2}{\partial z} = \frac{\alpha}{RePr}\left(\frac{\partial^2\tilde{\theta}_2}{\partial z^2} - k^2\tilde{\theta}_2\right) \tag{3.25}$$

Boundary conditions:

$$\begin{array}{c}\text{for } z = -d, \quad \tilde{u}_1 = \tilde{w}_1 = \tilde{\theta}_1 = 0 \\ \text{for } z = 1, \quad \tilde{u}_2 = \tilde{w}_2 = \tilde{\theta}_2 = 0\end{array}$$

Interface conditions (z=0):

Kinematical condition

$$\tilde{w}_1 = ik\tilde{h}(U_1 - c), \quad \tilde{w}_2 = ik\tilde{h}(U_2 - c) \tag{3.26}$$

Tangential stress

$$\mu\left(\frac{\partial\tilde{u}_2}{\partial z} + ik\tilde{w}_2\right) = \frac{\partial\tilde{u}_1}{\partial z} + ik\tilde{w}_1 \tag{3.27}$$

Normal stress

$$\tilde{p}_1 - \tilde{p}_2 + 2ik\left(\tilde{u}_1 - \mu\tilde{u}_2\right) = k^2\frac{Re}{We}\tilde{h} \tag{3.28}$$

Velocity condition

$$\tilde{u}_1 + \tilde{h}\frac{\partial U_1}{\partial z} = \tilde{u}_2 + \tilde{h}\frac{\partial U_2}{\partial z}, \quad \tilde{w}_1 = \tilde{w}_2 \tag{3.29}$$

Heat transfer conditions

$$\kappa\left(ik\tilde{h}\frac{\partial\Theta_2}{\partial x} - \frac{\partial\tilde{\theta}_2}{\partial z}\right) = ik\tilde{h}\frac{\partial\Theta_1}{\partial x} - \frac{\partial\tilde{\theta}_1}{\partial z}, \quad \tilde{\theta}_1 = \tilde{\theta}_2 \tag{3.30}$$

Since we are considering only a two-dimensional disturbance it is convenient to introduce a *stream function* for the perturbation velocity ϕ_j^*, defined in the usual way:

$$u_j = \frac{\partial\phi_j^*}{\partial z}, \quad w_j = -\frac{\partial\phi_j^*}{\partial x}, \quad j = \overline{1,2} \tag{3.31}$$

where

$$\phi_j^* = \Phi_j + \epsilon\phi_j(z)e^{ik(x-ct)}, \quad j = \overline{1,2} \tag{3.32}$$

and Φ_j is the "basic" stream function defined using the basic flow velocities, for each fluid.

Further, we plug-in the relation (3.32) into the definition formula (3.31) and collecting only the terms of order ϵ, we obtain the following relations for the perturbation:

$$\tilde{u}_j = \frac{\partial\phi_j}{\partial z}, \quad \tilde{w}_j = -ik\tilde{\phi}_j, \quad j = \overline{1,2}. \tag{3.33}$$

The stream function, by its definition, satisfies the incompressibility condition. Further, we obtain the following system of complex equations which governs the stability of the basic flow.

Orr-Sommerfeld equations:

$$\phi_1^{(iv)} - 2k^2\phi_1^{''} + k^4\phi_1 = ikRe(U_1 - c)(\phi_1^{''} - k^2\phi_1) - ikRe\phi_1\frac{\partial^2 U_1}{\partial z^2} + ik\frac{Gr}{Re}\tilde{\theta}_1 \tag{3.34}$$

$$\phi_2^{(iv)} - 2k^2\phi_2^{''} + k^4\phi_2 = ikRe\frac{\rho}{\mu}(U_2 - c)(\phi_2^{''} - k^2\phi_2) - ikRe\frac{\rho}{\mu}\phi_2\frac{\partial^2 U_2}{\partial z^2} + ik\frac{Gr\rho\beta}{\mu Re}\tilde{\theta}_2 \tag{3.35}$$

Energy equations:

$$ik\tilde{\theta}_1(U_1 - c) + \phi_1^{'}\frac{\partial\Theta_1}{\partial x} - ik\phi_1\frac{\partial\Theta_1}{\partial z} = \frac{1}{RePr}\left(\frac{\partial^2\tilde{\theta}_1}{\partial z^2} - k^2\tilde{\theta}_1\right) \tag{3.36}$$

$$ik\tilde{\theta}_2(U_2 - c) + \phi_2^{'}\frac{\partial\Theta_2}{\partial x} - ik\phi_2\frac{\partial\Theta_2}{\partial z} = \frac{\alpha}{RePr}\left(\frac{\partial^2\tilde{\theta}_2}{\partial z^2} - k^2\tilde{\theta}_2\right) \tag{3.37}$$

The advantage of using linear stability analysis with normal modes is that the derivatives in x direction for the perturbation disappear. Hence, we can express pressure perturbation from equations (3.19) and (3.23) and plug-in the results into equations (3.20) and (3.24). This is the technique used for obtaining the Orr-Sommerfeld equation for each fluid.

The above system is coupled with the following interface conditions:

Kinematical condition

$$\phi_1 = \tilde{h}(c - U_1), \quad \phi_2 = \tilde{h}(c - U_2) \rightarrow \phi_1 = \phi_2 \tag{3.38}$$

Tangential stress

$$\mu\left(\phi_2^{''} + k^2\phi_2\right) = \phi_1^{''} + k^2\phi_1 \tag{3.39}$$

Normal stress

$$\begin{gathered}\phi_1^{'''} - \mu\phi_2^{'''} - 3k^2(\phi_1^{'} - \mu\phi_2^{'}) - \\ -ikRe_1\left[(U_1 - c)\left(\phi_1^{'} - \rho\phi_2^{'}\right) + \phi_1 U_1^{'}\left(\frac{\rho}{\mu} - 1\right)\right] = ik^3\frac{Re}{We}\tilde{h}\end{gathered} \tag{3.40}$$

Velocity condition

$$\phi_1^{'} + \tilde{h}\frac{\partial U_1}{\partial z} = \phi_2^{'} + \tilde{h}\frac{\partial U_2}{\partial z} \tag{3.41}$$

Heat transfer conditions

$$\tilde{\theta}_1 = \tilde{\theta}_2, \quad \kappa\left(ik\tilde{h}\frac{\partial\Theta_2}{\partial x} - \frac{\partial\tilde{\theta}_2}{\partial z}\right) = ik\tilde{h}\frac{\partial\Theta_1}{\partial x} - \frac{\partial\tilde{\theta}_1}{\partial z} \tag{3.42}$$

Boundary conditions:

$$\begin{gathered}\text{for } z = -d,\ \phi_1 = \phi_1^{'} = \tilde{\theta}_1 = 0 \\ \text{for } z = 1,\ \phi_2 = \phi_2^{'} = \tilde{\theta}_2 = 0\end{gathered}$$

3.2.1 Orr-Sommerfeld equation

Orr-Sommerfeld equation was introduced in the beginning of the century by William Orr (1907) and Arnold Sommerfeld (1908) in two papers about the stability of fluid flows. The equation has the form of a general eigenvalue problem and it is solvable only for some specific values of the eigenvalue c. Taking into consideration the aspects of the given problem, for each real value of the wave number k there is a spectrum of wave speeds c, which can be continuous, infinite or finite discrete. For each k, the complete solution for the perturbation, (in our case temperature and stream function), is a combination between the wave speed together with the corresponding wave number and the coefficients which are computed from conditions [43, 45].

Nevertheless, the stability mechanism of a given flow can be understood without computing analitycally the perturbation solutions. The most used technique in linear analysis is to find a dependence between the wave speed c and the wave number k, described in the form of a dispersion relation. All the information about the development and propagation of a given wave mode is contained in the appropriate derived dispersion relation, which relates the two main parameters of a stability analysis using normal modes.

In order to perform a complete analysis of the stability we use two different approaches. The first one determine the critical values of our non-dimensional parameters (Reynolds, Grashof, Weber) from which the flow becomes first linearly unstable. The second approach determines, for fixed parameters and wide range of wave numbers k, the sign of the wave speed c which describes the stability of the flow.

Due to the complexity of the problem, an analytical solution for the dispersion relation is difficult to be found. Therefore, we apply asymptotic analysis, in two particular limits, long wave ($k \to 0$) and short wave ($k \to \infty$), and numerical methods in our attempt to solve the system of motion which characterize our problem and to determine its stability.

3.3 Long wave limit

The long wave stability problem corresponds to disturbances with wave length much longer than both layer's thickness. In this case the Weber number is large, so that the stabilizing effect of surface tension is small in comparison with the inertia effect.

The x and z directions are both scaled with the same characteristic length, the height of the thinner upper fluid, d_2. In the figure 3.3, is shown a comparison of the wave length and wave amplitude with the characteristic length. Thus, the wave length of a long wave, λ, is much larger than the height of the thinner upper fluid, when its amplitude is much smaller in comparison with the characteristic length. Thus, in the long wave limit the wave length tends to infinity (i.e. $\lambda \to \infty$).

Further, we investigate the development and the stability of the waves in this particular limit. In this case, our small parameter is the wave number $k = 2\pi/\lambda$, hence, the wave

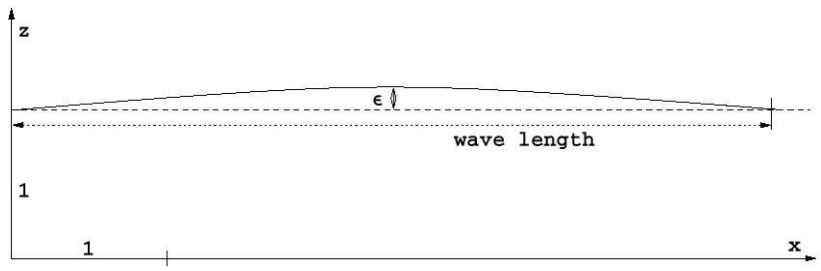

Figure 3.3: The wave form with respect to the scaling in the long wave limit

number tends to zero, $k \to 0$. Our analysis follows the classical approach, hence we look for solutions of the form:

$$\begin{aligned}
\phi^j &= \phi_0^j + k\phi_1^j + k^2\phi_2^j + ..., \\
\tilde{\theta}^j &= \tilde{\theta}_0^j + k\tilde{\theta}_1^j + k^2\tilde{\theta}_2^j + ..., \quad j = \overline{1,2}, \\
\tilde{h} &= \tilde{h}_0 + k\tilde{h}_1 + k^2\tilde{h}_2 + ... \\
c &= c_0 + kc_1 + k^2c_2 + ..., \quad k \to 0
\end{aligned} \tag{3.43}$$

In the following computations, the superscript shows which fluid is considered and the subscript emphasizes the order of each term which is reffered to.

We obtain the homogeneous *leading order* system of equations:

$$\phi_0^{1(iv)} = 0, \quad \phi_0^{2(iv)} = 0 \tag{3.44}$$

$$\tilde{\theta}_0^{1''} = RePr\phi_0^{1'}\frac{\partial\Theta_1}{\partial x}, \quad \tilde{\theta}_0^{2''} = \frac{RePr}{\alpha}\phi_0^{2'}\frac{\partial\Theta_2}{\partial x} \tag{3.45}$$

with the following interface conditions ($z = 0$):

$$\begin{aligned}
&\phi_0^1 = \phi_0^2, \quad \mu\phi_0^{2''} = \phi_0^{1''}, \quad \phi_0^{1'''} - \mu\phi_0^{2'''} = 0 \\
&\phi_0^{1'} + \tilde{h}_0\frac{\partial U_1}{\partial z} = \phi_0^{2'} + \tilde{h}_0\frac{\partial U_2}{\partial z}, \quad \phi_0^1 = \tilde{h}_0\,(c - U_1) \\
&\tilde{\theta}_0^1 = \tilde{\theta}_0^2, \quad \kappa\tilde{\theta}_0^{2'} = \tilde{\theta}_0^{1'}
\end{aligned} \tag{3.46}$$

and boundary conditions:

$$\begin{aligned}
&\text{for } z = -d,\ \phi_0^1 = \phi_0^{1'} = \tilde{\theta}_0^1 = 0 \\
&\text{for } z = 1,\ \phi_0^2 = \phi_0^{2'} = \tilde{\theta}_0^2 = 0.
\end{aligned}$$

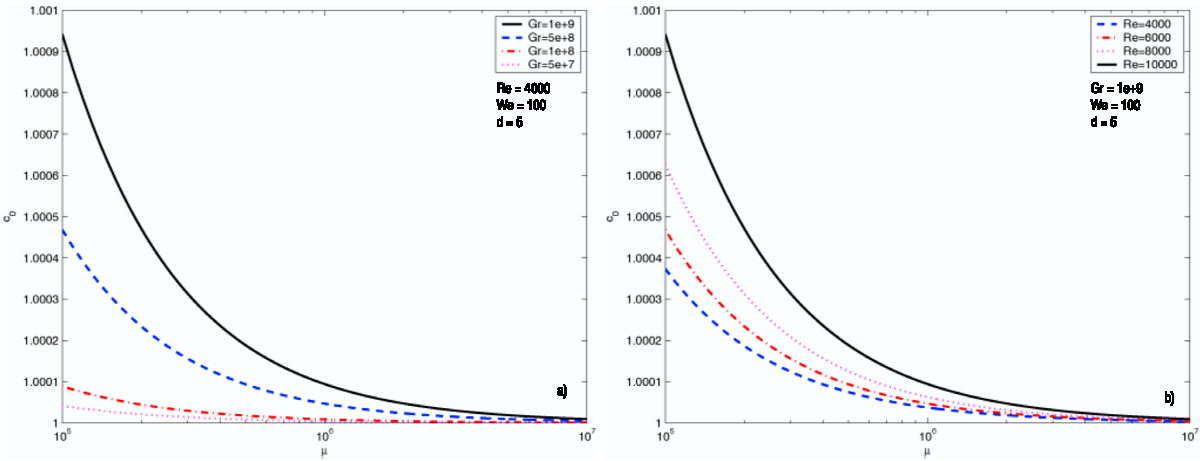

Figure 3.4: The wave speed with respect to the viscosities ratio for: (a) different values of Grashof number; (b) different values of Reynolds number.

The basic temperature field is a function depending on two variables, x and z, thus an additional term appears in each equation for the leading order temperature disturbances. Moreover, in order to observe the influence of the surface tension over the stability of the system, we assume that the Weber number is of order k^2.

The leading order system is an ODE system that can be solved analytically and its solution is plugged into the relation (3.38). Hence, we can compute the wave speed c_0, which has the following form:

$$c_0 = \frac{-2(C_{14} - C_{24})d^2(1+d)\mu + C_{15}(1 + 4d\mu + 6d^2\mu + 4d^3\mu + d^4\mu^2)}{1 + 4d\mu + 6d^2\mu + 4d^3\mu + d^4\mu^2} \tag{3.47}$$

In the long wave limit the wave speed c_0 depends on the Reynolds number of the lower fluid, the depth ratio of the liquid layers, the magnitude of the temperature gradient and the ratio of the viscosities. The following computations are made by taking into consideration a large depth ratio and mass flow rate ($d = 5, Q_2 = 1$).

The wave velocity is real, positive and becomes greater for higher temperature gradients as shown on figure 3.5(a). The wave propagates faster when the upper fluid is less viscous than the lower one. This results is verified for the no-temperature case, where the wave propagates in the direction of the less viscous flow [8, 10]. The speed of the disturbance is positive and grows further, whereas the inertia of the lower fluid increases (figure 3.5(b)). The wave propagates faster when the viscosity effects dominate in the lower fluid domain.

We investigate the influence of the depth ratio over the wave speed for high viscosity ratios (figure 3.6(a)). Thus, it is shown that the stability of the system depends on the depth ratio and it is important for the stability of the process that the height of the lower fluid to be equal or greater than the height of the upper one. From the literature it is known that in the case when the viscosities are equal, the wave propagates with the flow of the thinner layer [1, 10]. We found that this effect remains valid in our case, although

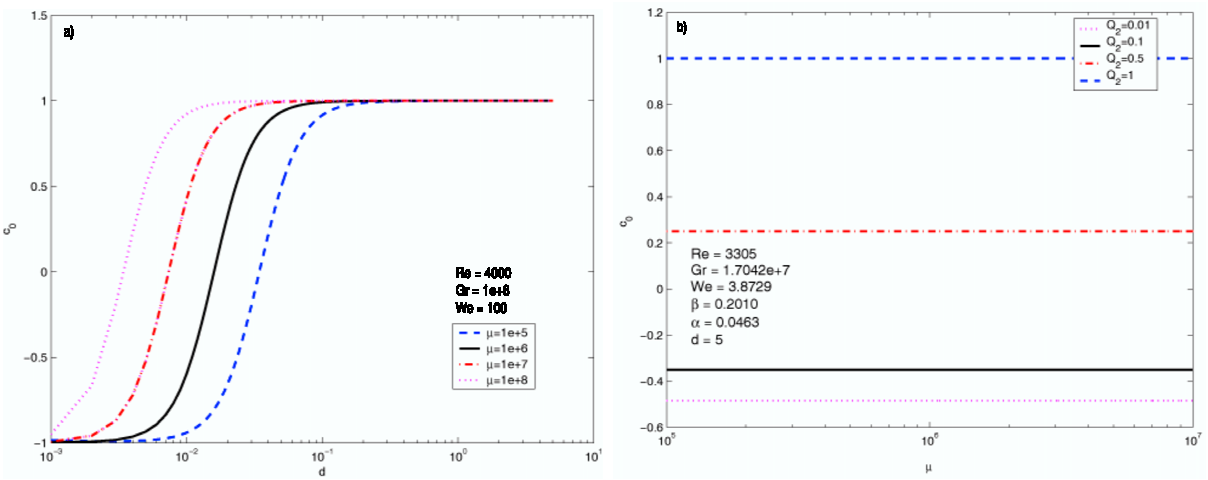

Figure 3.5: The wave speed with respect to: (a) the depth ratio for different values of the viscosities ratio; (b) the viscosities ratio for different values of the mass flow rate.

the viscosities ratio is considerably larger(figure 3.7(a)). The speed of the disturbance grows whereas the height of the lower layer becomes greater than the height of the upper one and the wave propagates quicklier when the upper fluid is more viscous than the lower one.

Further, we investigate the stability of the system taking into account parameters much closer to the real float glass process. Hence, we compare the value of the wave speed c_0 at small mass flow rates (figure 3.6(b)). We observed that for processes with the values of the upper fluid mass flow rates smaller than one, the waves are propagating upstream with half of the upper fluid velocity (i.e. molten glass). This result can be explained by the lack of kinematical viscosity in the lower fluid and by its high thermal diffusivity which contributes to the development of a strong buoyant motion unbalanced by small inertial effects already existent in the upper fluid layer.

The *first order* system of motion reads:

$$\begin{aligned}
\phi_1^{1(iv)} &= iRe(U_1 - c_0)\phi_0^{1''} - iRe\phi_0^1\frac{\partial^2 U_1}{\partial z^2} + i\frac{Gr}{Re}\tilde{\theta}_0^1 \\
\phi_1^{2(iv)} &= iRe\frac{\rho}{\mu}(U_2 - c_0)\phi_0^{2''} - iRe\frac{\rho}{\mu}\phi_0^2\frac{\partial^2 U_2}{\partial z^2} + i\frac{Gr\rho\beta}{Re\mu}\tilde{\theta}_0^2 \qquad (3.48) \\
\tilde{\theta}_1^{1''} &= RePr\left[\phi_1^{1'}\frac{\partial\Theta_1}{\partial x} + i\tilde{\theta}_0^1(U_1 - c_0) - i\phi_0^1\frac{\partial\Theta_1}{\partial z}\right] \\
\tilde{\theta}_1^{2''} &= \frac{RePr}{\alpha}\left[\phi_1^{2'}\frac{\partial\Theta_2}{\partial x} + i\tilde{\theta}_0^2(U_2 - c_0) - i\phi_0^2\frac{\partial\Theta_2}{\partial z}\right] \qquad (3.49)
\end{aligned}$$

with the corresponding interface conditions ($z = 0$):

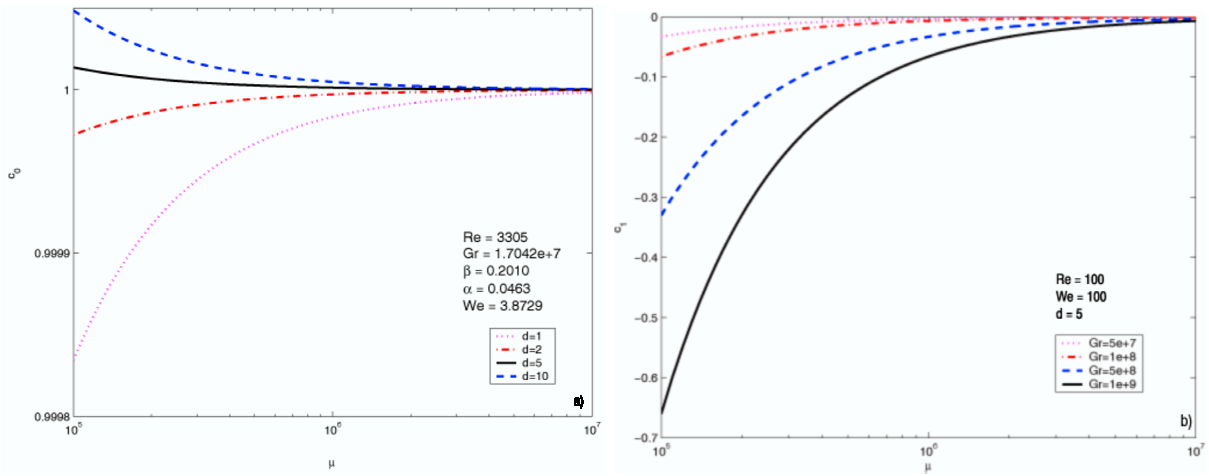

Figure 3.6: (a) The wave speed with respect to the viscosities ratio for different values of the depth ratio; (b) The eigenvalue c_1 with respect to viscosities ratio for different values of the Grashof number.

$$\phi_1^1 = \phi_1^2, \quad \mu\phi_1^{2''} = \phi_1^{1''}$$
$$\phi_1^{1'''} - \mu\phi_1^{2'''} - iRe\left[(U_1 - c_0)(\phi_0^{1'} - \rho\phi_0^{2'}) + \phi_0^1 U_1'\left(\frac{\rho}{\mu} - 1\right)\right] = i\frac{Re}{We}\tilde{h}_0$$
$$\phi_1^{1'} + \tilde{h}_1\frac{\partial U_1}{\partial z} = \phi_1^{2'} + \tilde{h}_1\frac{\partial U_2}{\partial z}, \quad \phi_1^1 = \tilde{h}_0 c_1 + \tilde{h}_1\left(c_0 - U_1\right)$$
$$\tilde{\theta}_1^1 = \tilde{\theta}_1^2, \quad \kappa\left(i\tilde{h}_0\frac{\partial\Theta_2}{\partial x} - \tilde{\theta}_1^{2'}\right) = i\tilde{h}_0\frac{\partial\Theta_1}{\partial x} - \tilde{\theta}_1^{1'} \tag{3.50}$$

and boundary conditions:

$$\text{for } z = -d,\ \phi_1^1 = \phi_1^{1'} = \tilde{\theta}_1^1 = 0$$
$$\text{for } z = 1,\ \phi_1^2 = \phi_1^{2'} = \tilde{\theta}_1^2 = 0.$$

The first order system is an ODE system that can be solved analytically and its solution, the growth rate c_1, is presented in the appendix D, due to its complexity. The eigenvalue c_1 computed from the system above is imaginary and depends on the flow inertia, magnitude of the temperature difference, depth ratio and the surface tension.

On figure 3.7(b), the eigenvalue c_1 is plotted with respect to the viscosity ratio μ for different values of the Grashof number. It is shown that temperature stabilizes the system and the effect arises much faster when the upper fluid is less viscous than the lower one.

The system is neutrally stable when the thickness of the lower fluid layer is comparable in value with the thickness of the upper one. An increase in the viscosity of the upper fluid

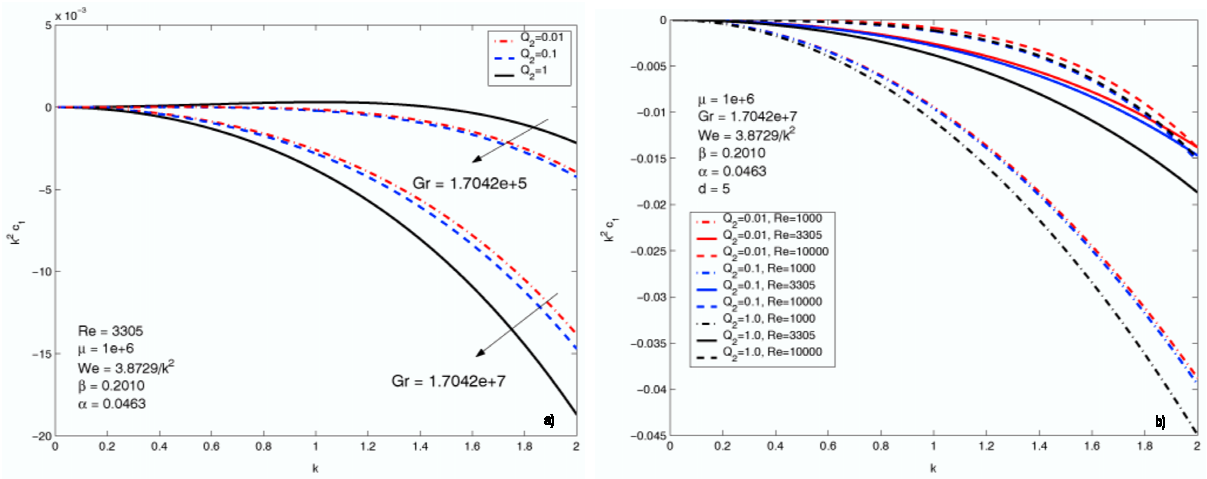

Figure 3.7: The growth rate with respect to the wave number for different values of the mass flow rate, with respect to: (a) Grashof number; (b) Reynolds number.

induces a faster loss of the stability. When the lower fluid is much thicker, the system becomes more stable. These results are computed in the case of low surface tension (large Weber number), thus the stabilizing effects which appear are the result of inertia, temperature and viscosity.

Having discussed the stability of the system (i.e. the sign of the eigenvalue c_1), now we analyze the growth rate of the perturbation, which in this case is k^2c_1, due to the fact that following the asymptotics $c = c_0 + kc_1$ and also taking into account the fact that c_1 is imaginary. Therefore, in the figure 3.8(b), we plotted the growth rate as a function of the wave number k for different values of the mass flow rate Q_2. It is shown that the temperature decreases the growth rate, hence stabilizing the process. Although, for smaller value of the Grashof number, the growth rate achieves a very small positive value around 10^{-4}. During the computations the surface tension changes according with the wave number and decreases in value, due to our assumption that the Weber number is of order k^2. The inertia destabilizes the flow, although slightly, whereas the difference in the mass flow rate for smaller values, $Q_2 = 0.1, 0.001$, has no noticeable effect over the gowth rate of the disturbance.

We make an estimation of how much an initial perturbation, (fixed wave number and amplitude), will grow during the entire process taking into account the linear evolution of the horizontal temperature gradient and the viscosities ratio. Figure 3.9, shows that the perturbation decreases fast at the beginning of the process; at this point parameters are $Gr = 1.7042 \cdot 10^7$, $\mu = 10^4$. Further, the amplitude of the perturbation grows slowly to an asymptotic value of one. From the right figure (the logarythmic plot of the growth rate) we can see that the initial droping take place only in a very small neighbourhood near inlet. The result of the estimation is that, the initial perturbation is conserved throughout the process.

In the next chapter, we compute numerically the value of the initial perturbation for the interface at different wave numbers and coupling this result with the above estimation we

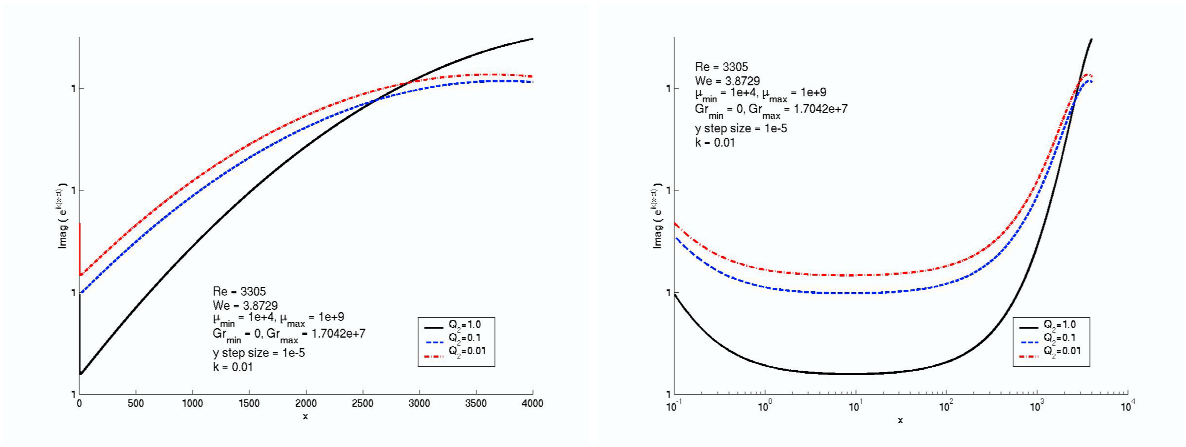

Figure 3.8: The growth rate with respect to the length of the bath for different values of the mass flow rate

find that the waves with wave lengths much larger than the amplitude are always stable. Moreover, this result is confirmed by the observations made on the real float glass process (see Chapter 6).

3.4 Short wave limit

Our primary concern is to focus on the development and the stability of short waves which appear close to the interface. Hence, we should construct another system of motion, devoted to emphasizing micro-patterns of waves which evolve, in the real process, at the contact surface between hot glass and molten tin.

Nevertheless, in the short wave limit, we are looking for waves which have an amplitude and a wave length of the same order of magnitude, although much smaller than the characteristic length, the height of the thinner upper fluid layer. Using the same system of motion which was developed in the last section and imposing the wave number k to tend to infinity, no reasonable results can be obtained (i.e. both stream functions become equal zero). Hence, we need to change our perspective by focusing on the micro-structures which can appear near the interface.

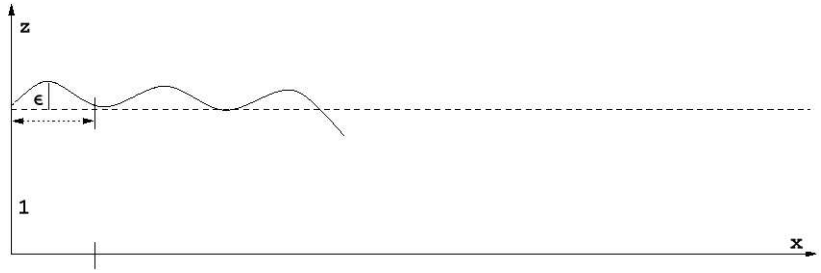

Figure 3.9: The wave form with respect to the scaling in the short wave limit

In order to keep x and z scales at the same order of magnitude, we perform a change in our scaling, corresponding to a short-scale structure concentrated close to the interface. Hence, we change our perspective from the macroscopic to the microscopic approach. In this case we enlarge the height z as follows:

$$z = \epsilon\tilde{z} \tag{3.51}$$

where $\epsilon \to 0$ is the linearization small parameter.

Moreover, we assume that our small parameter is the ratio $1/k$, where k is the wave number and $k \to \infty$ relation characteristic for the short wave limit. We consider the basic flow profile defined in the chapter 2 and we perturb the basic quantities in the same way as was presented in the last section. Thus, we have:

$$u_1 = U_1(\frac{1}{k}\tilde{z}) + \frac{1}{k}\tilde{u}_1(\frac{1}{k}\tilde{z})e^{ik(x-ct)}, \quad u_2 = U_2(\frac{1}{k}\tilde{z}) + \frac{1}{k}\tilde{u}_2(\frac{1}{k}\tilde{z})e^{ik(x-ct)} \tag{3.52}$$

$$w_1 = \frac{1}{k}\tilde{w}_1(\frac{1}{k}\tilde{z})e^{ik(x-ct)}, \quad w_2 = \frac{1}{k}\tilde{w}_2(\frac{1}{k}\tilde{z})e^{ik(x-ct)} \tag{3.53}$$

$$p_1 = P_1(\frac{1}{k}\tilde{z}) + \frac{1}{k}\tilde{p}_1(\frac{1}{k}\tilde{z})e^{ik(x-ct)}, \quad p_2 = P_2(\frac{1}{k}\tilde{z}) + \epsilon\tilde{p}_2(\frac{1}{k}\tilde{z})e^{ik(x-ct)} \tag{3.54}$$

$$h = \frac{1}{k}\tilde{h}e^{ik(x-ct)} \tag{3.55}$$

$$\theta_1 = \Theta_1(\frac{1}{k}\tilde{z}) + \frac{1}{k}\tilde{\theta}_1(\frac{1}{k}\tilde{z})e^{ik(x-ct)}, \quad \theta_2 = \Theta_2(\frac{1}{k}\tilde{z}) + \frac{1}{k}\tilde{\theta}_2(\frac{1}{k}\tilde{z})e^{ik(x-ct)} \tag{3.56}$$

Hence, we plug-in the above relations into the non-dimensional system of motion (2.22)-(2.35) and taking into account that the basic flow quantities satisfy the equations and keeping only the linear terms which contain perturbation quantities, we obtain the linearized system of motion, in the same way as was presented in chapter 1. Similarly, we introduce the stream function and performing the computations, we obtain the new Orr-Sommerfeld system of motion coupled with the energy equations and both boundary and interface conditions, written for both fluids (some computation examples are shown in appendix B):

$$k^4\left(\phi_1^{(iv)} - 2\phi_1^{''} + \phi_1\right) = ik^3Re(U_1 - c)(\phi_1^{''} - \phi_1) - ik^3Re\phi_1\frac{\partial^2 U_1}{\partial z^2} + ik\frac{Gr}{Re}\tilde{\theta}_1 \tag{3.57}$$

$$k^4\left(\phi_2^{(iv)} - 2\phi_2^{''} + \phi_2\right) = ik^3Re\frac{\rho}{\mu}(U_2 - c)(\phi_2^{''} - \phi_2) - ik^3Re\frac{\rho}{\mu}\phi_2\frac{\partial^2 U_2}{\partial z^2} + ik\frac{Gr\rho\beta}{\mu Re}\tilde{\theta}_2 \tag{3.58}$$

$$ik\tilde{\theta}_1(U_1 - c) + k\phi_1^{'}\frac{\partial\Theta_1}{\partial x} - ik^2\phi_1\frac{\partial\Theta_1}{\partial z} = \frac{k^2}{RePr}\left(\frac{\partial^2\tilde{\theta}_1}{\partial z^2} - \tilde{\theta}_1\right) \tag{3.59}$$

$$ik\tilde{\theta}_2(U_2 - c) + k\phi_2^{'}\frac{\partial\Theta_2}{\partial x} - ik^2\phi_2\frac{\partial\Theta_2}{\partial z} = \frac{\alpha k^2}{RePr}\left(\frac{\partial^2\tilde{\theta}_2}{\partial z^2} - \tilde{\theta}_2\right) \tag{3.60}$$

Interface conditions ($\tilde{z} = 0$):

Kinematical condition

$$\phi_1 = \phi_2 \tag{3.61}$$

Tangential stress

$$\mu\left(\phi_2^{''} + \phi_2\right) = \phi_1^{''} + \phi_1 \tag{3.62}$$

Normal stress

$$k^3(\phi_1^{'''} - \mu\phi_2^{'''}) - 3k^3(\phi_1^{'} - \mu\phi_2^{'}) -$$
$$-ik^2Re\left[(U - c)\left(\phi_1^{'} - \rho\phi_2^{'}\right) + \phi_1 U_1^{'}\left(\frac{\rho}{\mu} - 1\right)\right] = ik^3\frac{Re}{We}\tilde{h} \tag{3.63}$$

Velocity condition

$$\phi_1^{'} + \tilde{h}\frac{\partial U_1}{\partial z} = \phi_2^{'} + \tilde{h}\frac{\partial U_2}{\partial z} \tag{3.64}$$

Heat transfer conditions

$$\kappa\left(ik\tilde{h}\frac{\partial\Theta_2}{\partial x}-k\frac{\partial\tilde{\theta}_2}{\partial z}\right)=ik\tilde{h}\frac{\partial\Theta_1}{\partial x}-k\frac{\partial\tilde{\theta}_1}{\partial z},\quad \tilde{\theta}_1=\tilde{\theta}_2 \tag{3.65}$$

Further, for clarity, we drop the "tilde" symbol for the z direction. After scaling, the boundary conditions will change to plus and minus infinity.

$$\phi_1(-\infty)=\phi_1^{'}(-\infty)=\tilde{\theta}_1(-\infty)=0, \tag{3.66}$$

$$\phi_2(\infty)=\phi_2^{'}(\infty)=\tilde{\theta}_2(\infty)=0, \tag{3.67}$$

Thus, the eigenvectors of the perturbation system of motion should remain bounded, thus we are looking for solutions in the form:

$$\phi_1\sim\mathcal{O}(e^z),\quad \theta_1\sim\mathcal{O}(e^z) \tag{3.68}$$

$$\phi_2\sim\mathcal{O}(e^{-z}),\quad \theta_2\sim\mathcal{O}(e^{-z}) \tag{3.69}$$

Using the asymptotic expansions according with k, the wavenumber, we look for the solutions of the form:

$$\phi^j=\phi_0^j+\frac{1}{k}\phi_1^j+\frac{1}{k^2}\phi_2^j+... \tag{3.70}$$

$$\tilde{\theta}^j=\tilde{\theta}_0^j+\frac{1}{k}\tilde{\theta}_1^j+\frac{1}{k^2}\tilde{\theta}_2^j+... \tag{3.71}$$

$$c=c_0+\frac{1}{k}c_1+\frac{1}{k^2}c_2+... \tag{3.72}$$

$$\tilde{h}=\tilde{h}_0+\frac{1}{k}\tilde{h}_1+\frac{1}{k^2}\tilde{h}_2+... \tag{3.73}$$

with $1/k\to 0$ and the dimensionless numbers fixed.

3.4.1 No-thermal leading order effects

We consider the above system of motion without making further assumptions. Thus, we compute the first two eigenvalues, (i.e. leading, c_0, and first order, c_1) and using the expansion definition we construct the general eigenvalue c, ($c=c_0+1/kc_1$). The real part of the eigenvalue describes the wave speed of the perturbation whereas the imaginary part is the growth rate of the perturbation due to the fact that we are in the short wave limit. In this case, the influence of the temperature over the stability of the system is felt only through the basic flow parameters (i.e. basic flow velocities).

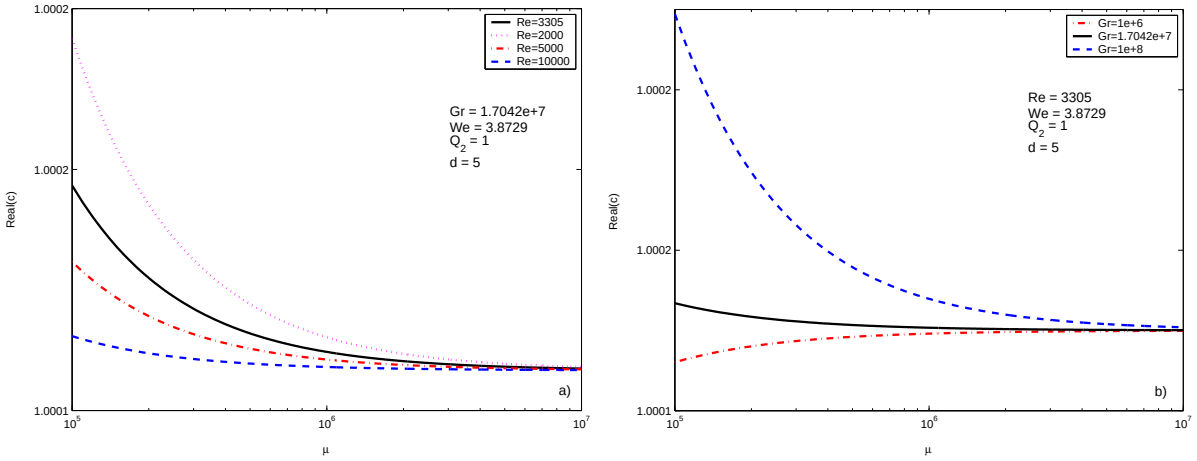

Figure 3.10: The wave speed of the perturbation with respect to the viscosities ratio for different values of the: a) Reynolds number; b) Grashof number.

Hence, we plug-in the above expansions into the short wave system of motion described by the eqs. (3.57)-(3.67) and collecting the leading order terms we obtain the leading order system of motion:

$$\phi_0^{1(iv)} - 2\phi_0^{1''} + \phi_0^1 = 0, \quad \phi_0^{2(iv)} - 2\phi_0^{2''} + \phi_0^2 = 0 \tag{3.74}$$

$$\frac{\partial^2 \tilde{\theta}_0^1}{\partial z^2} - \tilde{\theta}_0^1 + iRePr\phi_0^1 \frac{\partial \Theta_1}{\partial z} = 0, \quad \frac{\partial^2 \tilde{\theta}_0^2}{\partial z^2} - \tilde{\theta}_0^2 + i\phi_0^2 \frac{RePr}{\alpha} \frac{\partial \Theta_2}{\partial z} = 0 \tag{3.75}$$

coupled with the following interface conditions ($z = 0$):

$$\phi_0^1 = \phi_0^2, \quad \phi_0^{1'} + \tilde{h}_0 \frac{\partial U_1}{\partial z} = \phi_0^{2'} + \tilde{h}_0 \frac{\partial U_2}{\partial z}, \quad \phi_0^1 = \tilde{h}_0 \left(c - U_1\right)$$

$$\mu(\phi_0^{2''} + \phi_0^2) = \phi_0^{1''} + \phi_0^1, \quad \phi_0^{1'''} - \mu\phi_0^{2'''} - 3(\phi_0^{1'} - \mu\phi_0^{2'}) = i\frac{Re}{We} h_0$$

$$\tilde{\theta}_0^1 = \tilde{\theta}_0^2, \quad \kappa \left(i\tilde{h_0} \frac{\partial \Theta_2}{\partial x} - \frac{\partial \tilde{\theta}_0^2}{\partial z} \right) = i\tilde{h_0} \frac{\partial \Theta_1}{\partial x} - \frac{\partial \tilde{\theta}_0^1}{\partial z}. \tag{3.76}$$

In the leading order energy equation, the temperature is coupled with the stream function and also the basic flow temperature derivative with respect to x dimension appears in the heat transfer interface condition. These factors determine the complex form of the temperature perturbation.

The leading order system is an ODE system that can be solved analytically and its solution, the wave speed c_0, has the following form:

$$c_0 = C_{15} - i\frac{Re}{2We\left(1+\mu\right)}. \tag{3.77}$$

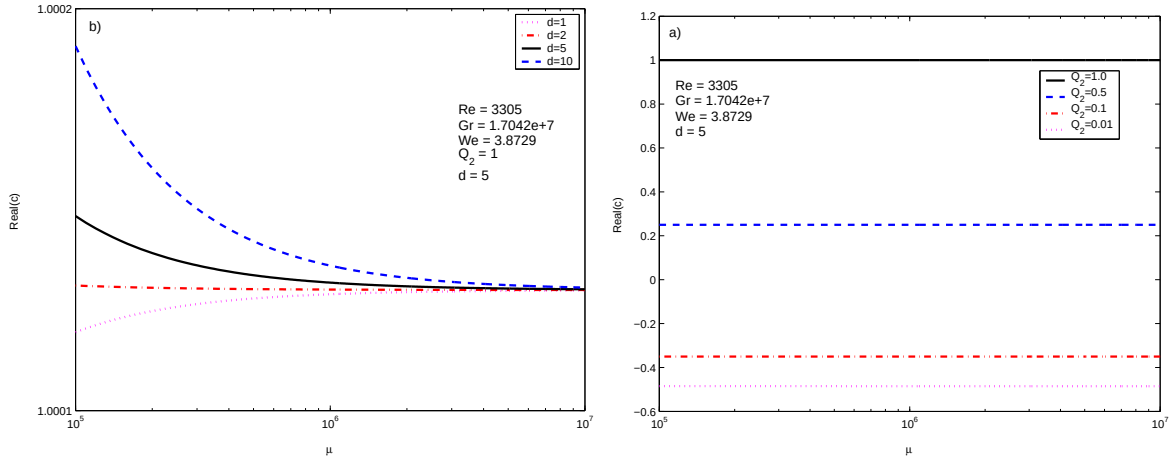

Figure 3.11: The wave speed of the perturbation with respect to the viscosities ratio for different values of the: a) depth ratio; b) mass flow rate.

The eigenvalue c_0 is complex and has an imaginary part which depends on the Reynolds number of the lower fluid, the viscosities ratio and the Weber number. Therefore, due to the large magnitude of the viscosities ratio, the imaginary part is negative and very small in magnitude. The existence of eigenvalue c_0 complex part is ensured by the appeareance of the term iRe/Weh_0 in the normal stress condition. Nevertheless, the real part of the eigenvalue c_0 represents the speed of the perturbation and has a non-dimensional value one, which corresponds to the dimensional velocity of the upper fluid layer.

The system becomes unstable whereas the inertia of the lower fluid decreases as shown on figure 3.11(a). Moreover, the wave velocity grows for higher temperature gradients, destabilizing the system and the wave propagates faster when the upper fluid layer is less viscous than the lower one. This results is verified for the no-temperature case, where the wave propagates in the direction of the less viscous flow [9, 10].

We investigate the influence of the depth ratio on the stability of the system and we shown that the system becomes unstable when the height of the lower liquid layer increases (figure 3.12(a)). This result is in contradiction with the long wave case where the depth ratio stabilizes the long waves, although the wave speed increases with a very small amount. From the figure 3.12(b) we can see that a change in the upper fluid mass flow rate has strong consequences on the speed of the disturbance and the effect is similar with the one observed in the long wave limit.

Further, collecting the first order terms from the system (3.57)-(3.67), we obtain the *first order* system of motion which is stated below:

$$\phi_1^{1(iv)} - 2\phi_1^{1''} + \phi_1^1 - iRe(U_1 - c_0)(\phi_0^{1''} - \phi_0^1) + iRe\phi_1^1 \frac{\partial^2 U_1}{\partial z^2} = 0$$

$$\phi_1^{2(iv)} - 2\phi_1^{2''} + \phi_1^2 - i\frac{\rho}{\mu}Re(U_2 - c_0)(\phi_0^{2''} - \phi_0^2) + iRe\frac{\rho}{\mu}\phi_1^2 \frac{\partial^2 U_2}{\partial z^2} = 0 \qquad (3.78)$$

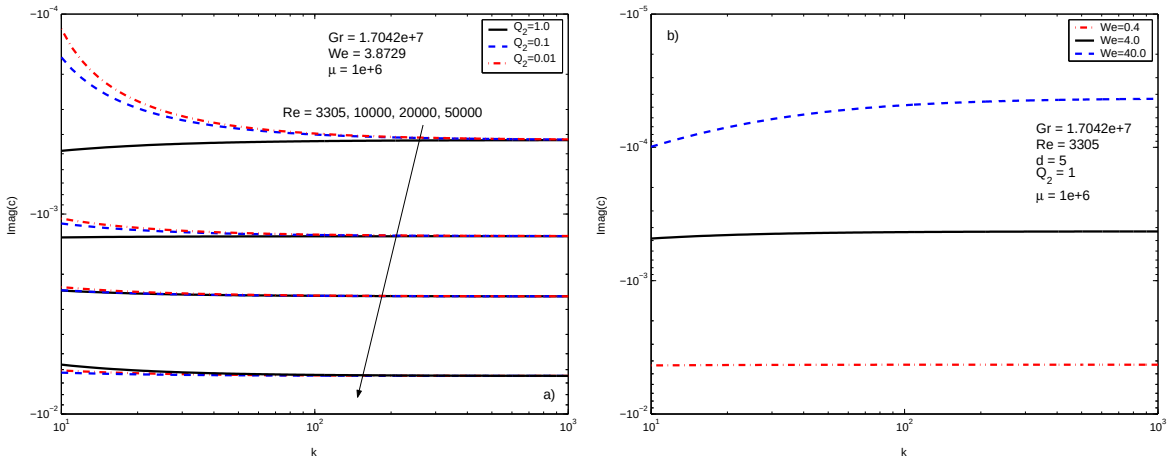

Figure 3.12: The growth rate with respect to the wave number for different values of the mass flow rate at various values for the: a) Reynolds number; b) Weber number.

$$i\tilde{\theta}_0^1(U_1 - c_0) - i\phi_0^1\frac{\partial\Theta_1}{\partial z} + \phi_1^1\frac{\partial\Theta_1}{\partial x} = \frac{1}{RePr}\left(\frac{\partial^2\tilde{\theta}_1^1}{\partial z^2} - \tilde{\theta}_1^1\right)$$
$$i\tilde{\theta}_0^2(U_2 - c_0) - i\phi_0^2\frac{\partial\Theta_2}{\partial z} + i\phi_1^2\frac{\partial\Theta_2}{\partial z} = \frac{\alpha}{RePr}\left(\frac{\partial^2\tilde{\theta}_1^2}{\partial z^2} - \tilde{\theta}_1^2\right) \tag{3.79}$$

The system is coupled with the following interface conditions ($z = 0$):

$$\phi_1^1 = \phi_1^2, \qquad \phi_1^{1'} + \tilde{h}_1\frac{\partial U_1}{\partial z} = \phi_1^{2'} + \tilde{h}_1\frac{\partial U_2}{\partial z}$$
$$\mu(\phi_1^{2''} + \phi_1^2) = \phi_1^{1''} + \phi_1^1, \qquad \phi_1^1 = \tilde{h}_0 c_1 + \tilde{h}_1\left(c_0 - U_1\right)$$
$$\phi_1^{1'''} - \mu\phi_1^{2'''} - 3(\phi_1^{1'} - \mu\phi_1^{2'}) - iRe\left[(U_1 - c_0)\left(\phi_0^{1'} - \rho\phi_0^{2'}\right) + \phi_0^1\frac{\partial U_1}{\partial z}\left(\frac{\rho}{\mu} - 1\right)\right] = i\frac{Re}{We}\tilde{h}_1$$
$$\tilde{\theta}_1^1 = \tilde{\theta}_1^2, \qquad \kappa\left(i\tilde{h}_1\frac{\partial\Theta_2}{\partial x} - \frac{\partial\tilde{\theta}_1^2}{\partial z}\right) = i\tilde{h}_1\frac{\partial\Theta_1}{\partial x} - \frac{\partial\tilde{\theta}_1^1}{\partial z}. \tag{3.80}$$

Hence, in the first order Orr-Sommerfeld equations appears the leading order eigenvalue c_0 and the second derivative of the basic flow velocities. Similarly, in the first order energy equations, we have the first derivative of the basic flow temperatures with respect to x and z dimensions, along with the leading order eigenvalue c_0. The interface conditions remain essentially the same, the noticeable changes appear only in the normal stress condition.

The eigenvalue c_1 computed from the system above is complex and depends on the flow inertia, magnitude of the temperature difference, depth ratio and the surface tension (see appendix D). The sign of the complex part of the first order eigenvalue, together with the complex part of the leading order eigenvalue c_0, determine the stability of the system.

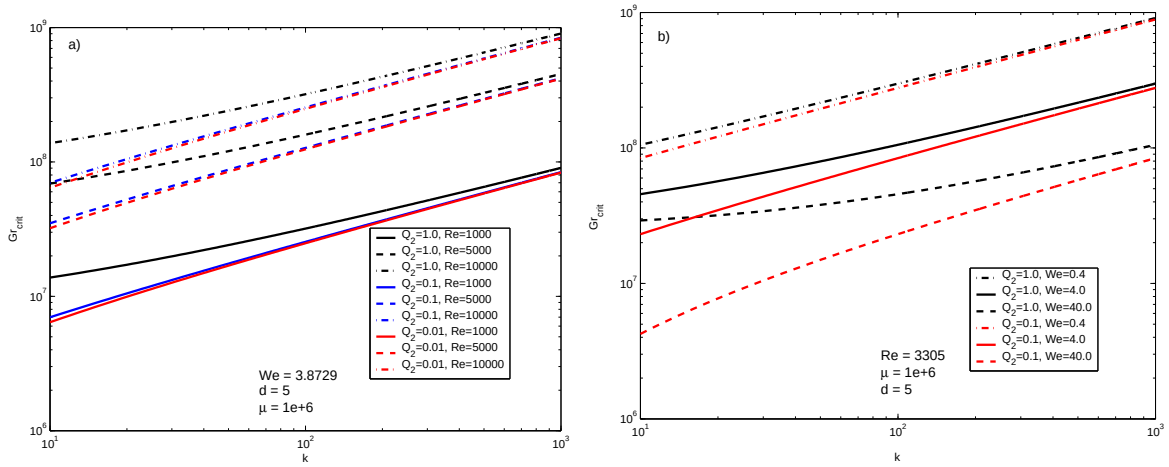

Figure 3.13: The critical Grashof number with respect to the wave number for different values of the mass flow rate at various values for the: a) Reynolds number; b) Weber number

On figure 3.13(a) is plotted the growth rate of the perturbation with respect to the wave number for large different values of the Reynolds number. Thus, it is shown that the inertia stabilizes the flow, result also obtained in the analysis of the wave speed. Moreover, inertia stabilizes the flow also when the upper layer is much more viscous than the lower one. The disturbances decrease in magnitude when the upper layer increases in thickness in comparison with the lower one.

Changes in the upper fluid mass flow rate destabilize the flow for wave numbers in a range between 10 and 100, although for larger values of the wavenumber k (i.e. $100 < k < 1000$) the decrease in the mass flow rate Q_2 has no effect for the stability of the system. Moreover, the flow becomes stable when the viscosity of the upper fluid layer increases, thus the more viscous fluid slows down the growth of the disturbance and the presence of surface tension stabilizes the flow (figure 3.13(b)).

We investigate the influence of the Grashof number on the stability of the system for different values of the Reynolds and Weber numbers. Hence, it is shown that the value of the critical Grashof number (i.e. the value of the temperature gradient from which the instability evolves) grows with the wave number k (figure 3.14(a)). Moreover, for large values of the wave number, the influence of the upper fluid mass flow rate decrease substantially and inertia and surface tension stabilize the flow, results presented above. On figure 3.14(b) is shown the critical Grashof number at a small Reynolds number (i.e. $Re = 3305$) whereas only the temperature is responsible for the development of the instability.

Following the same procedure as in the long wave case, we make an estimation of how much an initial perturbation, (fixed wavenumber and amplitude), will grow during the entire process taking into account the linear evolution of the horizontal temperature gradient and the viscosities ratio. In the figure 3.15, it is shown that the perturbation drops at the beginning of the process, and this effect is larger whereas the non-dimensional

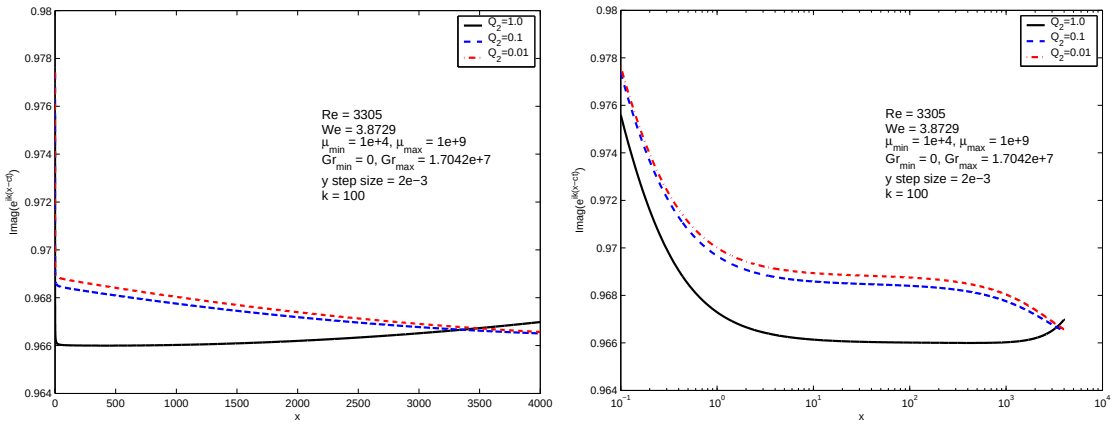

Figure 3.14: The growth rate with respect to the bath length for different values of the mass flow rate.

upper fluid mass flow rate has value one; at this point the viscosities ratio is $\mu = 10^4$ and fluids experience a large horizontal temperature gradient (i.e. $Gr = 1.7 \cdot 10^7$). Further, the amplitude of the perturbation remains at the same level with slightly changes which depend on the mass flow rate (i.e. for $Q_2 = 1.0$ increases its value from 0.966 to 0.968, whereas for $Q_2 = 0.1, 0.01$ decreases its value from 0.968 to 0.966). From the right figure (the logarythmic plot of the growth rate) we can see that the initial drop of the perturbation amplitude take place only in a very small neighbourhood near inlet. The result of the estimation is that, as in the long wave limit, that the initial perturbation is conserved throughout the process.

3.4.2 First order thermal effects

Further, it is interesting to investigate the case when the temperature appears in the leading order system of motion, due to its importance for the real process from the industrial point of view. Hence, we consider the term Gr/Re of the order k^2 to emphasize the magnitude of the thermal effects over the development of short waves and, also, We of the order k looking to reduce the stability effects induced by the surface tension.

Similarly, we use the expansions (3.101)-(3.104) into the system defined by equations (3.57)-(3.67) and collecting only the leading order terms, we obtain the *leading order* system of motion:

$$\phi_0^{1(iv)} - 2\phi_0^{1''} + \phi_0^1 = 0, \quad \phi_0^{2(iv)} - 2\phi_0^{2''} + \phi_0^2 = 0 \tag{3.81}$$

$$\frac{\partial^2 \tilde{\theta}_0^1}{\partial z^2} - \tilde{\theta}_0^1 + iRePr\phi_0^1 \frac{\partial \Theta_1}{\partial z} = 0, \quad \frac{\partial^2 \tilde{\theta}_0^2}{\partial z^2} - \tilde{\theta}_0^2 + i\phi_0^2 \frac{RePr}{\alpha} \frac{\partial \Theta_2}{\partial z} = 0 \tag{3.82}$$

coupled with the follwoing interface conditions ($z = 0$):

$$\phi_0^1 = \phi_0^2, \quad \phi_0^{1'} + \tilde{h}_0 \frac{\partial U_1}{\partial z} = \phi_0^{2'} + \tilde{h}_0 \frac{\partial U_2}{\partial z}$$

$$\mu(\phi_0^{2''}+\phi_0^2)=\phi_0^{1''}+\phi_0^1,\quad \phi_0^1=\tilde{h}_0\,(c-U_1)$$
$$\phi_0^{1'''}-\mu\phi_0^{2'''}-3(\phi_0^{1'}-\mu\phi_0^{2'})=0$$
$$\tilde{\theta}_0^1=\tilde{\theta}_0^2,\quad \kappa\left(i\tilde{h_0}\frac{\partial\Theta_2}{\partial x}-\frac{\partial\tilde{\theta}_0^2}{\partial z}\right)=i\tilde{h_0}\frac{\partial\Theta_1}{\partial x}-\frac{\partial\tilde{\theta}_0^1}{\partial z} \tag{3.83}$$

The leading order system is an ODE system that can be solved analytically and its solution, the eigenvalue c_0, has the following form:

$$c_0=C_{15} \tag{3.84}$$

The leading order eigenvalue c_0 is real, positive and, hence, represents the wave speed of the disturbance which is similar with the wave speed obtained for no-thermal leading order effects case. Thus, the wave speed of the perturbation has a non-dimensional value of one which corresponds to the dimensional value of the upper fluid layer speed. Also, all the effects presented in the last section remain valid in this case.

We collect the first order terms and construct the *first order* system of motion stated below:

$$\phi_1^{1(iv)}-2\phi_1^{1''}+\phi_1^1-i\frac{Gr}{Re}\tilde{\theta}_0^1-iRe(U_1-c_0)(\phi_0^{1''}-\phi_0^1)+iRe\phi_1^1\frac{\partial^2U_1}{\partial z^2}=0$$
$$\phi_1^{2(iv)}-2\phi_1^{2''}+\phi_1^2-i\frac{\rho\beta Gr}{\mu Re}\tilde{\theta}_0^2-i\frac{\rho}{\mu}Re(U_2-c_0)(\phi_0^{2''}-\phi_0^2)+iRe\frac{\rho}{\mu}\phi_1^2\frac{\partial^2U_2}{\partial z^2}=0 \tag{3.85}$$
$$i\tilde{\theta}_0^1(U_1-c_0)-i\phi_0^1\frac{\partial\Theta_1}{\partial z}+\phi_1^1\frac{\partial\Theta_1}{\partial x}=\frac{1}{RePr}\left(\frac{\partial^2\tilde{\theta}_1^1}{\partial z^2}-\tilde{\theta}_1^1\right)$$
$$i\tilde{\theta}_0^2(U_2-c_0)-i\phi_0^2\frac{\partial\Theta_2}{\partial z}+i\phi_1^2\frac{\partial\Theta_2}{\partial z}=\frac{\alpha}{RePr}\left(\frac{\partial^2\tilde{\theta}_1^2}{\partial z^2}-\tilde{\theta}_1^2\right) \tag{3.86}$$

together with the following interface conditions ($z=0$):

$$\phi_1^1=\phi_1^2,\quad \phi_1^{1'}+\tilde{h}_1\frac{\partial U_1}{\partial z}=\phi_1^{2'}+\tilde{h}_1\frac{\partial U_2}{\partial z}$$
$$\mu(\phi_1^{2''}+\phi_1^2)=\phi_1^{1''}+\phi_1^1,\qquad \phi_1^1=\tilde{h}_0c_1+\tilde{h}_1\,(c_0-U_1)$$
$$\phi_1^{1'''}-\mu\phi_1^{2'''}-3(\phi_1^{1'}-\mu\phi_1^{2'})-iRe\left[(U_1-c_0)\left(\phi_0^{1'}-\rho\phi_0^{2'}\right)+\phi_0^1\frac{\partial U_1}{\partial z}\left(\frac{\rho}{\mu}-1\right)\right]=i\frac{Re}{We}\tilde{h}_0$$
$$\tilde{\theta}_1^1=\tilde{\theta}_1^2,\quad \kappa\left(i\tilde{h_1}\frac{\partial\Theta_2}{\partial x}-\frac{\partial\tilde{\theta}_1^2}{\partial z}\right)=i\tilde{h_1}\frac{\partial\Theta_1}{\partial x}-\frac{\partial\tilde{\theta}_1^1}{\partial z}. \tag{3.87}$$

The first order system is an ODE system that can be solved analytically and its solution, the eigenvalue c_1, is presented in the appendix D, due to its complexity and, also, represents the growth rate of the perturbance. As in the first case presented, the short waves

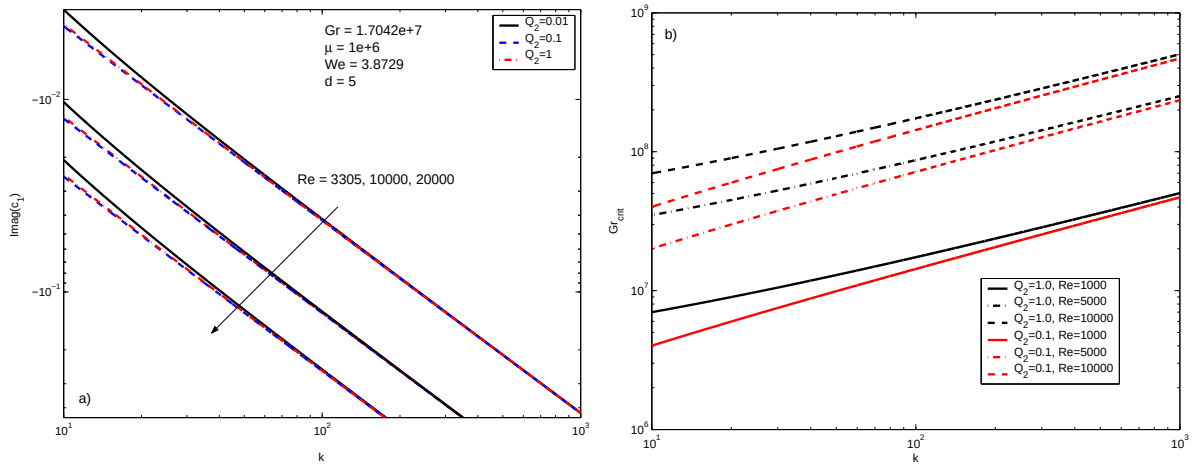

Figure 3.15: a) The growth rate and b) The critical Grashof number with respect to the wave number for different values of the mass flow rate at various values for the Reynolds number.

are stable and the inertia stabilizes the flow (figure 3.15(a)), although the magnitude of the growth rate is slightly smaller than in the no-thermal case. In the figure 3.15(b) we plotted the critical Grashof number with respect to the wave number for different values of the inertia and it is shown that the critical value is slightly smaller than in the no-thermal case, although the same profile can be observed. Moreover, the remark that inertia stabilizes the flow is once more validated.

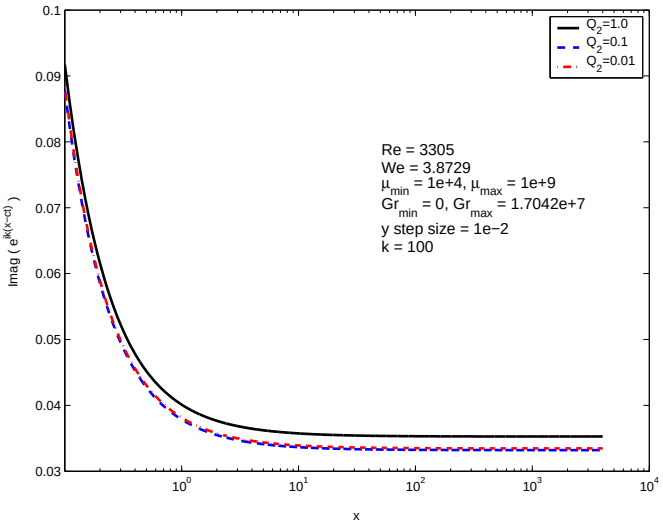

Figure 3.16: The growth rate with respect to the bath length for different values of the mass flow rate.

Further, as in the no-thermal case, we make the same estimation of how much an initial perturbation will grow during the entire process. In the figure 3.17, it is shown that the perturbation is damped throughout the process, the drop taking place at the beginning

of the process, near the inlet. This behaviour is different from the one observed in the non-thermal case, thus our conclusion is that the thermal effects stabilize the flow by damping the initial perturbation.

3.4.3 Discussions of the scaling parameter

As it is shown in section 3.4, in order to focus on the development of the short waves at the interface, we scale the z direction with respect to a small parameter ϵ:

$$z = \epsilon \tilde{z}. \tag{3.88}$$

The scaling parameter is related, further, to the wave number k, due to the fact in the short wave limit the wave number tends to infinity. In this section, we consider the dependence of the small parameter, ϵ, to the wave number, k, in a more general form as follows:

$$\epsilon = \frac{1}{k^n}, \quad n > 0. \tag{3.89}$$

Hence, we perform the linearization using the technique presented in section 3.4, and, thus, we obtain the following system of motion:

$$k^{4n}\phi_1^{(iv)} - 2k^{2n+2}\phi_1^{''} + k^4\phi_1 = iRe(U_1 - c)(k^{2n+1}\phi_1^{''} - k^3\phi_1) - iRek^{2n+1}\phi_1\frac{\partial^2 U_1}{\partial z^2} + ik\frac{Gr}{Re}\tilde{\theta}_1 \tag{3.90}$$

$$k^{4n}\phi_2^{(iv)} - 2k^{2n+2}\phi_2^{''} + k^4\phi_2 = iRe\frac{\rho}{\mu}(U_2 - c)(k^{2n+1}\phi_2^{''} - k^3\phi_2) - iRe\frac{\rho}{\mu}k^{2n+1}\phi_2\frac{\partial^2 U_2}{\partial z^2} + ik\frac{Gr\rho\beta}{\mu Re}\tilde{\theta}_2 \tag{3.91}$$

$$ik\tilde{\theta}_1(U_1 - c) + k^n\phi_1^{'}\frac{\partial \Theta_1}{\partial x} - ik^{n+1}\phi_1\frac{\partial \Theta_1}{\partial z} = \frac{1}{RePr}\left(k^{2n}\frac{\partial^2\tilde{\theta}_1}{\partial z^2} - k^2\tilde{\theta}_1\right) \tag{3.92}$$

$$ik\tilde{\theta}_2(U_2 - c) + k^n\phi_2^{'}\frac{\partial \Theta_2}{\partial x} - ik^{n+1}\phi_2\frac{\partial \Theta_2}{\partial z} = \frac{\alpha}{RePr}\left(k^{2n}\frac{\partial^2\tilde{\theta}_2}{\partial z^2} - k^2\tilde{\theta}_2\right) \tag{3.93}$$

The system is coupled with the following interface ($\tilde{z} = 0$) and boundary conditions:

Kinematical condition

$$\phi_1 = \phi_2 \tag{3.94}$$

Tangential stress

$$\mu\left(k^{2n}\phi_2^{''} + k^2\phi_2\right) = k^{2n}\phi_1^{''} + k^2\phi_1 \tag{3.95}$$

Normal stress

$$k^{3n}(\phi_1^{'''} - \mu\phi_2^{'''}) - 3k^{n+2}(\phi_1^{'} - \mu\phi_2^{'}) +$$

$$+iRe\left[(U_1-c)\left(k^{n+1}\phi_1^{'}-\rho k^{n+1}\phi_2^{'}\right)+k^{n+1}\phi_1 U_1^{'}\left(\frac{\rho}{\mu}-1\right)\right]=ik^3\frac{Re}{We}\tilde{h} \tag{3.96}$$

Velocity condition

$$\phi_1^{'}+\tilde{h}\frac{\partial U_1}{\partial z}=\phi_2^{'}+\tilde{h}\frac{\partial U_2}{\partial z} \tag{3.97}$$

Heat transfer conditions

$$\kappa\left(ik\tilde{h}\frac{\partial\Theta_2}{\partial x}-k^n\frac{\partial\tilde{\theta}_2}{\partial z}\right)=ik\tilde{h}\frac{\partial\Theta_1}{\partial x}-k^n\frac{\partial\tilde{\theta}_1}{\partial z},\qquad \tilde{\theta}_1=\tilde{\theta}_2 \tag{3.98}$$

Further, for clarity, we drop the "tilde" symbol for the z direction. After scaling, the boundary conditions will change to plus and minus infinity.

$$\phi_1(-\infty)=\phi_1^{'}(-\infty)=\tilde{\theta}_1(-\infty)=0, \tag{3.99}$$

$$\phi_2(\infty)=\phi_2^{'}(\infty)=\tilde{\theta}_2(\infty)=0, \tag{3.100}$$

Using the asymptotic expansions according with k, the wave number, we look for the solutions of the form:

$$\phi^j=\phi_0^j+\frac{1}{k^n}\phi_1^j+\frac{1}{k^{2n}}\phi_2^j+... \tag{3.101}$$

$$\tilde{\theta}^j=\tilde{\theta}_0^j+\frac{1}{k^n}\tilde{\theta}_1^j+\frac{1}{k^{2n}}\tilde{\theta}_2^j+... \tag{3.102}$$

$$c=c_0+\frac{1}{k^n}c_1+\frac{1}{k^{2n}}c_2+... \tag{3.103}$$

$$\tilde{h}=\tilde{h}_0+\frac{1}{k^n}\tilde{h}_1+\frac{1}{k^{2n}}\tilde{h}_2+... \tag{3.104}$$

with $1/k^n\to 0$ and the dimensionless numbers fixed. In the following computations, we drop the "tilde" symbol for the z direction for simplicity.

Further, we analyze three different cases: ($n=1,\ n<1,\ n>1$). The case for the parameter $n=1$ was discussed in the sections 3.4.1 and 3.4.2, thus we remain only with two cases presented as follows:

Case A: $n<1$

Following the same analysis as one presented above, in this case, in the Orr-Sommerfeld equation written for each fluid, the leading order term is ϕ_0^j, with $j=\overline{1,2}$. Thus, we have:

$$\phi_0^j=0,\quad j=\overline{1,2} \tag{3.105}$$

Moreover, taking into consideration the continuity of the velocity across the interface,(i.e. relation (3.97)), and due to the fact that the first derivatives of the basic flow velocities of each fluid with respect to the z direction are not equal at the interface (3.4), we have:

$$\tilde{h}_0=0 \tag{3.106}$$

The same result, we can obtain from the normal stress condition at the interface, whereas the leading order term, in this case, is $iRe/We\tilde{h}_0$. Thus, we have also $\tilde{h}_0 = 0$.

From the kinematical condition,

$$\phi_0^j = \tilde{h}_0(c_0 - U_1(0)) \tag{3.107}$$

we obtain that the leading order eigenvalue c_0 is undetermined.

Case B: $n > 1$

In this case, for each fluid, in the Orr-Sommerfeld equation, the leading order relation is ${\phi_0^j}^{(iv)}$, with $j = \overline{1,2}$. Thus, we have:

$$\phi_0^j = a_3^j z^3 + a_2^j z^2 + a_1^j z + a_0^j, \quad j = \overline{1,2}. \tag{3.108}$$

Hence, the leading order stream functions have a polynomial form and, in this case, do not satisfy the boundary conditions (3.99) and (3.100). Nevertheless, the boundary conditions are always satisfied by the trivial solution $\phi_0^j = 0, \quad j = \overline{1,2}$. Similarly, using velocity and kinematical condition we obtain that $\tilde{h}_0 = 0$ and the leading order eigenvalue c_0 is undetermined.

Chapter 4

Numerical method

In the last two chapters, we presented two analytical limits which characterize the stability of two different kinds of waves: long ($k \to 0$) and short ($k \to \infty$). Nevertheless, the wave spectrum, observed on the finite products, is much larger and covers all the wave number spectrum. Our analytical analysis cannot describe these "intermediate" waves, thus we solve our system of motion numerically using spectral methods.

4.1 Spectral methods in fluid dynamics

Since the pioneering work of Orszag [29], spectral methods have been intensively studied and considered to be extremely efficient for hydrodynamical stability problems due to their increased accuracy. It is shown by Orszag, and later by Schmid and Henningson [39], that a spectrum of Chebyshev polynomials is the most suitable for solving eigenvalue problems in a bounded domain, due to the fact that the approximation errors decrease more rapidly than in the finite difference case.

In order to solve an eigenvalue problem coupled with boundary conditions, several spectral methods have been applied by many authors for different kind of reasons, all in connection with the Chebyshev polynomials: Chebyshev-Tau [30, 31], Galerkin-Tau [32, 33], collocation method [34]. Further, we present some generalities about the Chebyshev polynomials, the definition of the derivative matrice and the construction of our numerical method using a collocation approach.

4.1.1 Chebyshev polynomials

Spectral methods, constructed with Chebyshev polynomials basis, are widely used for solving fluid dynamics problems. The definition of the n^{th} order polynomial of the first kind is

$$T_n(\cos\theta) = \cos n\theta, \quad \cos\theta \in [-1, 1] \tag{4.1}$$

or

$$T_n(x) = \cos(n \cos^{-1}(x)), \quad n \in \mathbf{N},\ x \in [-1, 1] \tag{4.2}$$

Many authors give also other definitions which can be found in their works [47, 39]. Further, we state below some of the Chebyshev polynomial properties which are used for computations:

$$T_{n+2}(x) = 2xT_{n+1}(x) - T_n(x),$$
$$T_n(x)T_m(x) = \frac{1}{2}\left(T_{n+m} + T_{|n-m|}\right)$$
$$T_n(\pm) = (\pm 1)^n, \quad \int_{-1}^{1} T_n(x)T_m(x)\omega(x)dx = \frac{\pi}{2}c_n\delta_{n,m} \quad n, m \in \mathbf{N},\ x \in [-1, 1] \tag{4.3}$$

where $\delta_{n,m}$ is the symbol of Kronecker, $\omega(x) = 1/\sqrt{1-x^2}$ is the Chebyshev weight and $c_j = 2$, if $j = 0$ or $c_j = 1$, if $j > 0$. The first relation states the definition of Chebyshev basis functions through recurrence, whereas the last formula ensures the orthogonality of polynomials spectrum.

Therefore, we can approximate the solution of our differential problem by a Chebyshev expansion:

$$\phi(x) = \sum_{n=0}^{N} a_n T_n(x) \tag{4.4}$$

4.1.2 Gauss-Lobatto points and Chebyshev differentiation matrice

In order to discretize partial differential equations, we need to express the derivatives of solutions in terms of Chebyshev polynomials. The following recurrence formulas express the relation between polynomials and their derivatives [29, 39, 47]:

$$T_0^{(k)}(x) = 0, \quad T_1^{(k)}(x) = T_0^{(k-1)}(x), \quad T_2^{(k)}(x) = 4T_1^{(k-1)}(x),$$
$$T_n^{(k)}(x) = 2nT_{n-1}^{(k-1)}(x) + \frac{n}{n-1}T_{n-1}^{k}(x), \quad n > 2 \tag{4.5}$$

where $k > 0$ denotes the differentiation order.

The accuracy of the Chebyshev methods increases substantially when the interpolation is made in unevenly spaced points (non-uniform grid points). Various sets of points are used for the discretization [47, 48], although we use the simplest physical points called *collocation* or *Gauss-Lobatto* points. These are the standard set of collocation points used for interpolating Chebyshev basis functions:

$$x_j = \cos\frac{2\pi j}{N}, j = \overline{0, N}. \tag{4.6}$$

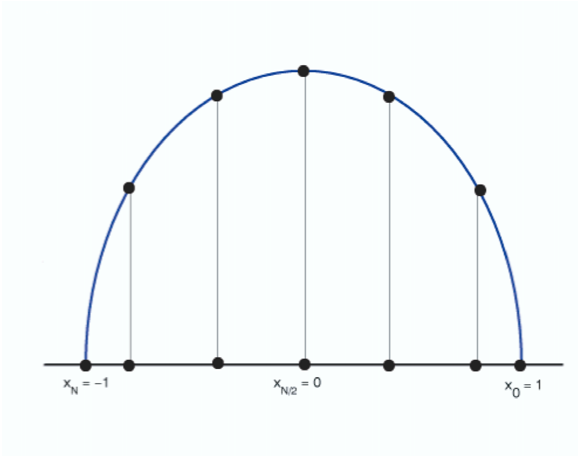

Figure 4.1: The projections of the unit circle onto the diameter axis

The Gauss-Lobatto points represent the projection onto the diameter axis of equally spaced points from the unit circle (figure 4.1) [48]. An important remark is that the domain $[-1, 1]$ is discretized from the end to the beginning (i.e. $x_0 = 1,\ x_N = -1$).

Using the above definitions, now we can introduce the differentiation matrice, $(D_k)_{ij}$ with $i, j = \overline{0, N}$, which allows us to express each solution of a partial differential equation as a Chebyshev basis functions expansion [39, 47, 48]:

$$(D_k)_{00} = \frac{2N^2+1}{6}, \quad (D_k)_{NN} = -\frac{2N^2+1}{6},$$
$$(D_k)_{jj} = -\frac{x_j}{2(1-x_j^2)}, \quad j = \overline{1, N-1},$$
$$(D_k)_{ij} = \frac{c_i}{c_j}\frac{(-1)^{i+j}}{(x_i - x_j)}, \quad i \neq j, \quad i, j = \overline{0, N}. \tag{4.7}$$

where $k > 0$ is the order of differentiation.

4.2 Collocation method

We apply the collocation method onto the system (3.34)-(3.42) in order to solve a general eigenvalue problem. Moreover, we choose to apply this method due to the fact that it is more convenient to implement our basic functions which have complicated forms. From technical point of view, we have to solve a general eigenvalue problem (Orr-Sommerfeld and energy equations) for each fluid coupled with interface and boundary conditions.

In order to apply the Chebysev discretization, we transform our given domains to the domain $[1, -1]$. The transformation function is stated below in a general form (transform

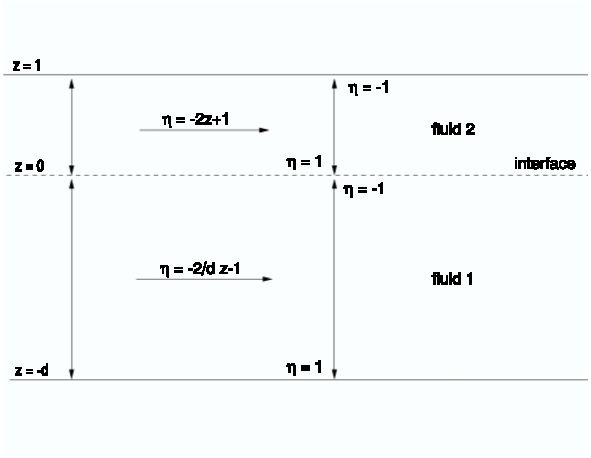

Figure 4.2: The projections of the unit circle onto the diameter axis

any domain $[a_d, b_d]$ into $[1, -1]$):

$$\eta = \frac{2z}{a_d - b_d} - \frac{a_d + b_d}{a_d - b_d} \tag{4.8}$$

Hence, any solution f, of our partial differential system, is computed as follows:

$$\frac{df}{dz}(z) = \frac{df}{d\eta} \cdot \frac{d\eta}{dz} \tag{4.9}$$

where

$$\frac{d\eta}{dz} = \frac{2}{a_d - b_d}. \tag{4.10}$$

Taking into account these remarks, we obtain, for our problem, the following transformation functions:

$$z \in [-d, 0] : \ \eta = -\frac{2}{d}z - 1, \qquad z \in [0, 1] : \ \eta = -2z + 1 \tag{4.11}$$

Thus, we approximate our solutions by Chebyshev expansions:

$$\phi_1(\eta) = \sum_{n=0}^{N} \tilde{a}_n T_n(\eta), \quad \phi_2(\eta) = \sum_{n=0}^{N} \tilde{b}_n T_n(\eta),$$

$$\tilde{\theta}_1(\eta) = \sum_{n=0}^{N} \tilde{c}_n T_n(\eta), \quad \tilde{\theta}_2(\eta) = \sum_{n=0}^{N} \tilde{d}_n T_n(\eta) \tag{4.12}$$

These expansions define $N+1$ unknowns for each equation and an additional one for the pertubation of the interface amplitude, $\tilde{h}$. The system contains the eigenvalue c which transform our intitial problem into a general eigenvalue problem of the form:

$$[A]\,\xi = c\,[B]\,\xi \tag{4.13}$$

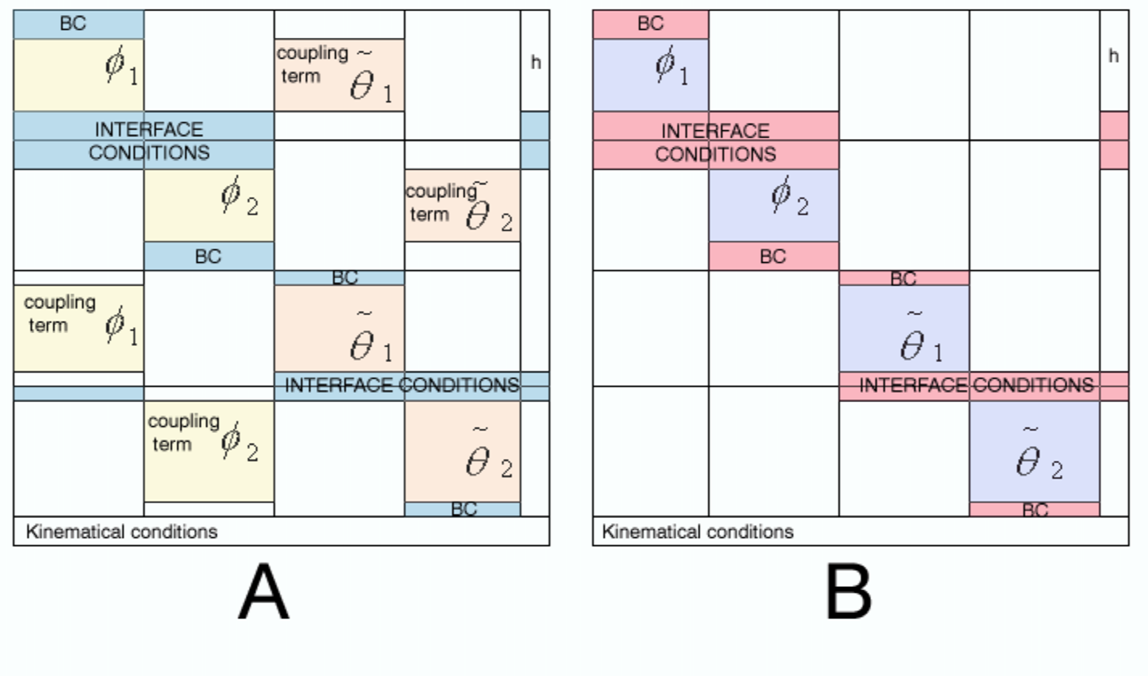

Figure 4.3: The distribution of the rows in the matrices A and B

where $\xi = \left[\tilde{a}_0, \tilde{a}_1, ..., \tilde{a}_N, \tilde{b}_0, \tilde{b}_1, ..., \tilde{b}_N, \tilde{c}_0, \tilde{c}_1, ..., \tilde{c}_N, \tilde{d}_0, \tilde{d}_1, ..., \tilde{d}_N, \tilde{h}\right]^T$ is the solutions vector. Twelve rows of matrices A and B contain the interface and boundary condition, whereas the last row is used with the kinematical condition which makes a connection between the stream function, the basic flow velocity, the perturbation of the interface amplitude and the eigenvalue (figure 4.3).

In our computation, we used a large number of modes for each equation (i.e. $N = 200$) in order to ensure a good accuracy although the computation time increased exponentially (0.64 sec. for solving one fluid without temperature in comparison with 27.3 sec. for the complete system). The code for solving our problem is written in MATLAB and for the general eigenvalue computation we use the EISPACK library routines which use the QZ algorithm [38].

One of the problem which appears in the general eigenvalue systems, derived from the stability related problems, is that the boundary conditions, for the system of the perturbations, are always equal with zero. Thus, the boundary conditions give zero entries for the matrice B, making it singular. Hence, the computation provides a number of wrong eigenvalues, called "spurious", which are very large in magnitude, do not converge when the number of modes is increased and do not correspond to the eigenvalues of the system [33, 47, 48]. Various authors gave different methods to solve this problem, although the most often used technique is to map the infinite eigenvalues to a specified point in the complex plane, allowing them to be distinguished easily from any finite eigenvalues [35, 36, 37].

We compare classical results from the literature with parts from our code, in order to

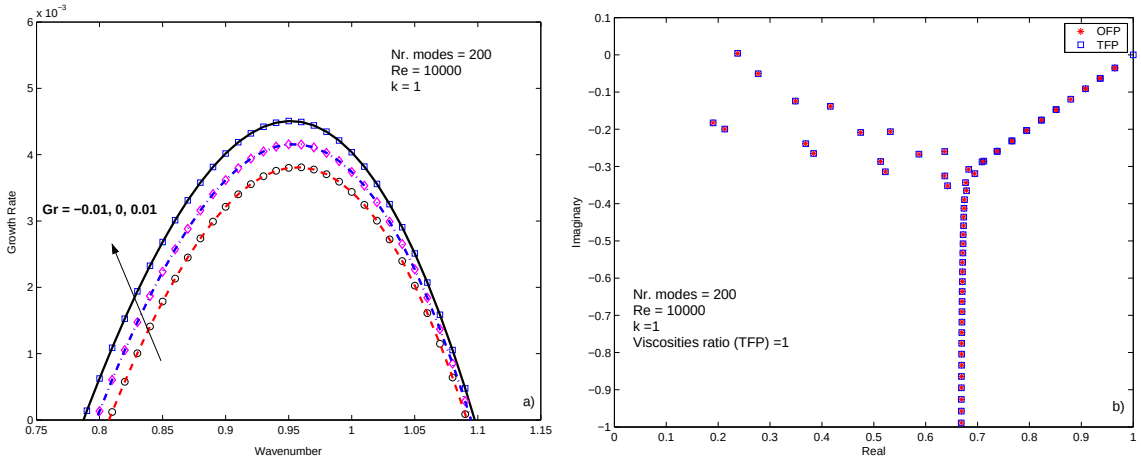

Figure 4.4: The comparison of the numerical method for: a) one Poiseuille fluid flow in a pipe coupled with temperature; b) one Poiseuille fluid flow (OFP) and two superposed Poiseuille fluids flow in a pipe (TFP).

validate the results. Hence, we construct the solution to the Poiseuille flow of a single fluid in a pipe, the same problem coupled with a vertical linear gradient of temperature and finally two superposed Poiseuille fluids flowing into a pipe. Thus, we investigate the accuracy of the collocation method by checking the following parts of the problem: one fluid flow coupled with the temperature (i.e. appears an additional equation for the temperature); two spuerposed fluids with a free interface between them (i.e. two equations, one for each fluid, are solved in two different domains, and are coupled through the interface conditions. In the figure 4.4(a) it is presented the growth rate with respect to the wavenumber for different values of the Grashof number, picture which is in a agreement with the results presented by Motsa [37]. For the two superposed fluids problem, we assume that the densities are equal, the position of the interface is in the middle of the channel and both fluids have Poiseuille velocity profiles. Thus, when the viscosities ratio tends to one the configuration becomes similar with the one fluid problem. In the figure 4.4(b) we have shown a comparison between the eigenvalues spectrum in both cases, and the result is in perfect agreement with the literature [29, 32, 35].

4.2.1 Long wave limit

We apply the collocation method on our system of motion. On figure 4.5 is shown a comparison between the analytical computations of the leading and first order eigenvalues, c_0 and c_1, and the numerical computations of real (figure 4.5(a)) and imaginary part (figure 4.5(b)) of the eigenvalue c near the interface. We recall that in the long wave limit the eigenvalue c is given by the following expansion: $c = c_0 + kc_1 + ...$, where c_0 is real and c_1 is imaginary.

Our main numerical result is shown in the figure 4.6, where we plotted the perturbation of the interface amplitude with respect to the wave number, k, for different values of

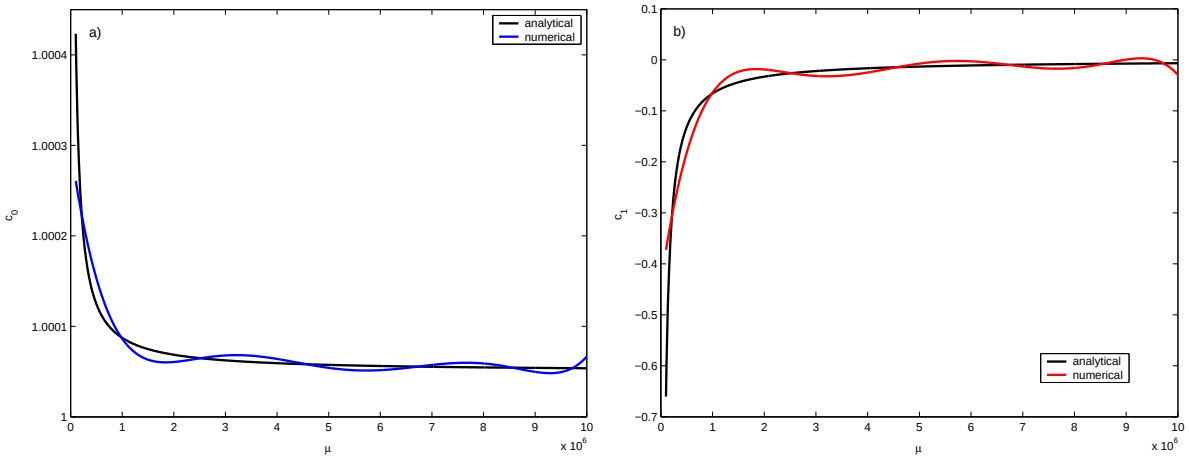

Figure 4.5: The comparison between the numerical and the analytical approach for: a) the wave speed, eigenvalue c_0; b) the eigenvalue c_1.

the lower fluid mass flow rate, Q_2. Hence, the absolute range of the perturbation is between $5 \cdot 10^{-12}$ and $5 \cdot 10^{-11}$, thus practically zero. This result is in agreement with the observations made on the float glass finite products which are perfectly flat from the long waves point of view.

4.2.2 Short wave limit

In the short wave limit, we obtain numerical results only for the no-thermal leading order effects case (section 3.4.1), due to the fact that in the first order thermal effects case the matrices become singular and stiff, fact which influence the accuracy of the method applied. Hence, in the figure 4.7 is plotted the perturbation of the interface amplitude with respect to the wave number, k, in range from 5 to 100, for different values of the lower fluid mass flow rate, $Q_2 = 1.0, 0.1, 0.001$. The absolute range of the perturbation is between 10^{-7} and $2.5 \cdot 10^{-6}$, whereas the largest amplitude is achieve for small wave numbers (i.e. k between 10 and 20) and the smallest amplitude is observed when k approaches value 100. This result is in perfect agreement with the observations made on the float glass finite products. Hence, the short wave patterns observed on the finite products have a dimensional wave length between $5 \cdot 10^{-4}$ and 10^{-2} meters and an amplitude between 10^{-9} and 10^{-7} meters. We recall that, in our case, the characteristic length is the height of the upper fluid layer, $d_2 = 0.01$ meters, thus the short waves, observed on the finite products, have a non-dimensional amplitude between 10^{-7} and 10^{-5} and, also, a non-dimensional wave number between 5 and 100. The results presented in the figure 4.7 cover the same ranges for wave number and amplitude.

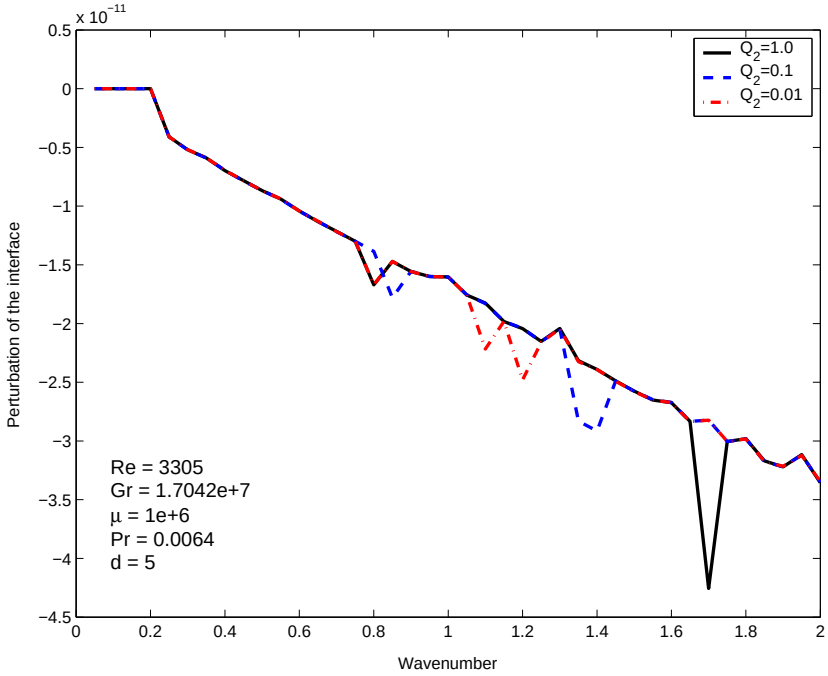

Figure 4.6: The interface amplitude perturbation with respect to the wave number for different values of the mass flow rate (long wave limit).

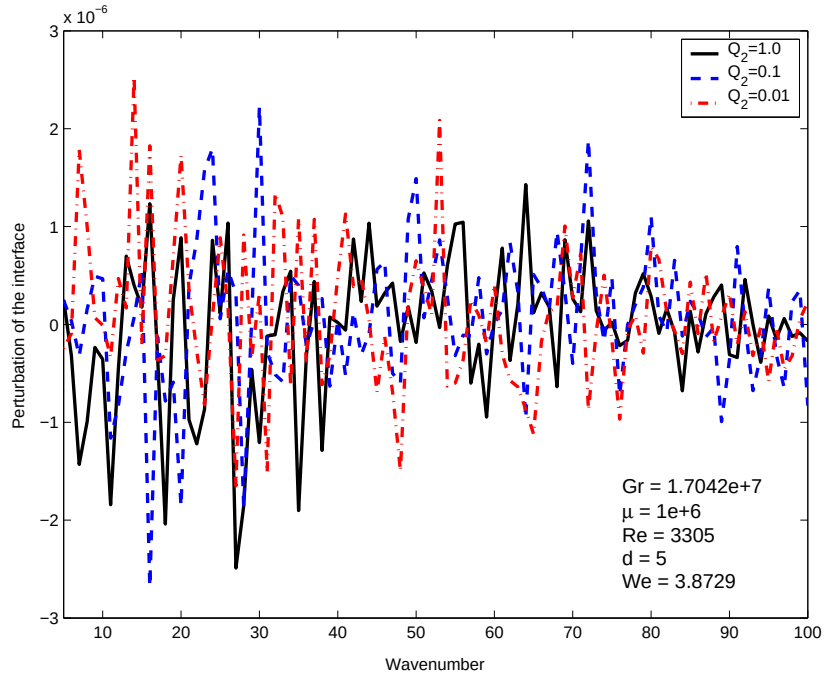

Figure 4.7: The amplitude perturbation with respect to the wave number for different values of the mass flow rate (short wave limit).

Chapter 5

Temperature dependent viscosity

In this chapter, we investigate the linear stability of two superposed fluids with temperature dependent viscosities. The fluids are confined between two rigid plates, maintained at different constant temperatures. The upper plate is moving with constant velocity, whereas the lower wall is kept fixed. It is known from literature [13, 14, 15], that in the case of one fluid, the heat, which causes viscosity to decrease along the domain, usually destabilizes the flow. We investigate the two dimensional stability problem by considering two different models for the viscosity dependence of each fluid. In the float glass process, temperature influences strongly the viscosity of the both fluids involved. Although, the temperature/viscosity relationships for glass and metal are more complex than one used in the following computations, our intentions is to emphasize the effects of this dependence over the stability of the system.

5.1 General system of motion

The governing equations of our problem respect the model introduced in section 2.1. Although, in the Navier-Stokes equations appear new terms due to the influence of the variable viscosity over the system of motion.

Mass:

$$\nabla \cdot \mathbf{u}_j = 0 \tag{5.1}$$

Momentum:

$$\bar{\rho}_j \left(\frac{\partial \mathbf{u}_j}{\partial \bar{t}} + \mathbf{u}_j \cdot \nabla \mathbf{u}_j \right) = -\nabla \bar{p}_j + \bar{\mu}_j(T_j)\Delta \mathbf{u}_j +$$

$$+\bar{\mu}_j^{'}(T_j)\left[2(\nabla T_j \cdot \nabla)\mathbf{u}_j + \nabla T_j \times (\nabla \times \mathbf{u}_j)\right] - \bar{\rho}_j \mathbf{g} \tag{5.2}$$

Energy:

$$\frac{\partial T_j}{\partial \bar{t}} + (\mathbf{u}_j \cdot \nabla)T_j = \alpha_j \Delta T_j, \quad j = \overline{1,2} \tag{5.3}$$

where $\mathbf{u}_j = (\bar{u}_j, \bar{w}_j)$, $\bar{u}_j$ is the velocity in $\bar{x}$ direction, $\bar{w}_j$ is the velocity in $\bar{z}$ direction, $\mathbf{g} = (0, g)$, g is the acceleration due to the gravity, $\bar{p}_j$ is the pressure, μ_j is the dynamic viscosity, $\bar{\rho}_j$ is the density, α_j is the thermal diffusivity and T_j is the temperature of the fluid for each phase ($j = \overline{1,2}$).

5.1.1 Interface and boundary conditions

The appropriate interface and boundary conditions, which model our problem, are similar with those introduced in section 2.2. The difference consists in the form of the stress tensor, which includes viscosity as a function of temperature.

In the following computations, τ denotes the stress tensor,

$$\bar{\tau} = \begin{bmatrix} -\bar{p} + 2\bar{\mu}(T)\frac{\partial \bar{u}}{\partial \bar{x}} & \bar{\mu}(T)\left(\frac{\partial \bar{u}}{\partial \bar{z}} + \frac{\partial \bar{w}}{\partial \bar{x}}\right) \\ \bar{\mu}(T)\left(\frac{\partial \bar{u}}{\partial \bar{z}} + \frac{\partial \bar{w}}{\partial \bar{x}}\right) & -\bar{p} + 2\bar{\mu}(T)\frac{\partial \bar{w}}{\partial \bar{z}} \end{bmatrix}, \tag{5.4}$$

$\mathbf{n}$, the normal vector pointing from phase 1 into phase 2, $\mathbf{t}$, the tangential vector,

$$\mathbf{n} = \left(\frac{-\bar{h}_{\bar{x}}}{(1+\bar{h}_{\bar{x}}^2)^{1/2}}, \frac{1}{(1+\bar{h}_{\bar{x}}^2)^{1/2}}\right) \tag{5.5}$$

$$\mathbf{t} = \left(\frac{1}{(1+\bar{h}_{\bar{x}}^2)^{1/2}}, \frac{\bar{h}_{\bar{x}}}{(1+\bar{h}_{\bar{x}}^2)^{1/2}}\right) \tag{5.6}$$

κ_j, the thermal conductivity ($j = \overline{1,2}$), σ, the surface tension and κ_S, the mean curvature of the interface, given by:

$$\kappa_S = -\frac{\bar{h}_{\bar{x}\bar{x}}}{(\bar{h}_{\bar{x}}^2 + 1)^{3/2}}. \tag{5.7}$$

The jump of the quantity f across the interface is denoted by $[f] = f_2 - f_1$. Thus, the interface conditions, (i.e. $\bar{z} = \bar{h}(\bar{x}, \bar{t})$), are stated below:

Kinematical condition

$$\bar{w}_j = \frac{\partial \bar{h}}{\partial \bar{t}} + \bar{u}_j \frac{\partial \bar{h}}{\partial \bar{x}}, \quad j = \overline{1,2} \tag{5.8}$$

Dynamical conditions

$$[\mathbf{n} \cdot \bar{\tau} \cdot \mathbf{n}] = \sigma \kappa_S \tag{5.9}$$

$$[\mathbf{t} \cdot \bar{\tau} \cdot \mathbf{n}] = 0 \tag{5.10}$$

Velocity condition (no-slip at the interface)

$$[\mathbf{u} \cdot \mathbf{t}] = 0 \tag{5.11}$$

Heat transfer conditions (fluxes and temperatures are equal at the interface)

$$T_1 = T_2, \quad \kappa_1 \frac{\partial T_1}{\partial \mathbf{n}} = \kappa_2 \frac{\partial T_2}{\partial \mathbf{n}}. \tag{5.12}$$

The velocity and the temperature, for both fluids, satisfy the following boundary conditions:

$$\begin{aligned} \bar{z} = -d_1, \quad \bar{u}_1 = \bar{w}_1 = 0, \quad T_1 = T_c(\bar{x}) \\ \bar{z} = d_2, \quad \bar{u}_2 = U, \quad \bar{w}_2 = 0, \, T_2 = T_h(\bar{x}). \end{aligned}$$

Further, we prescribe the mass flow rate condition for each fluid, in the same form that was introduced by the relation 2.19:

$$\bar{Q}_1 = \rho_1 \int_{-d_1}^{0} \bar{u}_1 d\bar{z}, \quad \bar{Q}_2 = \rho_2 \int_{0}^{d_2} \bar{u}_2 d\bar{z}. \tag{5.13}$$

5.1.2 Non-dimensional system of motion

In our computations, we use the following non-dimensionalizations:

$$\begin{aligned} \bar{p} = \rho_1 U^2 p, \quad \bar{\mu}_j = M\mu_j, \quad \bar{u}_j = U u_j, \quad \bar{w}_j = U w_j \\ \bar{x} = d_2 x, \quad \bar{z} = d_2 z, \quad \bar{t} = \frac{d_2}{U} t, \quad \theta_j = \frac{T_j - T_c}{T_h - T_c}, \quad j = \overline{1,2}. \end{aligned} \tag{5.14}$$

where d_2, ρ_1, U, M denote the height of the upper fluid, the density of the lower liquid, the velocity of the upper plate, and the viscosity of the lower fluid measured at the point $z = -d_1$ with constant temperature $T_1 = T_c$. The superscript "bar" emphasizes the dimensional parameters.

5.2 Basic Flow

The basic flow considered is the steady, fully developed laminar flow of two superposed fluid layers confined between two horizontal parallel plates in the presence of a small vertical gradient of temperature. The flow is generated by the combination of a pressure gradient applied to the upper fluid, the movement of the upper plate (parallel to the pressure gradient) relative to the lower plate, and the buoyancy movement of the lower fluid due to its small kinematic viscosity and high thermal diffusivity. The fluids have temperature dependent viscosities. In order to derive the basic flow profile, we make the following assumptions:

$$\bar{W}_1, \; \bar{W}_2 = 0 \Longrightarrow \bar{U}_j = \bar{U}_j(\bar{z}), \quad j = \overline{1,2} \tag{5.15}$$

$$T_1 = T_1(\bar{z}), \quad T_2 = T_2(\bar{z}), \quad T_c < T_h, \; \textit{constants} \tag{5.16}$$

where $\bar{W}_j, \bar{U}_j, T_j$ denote the basic velocities in x and z directions and the basic temperatures, all expressed for both fluids.

5.2.1 Basic temperature profiles

For the simplicity, we compute first the basic temperature profiles. In the steady state and following the above assumptions, the temperature is influenced by the vertical gradient. Thus, from the energy equation, we keep only the conductive term, which provides a first degree polynomial form for the temperature:

$$\frac{\partial^2 T_1}{\partial \bar{z}^2} = 0 \Longrightarrow T_1 = m_0 + m_1 \bar{z} \tag{5.17}$$

$$\frac{\partial^2 T_2}{\partial \bar{z}^2} = 0 \Longrightarrow T_2 = n_0 + n_1 \bar{z}. \tag{5.18}$$

The system is coupled with the corresponding interface and boundary conditions:

$$\bar{z} = 0: \quad T_1 = T_2, \quad \kappa_1 \frac{\partial T_1}{\partial \bar{z}} = \kappa_2 \frac{\partial T_2}{\partial \bar{z}} \tag{5.19}$$

$$\bar{z} = d_2: \quad T_2 = T_h; \quad \bar{z} = -d_1: \quad T_1 = T_c. \tag{5.20}$$

The dimensional temperature profiles for the steady state are:

$$T_1(\bar{z}) = \frac{d_2\kappa_1 T_c + d_1\kappa_2 T_h + \kappa_2(T_h - T_c)\bar{z}}{d_2\kappa_1 + d_1\kappa_2}, \tag{5.21}$$

$$T_2(\bar{z}) = \frac{d_2\kappa_1 T_c + d_1\kappa_2 T_h + \kappa_1(T_h - T_c)\bar{z}}{d_2\kappa_1 + d_1\kappa_2} \tag{5.22}$$

After applying the non-dimensional parameters introduced in section 5.1.2, we obtain the non-dimensional linear profiles for the basic temperature:

$$\Theta_1 = \frac{T_1 - T_c}{T_h - T_c}, \quad \Theta_2 = \frac{T_2 - T_c}{T_h - T_c} \Longrightarrow \tag{5.23}$$

$$\Theta_1 = \frac{\kappa_2(d_1 + \bar{z})}{d_2\kappa_1 + d_1\kappa_2}, \quad \Theta_2 = \frac{d_1\kappa_2 + \kappa_1\bar{z}}{d_2\kappa_1 + d_1\kappa_2} \tag{5.24}$$

Further, we use some notations which appear also in the previous chapters:

$$d = \frac{d_1}{d_2}, \quad \kappa = \frac{\kappa_2}{\kappa_1}, \quad z = \frac{\tilde{z}}{d_2} \Longrightarrow \Theta_1 = \frac{\kappa(d + z)}{1 + d\kappa}, \quad \Theta_2 = \frac{\kappa d + z}{1 + d\kappa} \tag{5.25}$$

and for the simplicity, we write the basic temperature profiles in the following form (figure 5.1):

$$\Theta_1(z) = a_0 + a_1 z, \quad \Theta_2(z) = b_0 + b_1 z \tag{5.26}$$

where

$$a_0 = \frac{kd}{1 + dk}, \quad a_1 = \frac{k}{1 + dk}, \tag{5.27}$$

$$b_0 = \frac{kd}{1 + dk}, \quad b_1 = \frac{1}{1 + dk}. \tag{5.28}$$

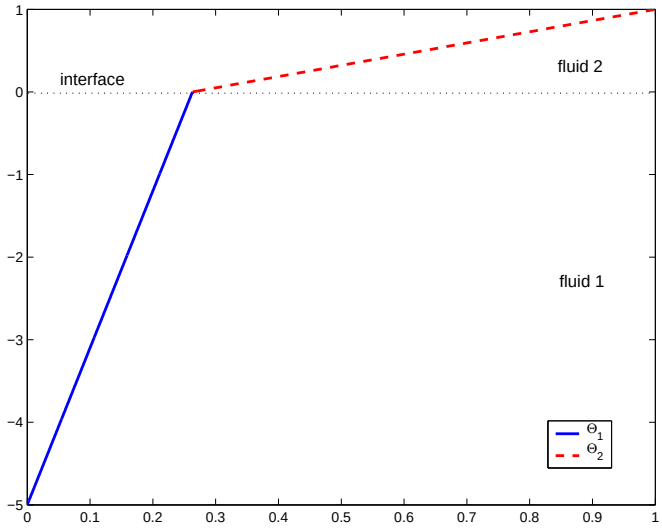

Figure 5.1: The basic temperature profiles

5.2.2 System of equations for the basic velocity profiles

In the steady state, velocities depend of the temperature, due to the viscosity, and the Boussinesq approximation. The dimensional system of equations, which describes the motion in this case, is the following:

$$\frac{\partial \bar{p}_1}{\partial \bar{x}} = \frac{\partial}{\partial \bar{z}}\left(\bar{\mu}_1(T_1)\frac{\partial \bar{U}_1}{\partial \bar{z}}\right), \quad \frac{\partial \bar{p}_1}{\partial \bar{z}} = \bar{\rho}_1 g \beta_1 (T_1 - T_c) \tag{5.29}$$

$$\frac{\partial \bar{p}_2}{\partial \bar{x}} = \frac{\partial}{\partial \bar{z}}\left(\bar{\mu}_2(T_2)\frac{\partial \bar{U}_2}{\partial \bar{z}}\right), \quad \frac{\partial \bar{p}_2}{\partial \bar{z}} = \bar{\rho}_2 g \beta_2 (T_2 - T_c). \tag{5.30}$$

Interface conditions describe the continuity of shear stress and the velocities across the interface. The appropriate boundary conditions represent the no-slip at the lower plate and the movement of the upper plate. Thus, we have:

$$\bar{U}_2(d_2) = U, \quad \bar{U}_1(-d_1) = 0 \tag{5.31}$$

$$\bar{z} = 0: \quad \bar{\mu}_1(T_1)\frac{\partial \bar{U}_1}{\partial \bar{z}} = \bar{\mu}_2(T_2)\frac{\partial \bar{U}_2}{\partial \bar{z}}, \quad \bar{U}_1 = \bar{U}_2. \tag{5.32}$$

Moreover, we non-dimensionalize the above system of equations, by using the parameters introduced in section 5.1.2, and we obtain the non-dimensional system of motion, stated below:

$$\frac{\partial \mu_1}{\partial z}(z)\frac{\partial U_1}{\partial z}(z) + \mu_1(z)\frac{\partial^2 U_1}{\partial z^2}(z) = C_1 \tag{5.33}$$

$$\frac{\partial \mu_2}{\partial z}(z)\frac{\partial U_2}{\partial z}(z) + \mu_2(z)\frac{\partial^2 U_2}{\partial z^2}(z) = C_2. \tag{5.34}$$

The above equations are coupled with the following boundary and interface conditions:

$$U_2(1) = 1, \quad U_1(-d) = 0 \tag{5.35}$$

$$z = 0: \quad \mu_1(0)\frac{\partial U_1}{\partial z}(0) = \mu_2(0)\frac{\partial U_2}{\partial z}(0), \quad U_1(0) = U_2(0), \tag{5.36}$$

plus two additional mass flow rate conditions, written for each fluid:

$$Q_1 = \int_0^{-d} U_1 dz, \qquad Q_2 = \int_1^0 U_2 dz. \tag{5.37}$$

Taking into account the complexity of the system and, in order to model reasonable our problem, in the following computations we assume that $C_2 = 0$ (condition which cancel the influence of the upper fluid thermal expansion on the basic velocity profiles) and $Q_1 = 0$ (condition which ensures the recirculation of the lower fluid).

The basic velocity profiles, as solutions of the above system of motion, can be computed after we prescribe a viscosity/temperature relationship which characterizes our fluids entirely. In the present work, we consider two different models for the temperature dependent viscosity, one for each fluid, and in this case, we compute the basic velocity profiles of each fluid. The models used in our computations appear also in the works of Wall and Wilson [15], Schäfer and Herwig [14], Potter and Graber [13].

5.2.3 Viscosity models

Model 1

For the lower fluid we assume an exponential viscosity/temperature relationship given by:

$$\mu_1(z) = e^{-K_1\theta_1(z)} \tag{5.38}$$

where $z \in [-d, 0]$.

In the float glass process, the lower fluid is molten tin, which is a metal liquid with very low kinematic viscosity. Thus, our assumption is justified, due to the fact the viscosity will drop fast when the temperature is increased.

Model 2

Moreover, for the upper fluid we consider a linear viscosity/temperature relationship given by:

$$\mu_2(z) = \mu - K_2\theta_2(z) \tag{5.39}$$

where $z \in [0, 1]$.

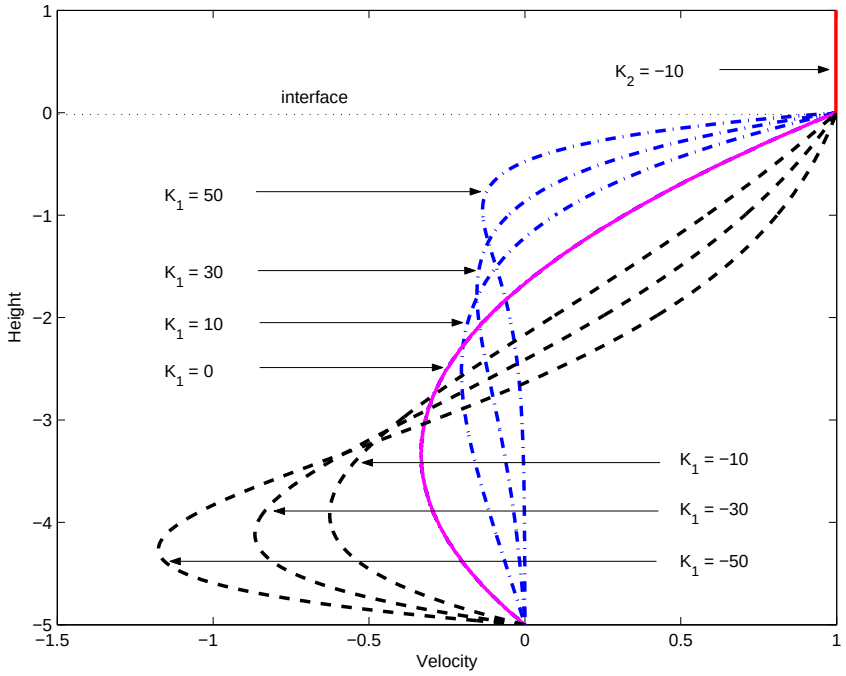

Figure 5.2: The basic velocity profiles

In the float glass, the upper fluid is hot glass, which has a large viscosity emphasized in this model by the coefficient μ, the ratio of the fluids viscosity in no-temperature conditions (i.e. the value of the temperature is equal to zero).

The viscosity of the upper fluid should have always positive value. Thus, we can prescribe some conditions for the constant K_2, in order to satisfy this property:

$$\mu_2 > 0 \implies K_2 < \mu/\theta_2(z). \tag{5.40}$$

In the reality, the temperature/viscosity dependence is much more complex and ussualy is a property of the material. In order to model industrial problems close to reality, many authors developed different kind of relationships which preserve the desired characteristics of the process [15, 13].

5.2.4 Basic velocity profiles

Using the viscosity models introduced in section 5.2.3, we compute the basic velocity profiles, stated below:

$$U_1(z) = \frac{e^{a_1 K_1 z}(C_1 e^{a_0 K_1}(-1 + a_1 K_1 z) + a_1 K_1 C t_1)}{a_1^2 K_1^2} + C t_2 \tag{5.41}$$

$$U_2(z) = C t_3 + \frac{C t_4 log(-1 + b_0 K_2 + b_1 K_2 z)}{b_1 K_2} \tag{5.42}$$

where $C_1, Ct_1, Ct_2, Ct_3, Ct_4$ are solutions of the system (5.33)-(5.36) and the forms of a_0, a_1, b_1 are given by (5.27) and (5.28).

For both these models, when viscosity of the lower fluid decreases monotonically across the channel, the basic profile skews towards the upper hot fluid. Moreover, when viscosity increases monotonically across the channel, due to the buoyancy movement of the lower fluid, the basic flow skews towards the cold wall (figure 5.2).

5.3 Linearized system of motion

In accordance with the classical linear stability theory, we perturb the basic solutions with small perturbations, which are assumed to have the normal mode form. We apply this procedure in two steps, due to the complexity of our system of motion. First, we seek solutions in the form:

$$\mathbf{u}_j = U_j + \epsilon\tilde{\mathbf{u}}_j, \quad p_j = P_j + \epsilon\tilde{p}_j, \quad \theta_j = \Theta_j + \epsilon\tilde{\theta}_j, \quad h = \epsilon\tilde{h} \tag{5.43}$$

where $\epsilon \to 0$ is a parameter introduced due to our assumption that the disturbances of the basic flow are small. The capital letters denote the solutions of the basic flow for velocity, pressure and temperature.

Further, we linearize our system taking into account that the solutions of the basic flow satisfy the equations. Although, according with Wall and Wilson [13], we notice that the viscosity contains both basic and perturbation temperatures which make the linearization more difficult. We apply the same technique and, thus, we introduce the following new terms:

$$\mu_j^* = \mu_j(\Theta_j + \epsilon\tilde{\theta}_j) - \mu_j(\Theta_j), \quad \mu_j^{*'} = \mu_j^{'}(\Theta_j + \epsilon\tilde{\theta}_j) - \mu_j^{'}(\Theta_j) \tag{5.44}$$

We expand the above relations in the Taylor series due to the fact that perturbations are considered to be small. Hence, we are able to keep only the viscosity terms in which appears the perturbed temperature only (basic flow temperature). More details about this procedure are given in the appendix C.

In the second step, we assume that the perturbations have the normal mode form:

$$\tilde{f} = \tilde{f}(z)e^{ik(x-ct)}. \tag{5.45}$$

Moreover, we follow the classical approach and introduce the stream function which, by its definition, satisfies the mass equation (section 3.2). Thus, we obtain the system of motion which characterize our problem in the case of temperature dependent viscosity:

Orr-Sommerfeld equations:

$$\mu_1(\Theta_1)(\phi_1^{iv} - 2k^2\phi_1^{''} + k^4\phi_1) + \mu_1^{'}(\Theta_1)(D_1\phi_1 + E_1\tilde{\theta}_1) + \mu_1^{''}(\Theta_1)(D_2\phi_1 + E_2\tilde{\theta}_1) +$$

$$+\mu_1^{'''}(\Theta_1)\frac{\partial U_1}{\partial z}\Theta_1^{'2}\tilde{\theta}_1 = iRek(U_1 - c)(\phi_1^{''} - k^2\phi_1) - iRek\phi_1\frac{\partial^2 U_1}{\partial z^2} + ik\frac{Gr}{Re}\tilde{\theta}_1 \tag{5.46}$$

$$\mu_2(\Theta_2)(\phi_2^{iv} - 2k^2\phi_2'' + k^4\phi_2) + \mu_2'(\Theta_2)(D_1\phi_2 + E_1\tilde{\theta}_2) + \mu_2''(\Theta_2)(D_2\phi_2 + E_2\tilde{\theta}_2) +$$
$$+\mu_2'''(\Theta_2)\frac{\partial U_2}{\partial z}\Theta_2'^2\tilde{\theta}_2 = ikRe\rho(U_2 - c)(\phi_2'' - k^2\phi_2) - ikRe\rho\phi_2\frac{\partial^2 U_2}{\partial z^2} + ik\frac{Gr\rho\beta}{Re}\tilde{\theta}_2 \quad (5.47)$$

where

$$D_1 = 2\Theta'\left(\frac{d^3}{dz^3} - k^2\frac{d}{dz}\right) + \Theta''\left(\frac{d^2}{dz^2} + k^2\right), \quad (5.48)$$

$$E_1 = U'\frac{d^2}{dz^2} + 2U''\frac{d}{dz} + (k^2U' + U'''), \quad (5.49)$$

$$D_2 = \Theta'^2\left(\frac{d^2}{dz^2} + k^2\right), \quad (5.50)$$

$$E_2 = 2U'\Theta'\frac{d}{dz} + 2\Theta'U'' + U'\Theta''. \quad (5.51)$$

Energy equations:

$$ik(U_1 - c)\tilde{\theta}_1 - ik\phi_1\frac{\partial\Theta_1}{\partial z} = \frac{1}{RePr}(\tilde{\theta}_1'' - k^2\tilde{\theta}_1), \quad (5.52)$$

$$ik(U_2 - c)\tilde{\theta}_2 - ik\phi_2\frac{\partial\Theta_2}{\partial z} = \frac{\alpha}{RePr}(\tilde{\theta}_2'' - k^2\tilde{\theta}_2). \quad (5.53)$$

The system is coupled with the following interface and boundary conditions ($z = 0$):

Kinematic condition

$$\phi_j = \tilde{h}(U_j - c),\ j = \overline{1,2} \quad \Longrightarrow \quad \phi_1 = \phi_2 \quad (5.54)$$

Normal Stress

$$\mu_1(\Theta_1)\phi_1''' - \mu_2(\Theta_2)\phi_2''' - 3k^2(\mu_1(\Theta_1)\phi_1' - \mu_2(\Theta_2)\phi_2') +$$
$$+\left[\mu_1'(\Theta_1)\tilde{\theta}_1\frac{\partial\Theta_1}{\partial z}\frac{\partial^2 U_1}{\partial z^2} + \mu_1''(\Theta_1)\tilde{\theta}_1\left(\frac{\partial\Theta_1}{\partial z}\right)^2\frac{\partial U_1}{\partial z}\right] +$$
$$+\mu_1'(\Theta_1)\left(\phi_1''\frac{\partial\Theta_1}{\partial z} + \tilde{\theta}_1'\frac{\partial U_1}{\partial z} + k^2\phi_1\frac{\partial\Theta_1}{\partial z}\right) -$$
$$-\left[\mu_2'(\Theta_2)\tilde{\theta}_2\frac{\partial\Theta_2}{\partial z}\frac{\partial^2 U_2}{\partial z^2} + \mu_2''(\Theta_2)\tilde{\theta}_2\left(\frac{\partial\Theta_2}{\partial z}\right)^2\frac{\partial U_2}{\partial z}\right] -$$
$$-\mu_2'(\Theta_2)\left(\phi_2''\frac{\partial\Theta_2}{\partial z} + \tilde{\theta}_2'\frac{\partial U_2}{\partial z} + k^2\phi_2\frac{\partial\Theta_2}{\partial z}\right) +$$
$$+ikRe_1\left\{\left[\phi_1\frac{\partial U_1}{\partial z} - \phi_1'(U_1 - c)\right] - \rho\left[\phi_2\frac{\partial U_2}{\partial z} - \phi_2'(U_2 - c)\right]\right\} = ik^3\frac{Re}{We}\tilde{h} \quad (5.55)$$

Tangetial Stress

$$\mu_2(\Theta_2)(\phi_2^{''}+k^2\phi_2)+\mu_2^{'}(\Theta_2)\tilde{\theta}_2\frac{\partial\Theta_2}{\partial z}\frac{\partial U_2}{\partial z}=\mu_1(\Theta_1)(\phi_1^{''}+k^2\phi_1)+\mu_1^{'}(\Theta_1)\tilde{\theta}_1\frac{\partial\Theta_1}{\partial z}\frac{\partial U_1}{\partial z} \quad (5.56)$$

Velocity condition

$$\phi_1+\tilde{h}\frac{\partial U_1}{\partial z}=\phi_2+\tilde{h}\frac{\partial U_2}{\partial z} \quad (5.57)$$

Heat Transfer conditions

$$\tilde{\theta}_1=\tilde{\theta}_2, \quad \kappa\frac{\partial\tilde{\theta}_2}{\partial z}=\frac{\partial\tilde{\theta}_1}{\partial z}. \quad (5.58)$$

Boundary conditions:

$$\begin{array}{c}\text{for } z=-d, \quad \phi_1=0, \quad \phi_1^{'}=0, \quad \tilde{\theta}_1=0\\ \text{for } z=1, \quad \phi_2=0, \quad \phi_2^{'}=0, \quad \tilde{\theta}_2=0\end{array}$$

Each equation which contains viscosity terms is compound from two parts. First part is the classical derivation of the relation, which can be found in section 2.2.1, whereas the second part contains viscosity and derivatives of the viscosity terms according with the basic flow temperature.

Moreover, due to the fact that the basic temperature profiles are first degree polynomials in z, all of the second and higher derivatives are equal zero.

$$\Theta_1=\frac{\kappa(d+z)}{1+d\kappa}\Longrightarrow\frac{\partial^2\Theta_1}{\partial z^2}=0, \quad \frac{\partial\Theta_1}{\partial z}=\frac{\kappa}{1+d\kappa}, \quad (5.59)$$

$$\Theta_2=\frac{\kappa d+z}{1+d\kappa}\Longrightarrow\frac{\partial^2\Theta_2}{\partial z^2}=0, \quad \frac{\partial\Theta_2}{\partial z}=\frac{1}{1+d\kappa}. \quad (5.60)$$

These changes will affect the operators D_1, E_1, D_2, E_2, thus the terms from Orr-Sommerfeld equations have the following forms:

$$D_1\phi_1+E_1\tilde{\theta}_1=2\frac{\partial\Theta_1}{\partial z}(\phi_1^{'''}-k^2\phi_1^{'})+\frac{\partial U_1}{\partial z}\tilde{\theta}_1^{''}+2\frac{\partial^2U_1}{\partial z^2}\tilde{\theta}_1^{'}+\left(k^2\frac{\partial U_1}{\partial z}+\frac{\partial^3U_1}{\partial z^3}\right)\tilde{\theta}_1,$$

$$D_2\phi_1+E_2\tilde{\theta}_1=\left(\frac{\partial\Theta_1}{\partial z}\right)^2(\phi_1^{''}+k^2\phi_1)+2\frac{\partial U_1}{\partial z}\frac{\partial\Theta_1}{\partial z}\tilde{\theta}_1^{'}+2\frac{\partial\Theta_1}{\partial z}\frac{\partial^2U_1}{\partial z^2}\tilde{\theta}_1, \quad (5.61)$$

$$D_1\phi_2+E_1\tilde{\theta}_2=2\frac{\partial\Theta_2}{\partial z}(\phi_2^{'''}-k^2\phi_2^{'})+\frac{\partial U_2}{\partial z}\tilde{\theta}_2^{''}+2\frac{\partial^2U_2}{\partial z^2}\tilde{\theta}_2^{'}+\left(k^2\frac{\partial U_2}{\partial z}+\frac{\partial^3U_2}{\partial z^3}\right)\tilde{\theta}_2,$$

$$D_2\phi_2+E_2\tilde{\theta}_2=\left(\frac{\partial\Theta_2}{\partial z}\right)^2(\phi_2^{''}+k^2\phi_2)+2\frac{\partial U_2}{\partial z}\frac{\partial\Theta_2}{\partial z}\tilde{\theta}_2^{'}+2\frac{\partial\Theta_2}{\partial z}\frac{\partial^2U_2}{\partial z^2}\tilde{\theta}_2. \quad (5.62)$$

Moreover, we take into account the viscosity models introduced in section 5.2.3 and we perform on our system of motion some required simplifications. Thus, for the upper fluid we have:

$$\mu_2^{'}(\theta_2) = -K_2, \quad \mu_2^{''}(\theta_2) = 0, \quad \mu_2^{'''}(\theta_2) = 0. \tag{5.63}$$

Similar, for the lower fluid:

$$\mu_1^{'}(\theta_1) = -K_1 e^{-K_1\theta_1}, \quad \mu_1^{''}(\theta_1) = K_1^2 e^{-K_1\theta_1}, \quad \mu_1^{'''}(\theta_1) = -K_1^3 e^{-K_1\theta_1}. \tag{5.64}$$

Hence, the Orr-Sommerfeld equations reduce at:

$$\begin{aligned}
&\mu_1(\theta_1)(\phi_1^{iv} - 2k^2\phi_1^{''} + k^4\phi_1) + \mu_1^{'}(\Theta_1)(D_1\phi_1 + E_1\tilde{\theta}_1) + \mu_1^{''}(\Theta_1)(D_2\phi_1 + E_2\tilde{\theta}_1) + \\
&+\mu_1^{'''}(\Theta_1)\frac{\partial U_1}{\partial z}\Theta_1^{'}\tilde{\theta}_1 = ikRe(U_1 - c)(\phi_1^{''} - k^2\phi_1) - ikRe\phi_1\frac{\partial^2 U_1}{\partial z^2} + ik\frac{Gr}{Re}\tilde{\theta}_1, \qquad (5.65)\\
&\mu_2(\theta_2)(\phi_2^{iv} - 2k^2\phi_2^{''} + k^4\phi_2) + \mu_2^{'}(\Theta_2)(D_1\phi_2 + E_1\tilde{\theta}_2) = \\
&= ikRe\rho(U_2 - c)(\phi_2^{''} - k^2\phi_2) - ikRe\rho\phi_2\frac{\partial^2 U_2}{\partial z^2} + ik\frac{Gr\rho\beta}{Re}\tilde{\theta}_2. \qquad (5.66)
\end{aligned}$$

Moreover, also some of the interface conditions experience few simplifications:

Normal Stress

$$\begin{aligned}
&\mu_1(\Theta_1)\phi_1^{'''} - \mu_2(\Theta_2)\phi_2^{'''} - 3k^2(\mu_1(\Theta_1)\phi_1^{'} - \mu_2(\Theta_2)\phi_2^{'}) + \\
&+\left[\mu'_1(\Theta_1)\tilde{\theta}_1\frac{\partial\Theta_1}{\partial z}\frac{\partial^2 U_1}{\partial z^2} + \mu_1^{''}(\Theta_1)\tilde{\theta}_1\left(\frac{\partial\Theta_1}{\partial z}\right)^2\frac{\partial U_1}{\partial z}\right] + \\
&+\mu_1^{'}(\Theta_1)\left(\phi_1^{''}\frac{\partial\Theta_1}{\partial z} + \tilde{\theta}_1^{'}\frac{\partial U_1}{\partial z} + k^2\phi_1\frac{\partial\Theta_1}{\partial z}\right) - \\
&-\mu_2^{'}(\Theta_2)\left[\tilde{\theta}_2\frac{\partial\Theta_2}{\partial z}\frac{\partial^2 U_2}{\partial z^2} + \left(\phi_2^{''}\frac{\partial\Theta_2}{\partial z} + \tilde{\theta}_2^{'}\frac{\partial U_2}{\partial z} + k^2\phi_2\frac{\partial\Theta_2}{\partial z}\right)\right] + \\
&+ikRe_1\left\{\left[\phi_1\frac{\partial U_1}{\partial z} - \phi_1^{'}(U_1 - c)\right] - \rho\left[\phi_2\frac{\partial U_2}{\partial z} - \phi_2^{'}(U_2 - c)\right]\right\} = ik^3\frac{Re}{We}\tilde{h} \qquad (5.67)
\end{aligned}$$

Tangential Stress

$$\mu_2(\Theta_2)(\phi_2^{''} + k^2\phi_2) + \mu_2^{'}(\Theta_2)\tilde{\theta}_2\frac{\partial\Theta_2}{\partial z}\frac{\partial U_2}{\partial z} = \mu_1(\Theta_1)(\phi_1^{''} + k^2\phi_1) + \mu_2^{'}(\Theta_2)\tilde{\theta}_1\frac{\partial\Theta_1}{\partial z}\frac{\partial U_1}{\partial z}. \tag{5.68}$$

All the other equations remain unchanged. An analytical dispersion relation for the eigenvalue c is very difficult to obtain, due to the complexity of the system. Hence, we solve the above system of equations numerically, using the Chebyshev collocation spectral method introduced in chapter 4. In this case, we consider the basic flow profiles defined in sections 5.2.4 and 5.2.1, together with the equations (5.46)-(5.53) and the conditions (5.54)-(5.58). The implementation is similar with the one described in chapter 4.

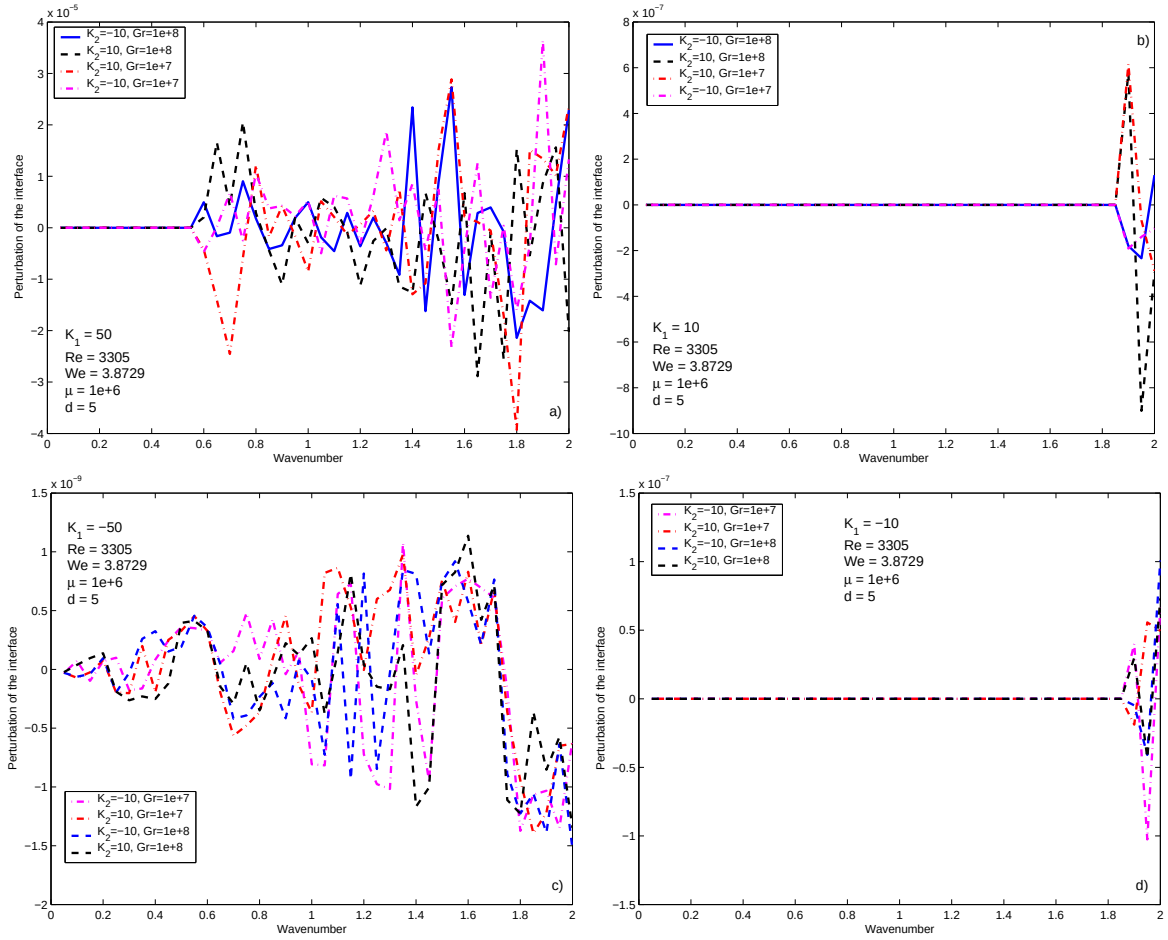

Figure 5.3: The perturbation of the interface with respect to the wave number for different values of the Grashof number at: a) $K_1 = 50$; b) $K_1 = 10$; c)$K_1 = -50$; d)$K_1 = -10$.

From the viscosities definition (section 5.2.3), it can be seen that when the parameters K_1 and K_2 are positive, the value of the viscosities decrease and, analogous, when the parameters are negative, the value of the viscosities increase. In the figure 5.3, we plotted the amplitude of the perturbation at the interface, $\tilde{h}$, with respect to the wave number at different values of the Grashof numbers and the parameters K_1 and K_2. Thus, the absolute value of the the interface perturbation amplitude vary between $5 \cdot 10^{-6}$ and $4 \cdot 10^{-5}$, whereas the viscosity of the lower fluid strongly decreases (i.e. $K_1 = 50$). In this case, the variation in the viscosity of the upper fluid has almost no effect, although for large temperature gradients (i.e. $Gr = 10^8$), the absolute value of the amplitude perturbation tends to decrease slightly (figure 5.3(a)). Hence, the temperature stabilizes the system.

Moreover, for smaller positive values of the lower fluid viscosity parameter (i.e. $K_1 = 10$) and for large wave number (between 1.8 and 2), the amplitude of the perturbation is much smaller, with absolute values between $2 \cdot 10^{-7}$ and $6 \cdot 10^{-7}$ (figure 5.3(b)). Temperature, in this case, has no effect over the amplitude of the interface perturbation. Nevertheless, when the lower fluid viscosity is increased faster (i.e. $K_1 = -50$), the absolute value

of the amplitude of the interface perturbation decreases and varies between 10^{-11} and $1.5 \cdot 10^{-9}$ (figure 5.3(c)). The amplitude raises with the wave number and, also, in this case, the temperature has almost no effect over the stability of the system. An interesting result is the fact that when the lower fluid viscosity increases slowly (i.e. $K_1 = -10$), the absolute values of the amplitude perturbation remain in the range 10^{-7}, as in the case when the lower fluid viscosity decreases slowly (i.e. $K_1 = 10$)(figure 5.3(d)).

The main result of the above analysis is that the amplitude of the interface perturbation is very small in absolute value with respect to the wave length. Hence, following this analysis, the sheets of glass produced by the float glass process in the conditions presented in our model, experience waves with very large wave length and very small amplitude, thus, practically negligeable. From the long waves point of view, the sheets of glass are perfectly flat, result which is in agreement with the real float glass process.

5.4 Short wave limit

The primary concern of our work is to focus over the development of the waves with wave length and amplitude comparable in magnitude, although much smaller than the characteristic length, the height of the upper fluid layer. We follow the same procedure which was introduced in section 3.4, thus, the small parameter used in the expansions is $1/k \to 0$. Also, we assume a change in our scaling, corresponding to a short-scale structure concentrated close to the interface and we linearize our system by using relations (3.52)-(3.56).

Nevertheless, in this case, the terms from Orr-Sommerfeld equation which contain the operators D_1, D_2, E_1, E_2 take the following forms ($j = \overline{1,2}$):

$$D_1\phi_j + E_1\tilde{\theta}_j = 2k^3\frac{\partial\Theta_j}{\partial z}(\phi_j^{'''} - \phi_j^{'}) + k^3\left(\frac{\partial U_j}{\partial z}\tilde{\theta}_j^{''}\right) + 2k^3\frac{\partial^2 U_j}{\partial z^2}\tilde{\theta}_j^{'} + k^3\left(\frac{\partial U_j}{\partial z} + \frac{\partial^3 U_j}{\partial z^3}\right)\tilde{\theta}_j$$

$$D_2\phi_j + E_2\tilde{\theta}_j = k^4\left(\frac{\partial\Theta_j}{\partial z}\right)^2\left(\phi_j^{''} + \phi_j\right) + 2k^4\frac{\partial U_j}{\partial z}\frac{\partial\Theta_j}{\partial z}\tilde{\theta}_j^{'} + 2k^3\frac{\partial\Theta_j}{\partial z}\frac{\partial^2 U_j}{\partial z^2}\tilde{\theta}_j. \qquad (5.69)$$

Thus, the system of motion which characterizes our problem has the following form:

Orr-Sommerfeld equations

$$\mu_1(\theta_1)k^4(\phi_1^{iv} - 2\phi_1^{''} + \phi_1) + \mu_1^{'}(\Theta_1)(D_1\phi_1 + E_1\tilde{\theta}_1) + \mu_1^{''}(\Theta_1)(D_2\phi_1 + E_2\tilde{\theta}_1) +$$

$$+\mu_1^{'''}(\Theta_1)\frac{\partial U_1}{\partial z}\Theta_1^{'}\tilde{\theta}_1 = ik^3Re(U_1 - c)(\phi_1^{''} - \phi_1) - ik^3Re\phi_1\frac{\partial^2 U_1}{\partial z^2} + ik\frac{Gr}{Re}\tilde{\theta}_1, \qquad (5.70)$$

$$\mu_2(\theta_2)k^4(\phi_2^{iv} - 2\phi_2^{''} + \phi_2) + \mu_2^{'}(\Theta_2)(D_1\phi_2 + E_1\tilde{\theta}_2) =$$

$$= ik^3Re\rho(U_2 - c)(\phi_2^{''} - \phi_2) - ik^3Re\rho\phi_2\frac{\partial^2 U_2}{\partial z^2} + ik\frac{Gr\rho\beta}{Re}\tilde{\theta}_2. \qquad (5.71)$$

Energy equations

$$ik(U_1 - c)\tilde{\theta}_1 - ik^2\phi_1\frac{\partial\Theta_1}{\partial z} = \frac{k^2}{RePr}(\tilde{\theta}_1'' - \tilde{\theta}_1), \tag{5.72}$$

$$ik(U_2 - c)\tilde{\theta}_2 - ik^2\phi_2\frac{\partial\Theta_2}{\partial z} = \frac{k^2\alpha}{RePr}(\tilde{\theta}_2'' - \tilde{\theta}_2). \tag{5.73}$$

The system of motion in the short wave limit is coupled with the following interface conditions ($z = 0$):

Kinematic condition

$$\phi_1 = \phi_2 \tag{5.74}$$

Normal Stress

$$\begin{aligned}
&\mu_1(\Theta_1)k^3\phi_1''' - \mu_2(\Theta_2)k^3\phi_2''' - 3k^3(\mu_1(\Theta_1)\phi_1' - \mu_2(\Theta_2)\phi_2') + \\
&+\left[\mu'_1(\Theta_1)k^3\tilde{\theta}_1\frac{\partial\Theta_1}{\partial z}\frac{\partial^2 U_1}{\partial z^2} + \mu_1''(\Theta_1)\tilde{\theta}_1 k^3\left(\frac{\partial\Theta_1}{\partial z}\right)^2\frac{\partial U_1}{\partial z}\right] + \\
&+\mu_1'(\Theta_1)\left(k^3\phi_1''\frac{\partial\Theta_1}{\partial z} + k^2\tilde{\theta}_1'\frac{\partial U_1}{\partial z} + k^3\phi_1\frac{\partial\Theta_1}{\partial z}\right) - \\
&-\mu_2'(\Theta_2)\left[k^3\tilde{\theta}_2\frac{\partial\Theta_2}{\partial z}\frac{\partial^2 U_2}{\partial z^2} + \left(k^3\phi_2''\frac{\partial\Theta_2}{\partial z} + k^2\tilde{\theta}_2'\frac{\partial U_2}{\partial z} + k^3\phi_2\frac{\partial\Theta_2}{\partial z}\right)\right] + \\
&+ik^2 Re_1\left\{\left[\phi_1\frac{\partial U_1}{\partial z} - \phi_1'(U_1 - c)\right] - \rho\left[\phi_2\frac{\partial U_2}{\partial z} - \phi_2'(U_2 - c)\right]\right\} = ik^3\frac{Re}{We}\tilde{h}
\end{aligned} \tag{5.75}$$

Tangential Stress

$$\mu_2(\Theta_2)k^2(\phi_2'' + \phi_2) + \mu_2'(\Theta_2)k^2\tilde{\theta}_2\frac{\partial\Theta_2}{\partial z}\frac{\partial U_2}{\partial z} = \mu_1(\Theta_1)k^2(\phi_1'' + \phi_1) + \mu_2'(\Theta_2)k^2\tilde{\theta}_1\frac{\partial\Theta_1}{\partial z}\frac{\partial U_1}{\partial z} \tag{5.76}$$

Velocity condition

$$\phi_1 + \tilde{h}\frac{\partial U_1}{\partial z} = \phi_2 + \tilde{h}\frac{\partial U_2}{\partial z} \tag{5.77}$$

Heat Transfer conditions

$$\tilde{\theta}_1 = \tilde{\theta}_2, \quad \kappa\frac{\partial\tilde{\theta}_2}{\partial z} = \frac{\partial\tilde{\theta}_1}{\partial z} \tag{5.78}$$

Boundary conditions which complete the system of motion in the short wave limit are defined in section 5.3.

We solve the above system of equations numerically, using Chebyshev collocation spectral method introduced in chapter 4. In the figure 5.4(a), we plotted the amplitude of the perturbation at the interface, $\tilde{h}$, with respect to the wave number at different values of the Grashof numbers and the parameters K_1 and K_2. Thus, the absolute value of the

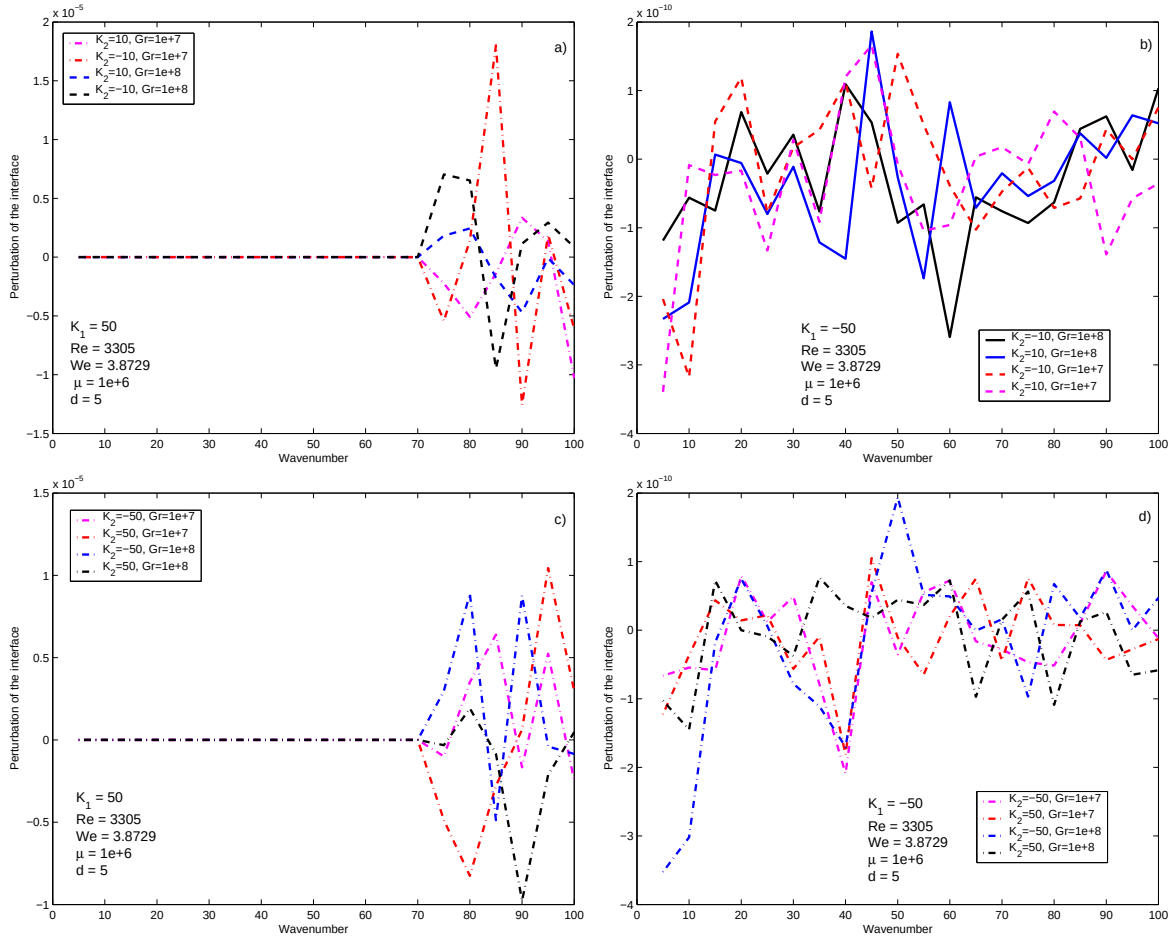

Figure 5.4: The perturbation of the interface with respect to the wave number for different values of the Grashof number at: a) $K_1 = 50$, $K_2 = -10, 10$; b) $K_1 = -50$, $K_2 = -10, 10$; c) $K_1 = 50$, $K_2 = -50, 50$; d) $K_1 = -50$, $K_2 = -50, 50$.

the interface perturbation amplitude vary between $2 \cdot 10^{-6}$ and $1.8 \cdot 10^{-5}$, whereas the viscosity of the lower fluid strongly decreases (i.e. $K_1 = 50$) and the viscosity of the upper fluid vary smoothly (i.e. $K_2 = -10, 10$). Moreover, it is shown that the variation in the viscosity of the upper fluid has almost no effect (figure 5.4(c)), although in the case when upper fluid viscosity varies smoothly, the temperature tends to stabilize the system (i.e. decreasing the amplitude of the perturbation).

We consider the case when the value of the lower fluid viscosity increases (figure 5.4(b)) and it is shown that the range, for the variation of the absolute value of the perturbation amplitude, is very small (i.e. smaller than $2 \cdot 10^{-10}$). Hence, in this case, we can neglect the perturbation of the interface and consider that the basic flow is unperturbed. Moreover, it is shown that changes in temperature and variations of the upper fluid viscosity have no effect over the stability of the system (figure 5.4(d)).

Nevertheless, inertia plays a very important role in the short waves stability, thus we focus on its influence on our system of motion. It is shown that the inertia destabilizes

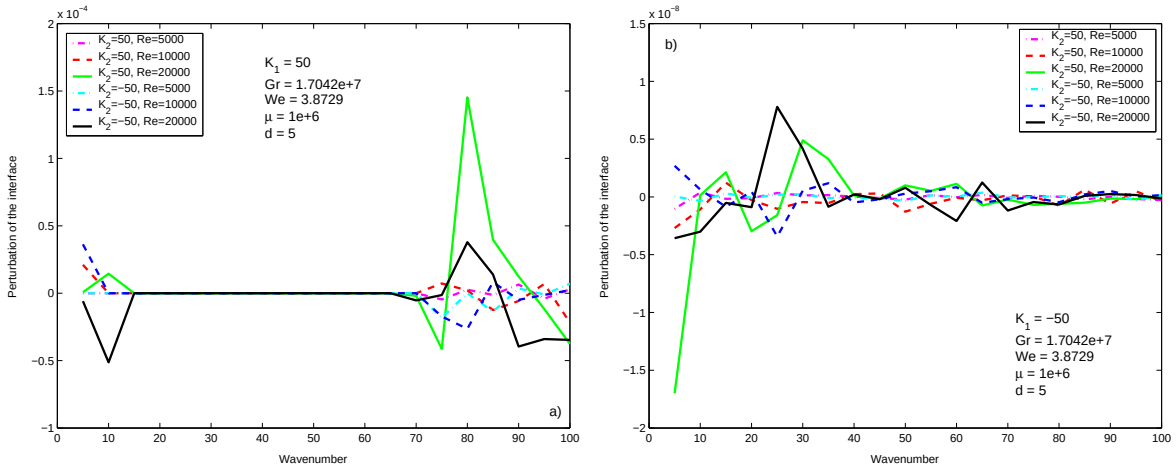

Figure 5.5: The perturbation of the interface with respect to the wave number for different values of the Reynolds number at: a) $K_1 = 50$; b) $K_1 = -50$.

the flow, for large values of the wave number (i.e. for k between 75 and 90), although the effect is stronger when the value of the upper fluid viscosity decreases (figure 5.5(a)). For wavenumbers larger than 90, the value of the perturbation amplitude tends to stabilize in a range between 10^{-6} and $5 \cdot^{-5}$.

The amplitude of the interface perturbation has smaller values when the lower fluid viscosity increases, varying between 10^{-10} and $1.6 \cdot 10^{-8}$ (figure 5.5(b)). In this case, the inertia, the temperature and the variation of the upper fluid viscosity have no effect over the amplitude of the interface perturbation.

Chapter 6

Discussions and conclusions

In this paper, we model the floating part of the float glass process, by an two dimensional theoretical study of the stability of two superposed fluids confined between two infinite plates and subjected to a large horizontal temperature gradient. We investigate the problem analytically (linear stability analysis), in two limit cases (long and short wave), and numerically, using Chebyshev spectral methods for fluid dynamics.

In the float glass process, the temperature influences strongly the viscosity of both fluids involved, molten metal and hot glass, which has direct consequences on the stability of the system. Hence, we investigate the linear stability of two superposed fluids with temperature dependent viscosities by considering two different temperature/viscosity relationships, one for each fluid. The new derived system of motion was solved numerically, using the same technique as in the case of constant viscosity.

The motivation of our work was the experiments and observations made on the float glass finite products, which emphasized the presence of continuous patterns of small amplitude waves. Our task was to investigate the hydrodynamical waves development mechanism, taking into account all possible factors that can influence its appearance. The waves observed on the final glass products have the wavelength between $5 \cdot 10^{-4}$ meters and 10^{-2} meters, and the amplitude between 10^{-9} meters and 10^{-7} meters.

In our computations, we use parameters which characterize the industrial float glass process. Further, we state below the values of some of the most important parameters, which were kept constant in our computations:

- The densities ratio, $\rho = 0.3872$, which emphasizes the fact that the lower fluid, the metal tin, is heavier than the upper fluid, hot glass. Thus, we neglected, from the beginning, the investigations of Rayleigh-Taylor instabilities.

- The viscosities ratio, μ, has values between 10^4 and 10^9, which emphasizes the fact that the hot glass is liquid at the inlet of the bath, and also, that the glass is almost solid at the outlet. Nevertheless, the large value of the viscosites ratio shows that the molten tin is much less viscous than the glass.

- The thermal diffusivities ratio, $\alpha = 0.0463$, shows that the thermal effects have strong consequences on the stability of the lower fluid, the molten metal (i.e. fast appeareance of the buoyant recirculation).

- The thermal expansion coefficients ratio, $\beta = 0.2010$, which emphasize the thermal expansion of the fluids, an effect which can not be neglected during the process.

The results of our analysis are in good agreement with the observations made on the final products and on the industrial process. We investigate the stability of the long waves (i.e. the wavelength much larger than the amplitude and the characteristic length) and the results are presented in sections 3.3, 4.2.1 and 5.3. Hence, it is shown that the long waves are always stable, and due to their very small amplitude (around 10^{-9} meters), do not affect the flatness and the shape of the glass sheets. This result is verified in reality by the overall quality of the float glass final products. Moreover, it is shown that the height and the viscosity of the lower fluid layer, (i.e. molten tin), influence directly the long waves stability. In section 3.3, we performed an analytical estimation of the perturbation evolution during the entire process and we showed that, in the long wave limit, the initial perturbation is conserved throughout the process.

Moreover, we investigate the stability of the short waves (i.e. the wavelength much smaller than the characteristic length) and the results are presented in sections 3.4, 4.2.2 and 5.4. Hence, the numerical analysis shown the existence of a short waves pattern with the amplitude and the wave length in good agreement with the amplitude and the wavelength of the observed waves (see figure 4.7). Moreover, the large temperature gradients, the inertia and the upper fluid mass flow rate stabilize the short waves. The analytical estimation performed in the short wave limit show that the initial perturbation is conserved throughout the process. Also, when the thermal effects dominate, any initial perturbation is damped by the flow. More details are given in sections 3.4and 4.2.2.

Nevertheless, our temperature dependent viscosity analysis comes to conclude the two dimensional linear stability of our model for the float glass process. The main numerical result of the long wave analysis is that the amplitude of the interface perturbation is very small in absulte value with respect to the wave length. Thus, the sheets of glass do not experience any shape changes, and from the long waves point of view, are perfectly flat (see section 5.3). In the short wave limit, the numerical analysis shows that the changes in temperature and variations of the upper fluid viscosity have no effect over the stability of the system, whereas the lower fluid viscosity increases. Moreover, when the viscosity of the lower fluid decreases, the temperature tends to stabilize the system. Also, it is shown that the inertia destabilizes the flow for large values of the wave number (between 75 and 90). More details are presented in section 5.4.

In order to describe more accurate the float glass process, this work can be continued with a three dimensional linear stability analysis, investigations of the radiation effects and nevertheless, a non-linear stability analysis and an optimization of the floating part of the process.

Appendix A

Considerations on the initial scalings

Asymptotic analysis is used to obtain a dispersion relation between the wave number, k, and the wave speed, c. In this chapter, we investigate, starting with some general assumptions, the existence of other limit cases, beside short and long wave. Moreover, we perform this analysis in order to check our scaling, used in the short wave limit.

Therefore, we start with the non-dimensional system of motion introduced in chapter 2 and with the non-dimensional basic flow profile constructed in chapter 3. Further, we apply the following perturbations:

$$u_1 = U_1 + \epsilon^{\alpha}\tilde{u}_1, \quad u_2 = U_2 + \epsilon^{\alpha}\tilde{u}_2 \tag{A.1}$$

$$w_1 = \epsilon^{\beta}\tilde{w}_1, \quad w_2 = \epsilon^{\beta}\tilde{w}_2 \tag{A.2}$$

$$p_1 = P_1 + \epsilon^{\eta}\tilde{p}_1, \quad p_2 = P_2 + \epsilon^{\eta}\tilde{p}_2 \tag{A.3}$$

$$h = \epsilon^{\gamma}\tilde{h} \tag{A.4}$$

$$\theta_1 = \Theta_1 + \epsilon^{\tau}\tilde{\theta}_1, \quad \theta_2 = \Theta_2 + \epsilon^{\tau}\tilde{\theta}_2 \tag{A.5}$$

We scale the x and z directions as follows:

$$x = \epsilon^{\delta_x}\tilde{x}, \quad z = \epsilon^{\delta_z}\tilde{z}, \quad t = \epsilon^{\delta_t}\tilde{t} \tag{A.6}$$

where δ_x, δ_z and δ_t denote the characteristic length for x and z directions, respectively the characteristic time.

Therefore, we can, now, derive the new system of motion which is stated below:

Mass:

$$\epsilon^{\alpha-\delta_x}\frac{\partial\tilde{u}_1}{\partial\tilde{x}} + \epsilon^{\beta-\delta_z}\frac{\partial\tilde{w}_1}{\partial\tilde{z}} = 0 \tag{A.7}$$

$$\epsilon^{\alpha-\delta_x}\frac{\partial\tilde{u}_2}{\partial\tilde{x}} + \epsilon^{\beta-\delta_z}\frac{\partial\tilde{w}_2}{\partial\tilde{z}} = 0 \tag{A.8}$$

Momentum:

$$Re\left(\epsilon^{\alpha-\delta_t}\frac{\partial\tilde{u}_1}{\partial\tilde{t}}+\epsilon^{\alpha-\delta_x}U_1\frac{\partial\tilde{u}_1}{\partial\tilde{x}}+\epsilon^{\beta-\delta_z}\tilde{w}_1\frac{\partial U_1}{\partial\tilde{z}}\right)=-\epsilon^{\eta-\delta_x}\frac{\partial\tilde{p}_1}{\partial\tilde{x}}+\epsilon^{\alpha-2\delta_x}\frac{\partial^2\tilde{u}_1}{\partial\tilde{x}^2}+\epsilon^{\alpha-2\delta_z}\frac{\partial^2\tilde{u}_1}{\partial\tilde{z}^2} \tag{A.9}$$

$$\frac{\rho Re}{\mu}\left(\epsilon^{\alpha-\delta_t}\frac{\partial\tilde{u}_2}{\partial\tilde{t}}+\epsilon^{\alpha-\delta_x}U_2\frac{\partial\tilde{u}_2}{\partial\tilde{x}}+\epsilon^{\beta-\delta_z}\tilde{w}_2\frac{\partial U_2}{\partial\tilde{z}}\right)=-\epsilon^{\eta-\delta_x}\frac{\partial\tilde{p}_2}{\partial\tilde{x}}+\epsilon^{\alpha-2\delta_x}\frac{\partial^2\tilde{u}_2}{\partial\tilde{x}^2}+\epsilon^{\alpha-2\delta_z}\frac{\partial^2\tilde{u}_2}{\partial\tilde{z}^2} \tag{A.10}$$

$$\epsilon^{\beta-\delta_t}\frac{\partial\tilde{w}_1}{\partial\tilde{t}}+\epsilon^{\beta-\delta_x}U_1\frac{\partial\tilde{w}_1}{\partial\tilde{x}}=\frac{1}{Re}\left(-\epsilon^{\eta-\delta_z}\frac{\partial\tilde{p}_1}{\partial\tilde{z}}+\epsilon^{\beta-2\delta_x}\frac{\partial^2\tilde{w}_1}{\partial\tilde{x}^2}+\epsilon^{\beta-2\delta_z}\frac{\partial^2\tilde{w}_1}{\partial\tilde{z}^2}\right)+\epsilon^{\tau}\frac{Gr}{Re^2}\tilde{\theta}_1 \tag{A.11}$$

$$\epsilon^{\beta-\delta_t}\frac{\partial\tilde{w}_2}{\partial\tilde{t}}+\epsilon^{\beta-\delta_x}U_2\frac{\partial\tilde{w}_2}{\partial\tilde{x}}=\frac{\mu}{\rho Re}\left(-\epsilon^{\eta-\delta_z}\frac{\partial\tilde{p}_2}{\partial\tilde{z}}+\epsilon^{\beta-2\delta_x}\frac{\partial^2\tilde{w}_2}{\partial\tilde{x}^2}+\epsilon^{\beta-2\delta_z}\frac{\partial^2\tilde{w}_2}{\partial\tilde{z}^2}\right)+\epsilon^{\tau}\beta\frac{Gr}{Re^2}\tilde{\theta}_2 \tag{A.12}$$

Energy:

$$\epsilon^{\tau-\delta_t}\frac{\partial\tilde{\theta}_1}{\partial t}+\epsilon^{\alpha-\delta_x}\tilde{u}_1\frac{\partial\Theta_1}{\partial\tilde{x}}+\epsilon^{\tau-\delta_x}U_1\frac{\partial\tilde{\theta}_1}{\partial\tilde{x}}+\epsilon^{\beta-\delta_z}\tilde{w}_1\frac{\partial\Theta_1}{\partial\tilde{z}}=\frac{1}{RePr}\left(\epsilon^{\tau-2\delta_x}\frac{\partial^2\tilde{\theta}_1}{\partial\tilde{x}^2}+\epsilon^{\tau-2\delta_z}\frac{\partial^2\tilde{\theta}_1}{\partial\tilde{z}^2}\right) \tag{A.13}$$

$$\epsilon^{\tau-\delta_t}\frac{\partial\tilde{\theta}_2}{\partial t}+\epsilon^{\alpha-\delta_x}\tilde{u}_2\frac{\partial\Theta_2}{\partial\tilde{x}}+\epsilon^{\tau-\delta_x}U_2\frac{\partial\tilde{\theta}_2}{\partial\tilde{x}}+\epsilon^{\beta-\delta_z}\tilde{w}_2\frac{\partial\Theta_2}{\partial\tilde{z}}=\frac{\tilde{\alpha}}{RePr}\left(\epsilon^{\tau-2\delta_x}\frac{\partial^2\tilde{\theta}_2}{\partial\tilde{x}^2}+\epsilon^{\tau-2\delta_z}\frac{\partial^2\tilde{\theta}_2}{\partial\tilde{z}^2}\right) \tag{A.14}$$

The system is coupled with the following boundary and interface conditions (z=0):

Kinematical condition:

$$\epsilon^{\beta}\tilde{w}_1=\epsilon^{\gamma-\delta_t}\frac{\partial\tilde{h}}{\partial\tilde{t}}+\epsilon^{\gamma-\delta_x}U_1\frac{\partial\tilde{h}}{\partial\tilde{x}} \tag{A.15}$$

$$\epsilon^{\beta}\tilde{w}_2=\epsilon^{\gamma-\delta_t}\frac{\partial\tilde{h}}{\partial\tilde{t}}+\epsilon^{\gamma-\delta_x}U_2\frac{\partial\tilde{h}}{\partial\tilde{x}} \tag{A.16}$$

Dynamical condition (normal stress):

$$\epsilon^{\eta}(\tilde{p}_1-\tilde{p}_2)-2\mu\left(\epsilon^{\alpha-\delta_x}\frac{\partial\tilde{u}_2}{\partial\tilde{x}}+\epsilon^{\gamma-\delta_x-\delta_z}\tilde{h}_{\tilde{x}}\frac{\partial U_2}{\partial\tilde{z}}\right)+2\left(\epsilon^{\alpha-\delta_x}\frac{\partial\tilde{u}_1}{\partial\tilde{x}}+\epsilon^{\gamma-\delta_x-\delta_z}\tilde{h}_{\tilde{x}}\frac{\partial U_1}{\partial\tilde{z}}\right)=\epsilon^{\gamma-2\delta_x}\frac{Re}{We}\tilde{h}_{\tilde{x}\tilde{x}} \tag{A.17}$$

Dynamical condition (tangential stress):

$$\mu\left(\epsilon^{\alpha-\delta_z}\frac{\partial\tilde{u}_2}{\partial\tilde{z}}+\epsilon^{\beta-\delta_x}\frac{\partial\tilde{w}_2}{\partial\tilde{x}}\right)=\left(\epsilon^{\alpha-\delta_z}\frac{\partial\tilde{u}_1}{\partial\tilde{z}}+\epsilon^{\beta-\delta_x}\frac{\partial\tilde{w}_1}{\partial\tilde{x}}\right) \tag{A.18}$$

Velocity condition:

$$\tilde{u}_1=\tilde{u}_2 \tag{A.19}$$

Heat Transfer conditions:

$$\tilde{\theta}_1=\tilde{\theta}_2,\qquad \epsilon^{\gamma-2\delta_x}\tilde{h}_{\tilde{x}}\frac{\partial\Theta_1}{\partial\tilde{x}}-\epsilon^{\tau-\delta_z}\frac{\partial\tilde{\theta}_1}{\partial\tilde{z}}=\kappa\left(\epsilon^{\gamma-2\delta_x}\tilde{h}_{\tilde{x}}\frac{\partial\Theta_2}{\partial\tilde{x}}-\epsilon^{\tau-\delta_z}\frac{\partial\tilde{\theta}_2}{\partial\tilde{z}}\right) \tag{A.20}$$

Further, we introduce the stream function, defined in section 3.2, and using the fact that the mass equation should be always satisfied, we derive the new system of motion:

$$\epsilon^{\alpha-\delta_x}ik\phi_1'-\epsilon^{\beta-\delta_z}ik\phi_1'=0\quad\Longrightarrow\quad\alpha-\delta_x=\beta-\delta_z \tag{A.21}$$

$$\begin{aligned}&\epsilon^{\alpha-\eta-2\delta_z+\delta_x}\phi_1''''-2k^2\epsilon^{\alpha-\eta-\delta_x}\phi_1''+k^4\epsilon^{\alpha-3\delta_x-\eta+2\delta_z}\phi_1=\\&=ikRe_1(U_1-c)(\epsilon^{\alpha-\eta}\phi_1''-\epsilon^{\alpha-2\delta_x-\eta+2\delta_z}k^2\phi_1)-ikRe_1\epsilon^{\alpha-\eta}\phi_1U_1''+ik\epsilon^{\tau-\eta+\delta_z}\frac{Gr_1}{Re_1}\tilde{\theta}_1\end{aligned} \tag{A.22}$$

$$\begin{aligned}&\epsilon^{\alpha-\eta-2\delta_z+\delta_x}\phi_2''''-2k^2\epsilon^{\alpha-\eta-\delta_x}\phi_2''+k^4\epsilon^{\alpha-3\delta_x-\eta+2\delta_z}\phi_2=\\&=ikRe_1\frac{\rho}{\mu}(U_2-c)(\epsilon^{\alpha-\eta}\phi_2''-\epsilon^{\alpha-2\delta_x-\eta+2\delta_z}k^2\phi_2)-ikRe_1\frac{\rho}{\mu}\epsilon^{\alpha-\eta}\phi_2U_2''+ik\epsilon^{\tau-\eta+\delta_z}\frac{\rho\beta Gr_1}{\mu Re_1}\tilde{\theta}_2\end{aligned} \tag{A.23}$$

$$\epsilon^{\tau-2\delta_z}\tilde{\theta}_1''-k^2\epsilon^{\tau-2\delta_x}\tilde{\theta}_1=Re_1Pr_1\left[ik\epsilon^{\tau-\delta_x}\tilde{\theta}_1(U_1-c)+ik\epsilon^{\alpha-\delta_x}\left(\phi_1'\frac{\partial\Theta_1}{\partial\tilde{x}}-\phi_1\frac{\partial\Theta_1}{\partial\tilde{z}}\right)\right] \tag{A.24}$$

$$\epsilon^{\tau-2\delta_z}\tilde{\theta}_2''-k^2\epsilon^{\tau-2\delta_x}\tilde{\theta}_2=\frac{\tilde{\alpha}}{Re_1Pr_1}\left[ik\epsilon^{\tau-\delta_x}\tilde{\theta}_2(U_2-c)+ik\epsilon^{\alpha-\delta_x}\left(\phi_2'\frac{\partial\Theta_2}{\partial\tilde{x}}-\phi_2\frac{\partial\Theta_2}{\partial\tilde{z}}\right)\right] \tag{A.25}$$

Conditions at the interface:

$$\phi_1=\tilde{h}\left(\epsilon^{\gamma-\delta_t-\beta}c-\epsilon^{\gamma-\delta_x-\beta}U_1\right),\quad\phi_2=\tilde{h}\left(\epsilon^{\gamma-\delta_t-\beta}c-\epsilon^{\gamma-\delta_x-\beta}U_2\right)\quad\Longrightarrow\quad\delta_t=\delta_x \tag{A.26}$$

$$\epsilon^{\alpha-2\delta_z+\delta_x}(\phi_1'''-\mu\phi_2''')-3k^2\epsilon^{\alpha-\delta_x}(\phi_1'-\mu\phi_2')-ikRe_1\epsilon^{\alpha}\left[(U_1-c)\left(\phi_1'-\rho\phi_2'\right)\right]=ik^3\epsilon^{\gamma-2\delta_x}\frac{Re_1}{We_1}\tilde{h} \tag{A.27}$$

$$\mu\left(\epsilon^{\alpha-\delta_z}\phi_2'' + k^2\epsilon^{\beta-\delta_x}\phi_2\right) = \epsilon^{\alpha-\delta_z}\phi_1'' + k^2\epsilon^{\beta-\delta_x}\phi_1 \tag{A.28}$$

$$\phi_1 = \phi_2, \quad \phi_1' = \phi_2' + \tilde{h}(U_2' - U_1') \tag{A.29}$$

$$\tilde{\theta}_1 = \tilde{\theta}_2, \quad \epsilon^{\gamma-2\delta_x} ik\tilde{h}\frac{\partial\Theta_1}{\partial\tilde{x}} - \epsilon^{\tau-\delta_z}\frac{\partial\tilde{\theta}_1}{\partial\tilde{z}} = \kappa\left(\epsilon^{\gamma-2\delta_x} ik\tilde{h}\frac{\partial\Theta_2}{\partial\tilde{x}} - \epsilon^{\tau-\delta_z}\frac{\partial\tilde{\theta}_2}{\partial\tilde{z}}\right) \tag{A.30}$$

A.1 Analysis: Long Wave Limit

In the long wave limit, the wave length tends to infinity, hence the wave number, k, tends to zero. We make the following assumption due to the fact that now the wave number can be used as small parameter:

$$\epsilon = k \tag{A.31}$$

Therefore, plugging the above relation in the equations (A.21)-(A.30), we obtain the following relations:

$$\epsilon^{\alpha-\eta-2\delta_z+\delta_x}\phi_1'''' - 2\epsilon^{\alpha-\eta-\delta_x+2}\phi_1'' + \epsilon^{\alpha-3\delta_x-\eta+2\delta_z+4}\phi_1 =$$

$$= iRe_1(U_1-c)(\epsilon^{\alpha-\eta+1}\phi_1'' - \epsilon^{\alpha-2\delta_x-\eta+2\delta_z+3}\phi_1) - iRe_1\epsilon^{\alpha-\eta+1}\phi_1 U_1'' + i\epsilon^{\tau-\eta+\delta_z+1}\frac{Gr_1}{Re_1}\tilde{\theta}_1 \tag{A.32}$$

$$\phi_1'''' - 2\epsilon^{2\delta_z-2\delta_x+2}\phi_1'' + \epsilon^{4\delta_z-4\delta_x+4}\phi_1 =$$

$$= iRe_1(U_1 - c)(\epsilon^{2\delta_z-\delta_x+1}\phi_1'' - \epsilon^{4\delta_z-3\delta_x+3}\phi_1) - iRe_1\epsilon^{2\delta_z-\delta_x+1}\phi_1 U_1'' + i\epsilon^{\tau-\alpha+3\delta_z-\delta_x+1}\frac{Gr_1}{Re_1}\tilde{\theta}_1 \tag{A.33}$$

It is known from literature that, in the long wave analysis, the term ϕ_j'''', $j = \overline{1,2}$, is the leading order term in the Orr-Sommerfeld equation, written for each fluid [1, 2, 5, 8]. All the other terms should have orders greater than the leading one and, thus, we have:

$$2\delta_z - 2\delta_x + 2 > 0, \quad 4\delta_z - 4\delta_x + 4 > 0 \quad \Longrightarrow \quad \delta_z - \delta_x + 1 > 0 \tag{A.34}$$

$$2\delta_z - \delta_x + 1 > 0, \quad 4\delta_z - 3\delta_x + 3 > 0, \quad \tau - \alpha + 3\delta_z - \delta_x + 1 > 0 \tag{A.35}$$

$$\gamma - \alpha - 3\delta_x + 2\delta_z + 3 > 0, \quad 2\delta_z - \delta_x + 1 + \alpha - \tau > 0 \tag{A.36}$$

$$\gamma - 2\delta_x + 1 - \tau + \delta_z > 0 \tag{A.37}$$

From the relation (A.34) we obtain:

$$\delta_z + \delta_z - \delta_x + 1 > 0 \tag{A.38}$$

Although, using formula (A.35), we arrive to the following cases:

$$\delta_z - \delta_x + 1 > \delta_z \quad \Longrightarrow \quad \delta_x < 1 \tag{A.39}$$

or

$$\delta_z \geq 0 \tag{A.40}$$

Taking all these results into consideration, we easily remark that the only suitable case, for these relations to be satisfied all-at-once,is $\delta_x = \delta_z$. Hence, in the long wave limit, the x and z direction should be scaled with the same factor and, moreover, we can assume without losing the generality that $\delta_x = \delta_z = 0$, due to the fact that the mass equation should be always satisfied. These results are verified with the literature [2, 4, 5, 26], and thus, our scaling assumption, applied for the long wave limit, is correct.

A.2 Analysis: Short Wave Limit

In this case, we look for waves with the amplitude and the wave length comparable in magnitude, although very small in comparison with the characteristic length of the problem (i.e. the height of the upper fluid layer). Hence, the wave number, k, tends to infinity. Therefore, we consider in our expansions, as small parameter, the ratio $1/k$ which tends to zero. This is a trivial choice and we want to investigate, in this case, the impact on our initial scalings. Hence, we have:

$$\epsilon = \frac{1}{k} \quad \Longrightarrow \quad k = \epsilon^{-1} \tag{A.41}$$

The system of motion has the following new form:

$$\epsilon^{\alpha-\eta-2\delta_z+\delta_x}\phi_1'''' - 2\epsilon^{\alpha-\eta-\delta_x-2}\phi_1'' + \epsilon^{\alpha-3\delta_x-\eta+2\delta_z-4}\phi_1 =$$

$$= iRe_1(U_1-c)(\epsilon^{\alpha-\eta-1}\phi_1''-\epsilon^{\alpha-2\delta_x-\eta+2\delta_z-3}\phi_1)-iRe_1\epsilon^{\alpha-\eta-1}\phi_1 U_1''+i\epsilon^{\tau-\eta+\delta_z-1}\frac{Gr_1}{Re_1}\tilde{\theta}_1 \tag{A.42}$$

$$\mu\left(\epsilon^{\alpha-\delta_z}\phi_2'' + \epsilon^{\beta-\delta_x-2}\phi_2\right) = \epsilon^{\alpha-\delta_z}\phi_1'' + \epsilon^{\beta-\delta_x-2}\phi_1 \tag{A.43}$$

From literature [3, 9, 10], it is known that, in the short wave analysis, the first three terms are the leading order terms in the Orr-Sommerfeld equation, written for each fluid. Moreover, all the terms, from the tangential stress condition at the interface, are also leading order terms. Thus, we have:

$$\alpha - \eta - 2\delta_z + \delta_x = \alpha - \eta - \delta_x - 2 = \alpha - 3\delta_x - \eta + 2\delta_z - 4 \tag{A.44}$$

$$\alpha - \delta_z = \beta - \delta_x - 2 \tag{A.45}$$

From the relations (A.44) and (A.45), we obtain:

$$\delta_x - \delta_z + 1 = 0, \quad \delta_x - 2\delta_z + 2 = 0 \quad \Longrightarrow \quad \delta_z = 1, \quad \delta_x = 0 \tag{A.46}$$

which corresponds with our scalings used in the case of short wave limit, due to the fact that we change our perspective from the macroscopical to the microscopical point of view.

Hence, we focus over the micro-structures developed close to the contact surface of the fluids.

Remark: When all the perturbations are equal in magnitude, from the mass equation and the kinematical condition, we obtain the classical case, whereas:

$$\delta_x = \delta_z = \delta_t = 0. \tag{A.47}$$

Appendix B

Derivation of the Orr-sommerfeld equation in the short wave limit

First, we consider the lower fluid momentum equations (relations (2.24)-(2.25)):

$$Re\left(\frac{\partial u_1}{\partial t}+u_1\frac{\partial u_1}{\partial x}+w_1\frac{\partial u_1}{\partial z}\right)=-\frac{\partial p_1}{\partial x}+\left(\frac{\partial^2 u_1}{\partial x^2}+\frac{\partial^2 u_1}{\partial z^2}\right) \tag{B.1}$$

$$\frac{\partial w_1}{\partial t}+u_1\frac{\partial w_1}{\partial x}+w_1\frac{\partial w_1}{\partial z}=\frac{1}{Re}\left(-\frac{\partial p_1}{\partial z}+\frac{\partial^2 w_1}{\partial x^2}+\frac{\partial^2 w_1}{\partial z^2}\right)+\frac{Gr}{Re^2}\theta_1 \tag{B.2}$$

In order to obtain the equation in the short wave limit, first we scale the z direction with the wave number k, technique presented in section 3.4, second, we linearize our system of motion with respect to the small perturbations and, third, we introduce the stream function and the exponential form of the perturbation and we perform the computations.

Hence, we consider the relations:

$$u_1=U_1(\frac{1}{k}\tilde{z})+\frac{1}{k}\tilde{u}_1(x,\frac{1}{k}\tilde{z}),\quad u_2=U_2(\frac{1}{k}\tilde{z})+\frac{1}{k}\tilde{u}_2(x,\frac{1}{k}\tilde{z}) \tag{B.3}$$

$$w_1=\frac{1}{k}\tilde{w}_1(x,\frac{1}{k}\tilde{z}),\quad w_2=\frac{1}{k}\tilde{w}_2(x,\frac{1}{k}\tilde{z}) \tag{B.4}$$

$$p_1=P_1(\frac{1}{k}\tilde{z})+\frac{1}{k}\tilde{p}_1(x,\frac{1}{k}\tilde{z}),\quad p_2=P_2(\frac{1}{k}\tilde{z})+\epsilon\tilde{p}_2(x,\frac{1}{k}\tilde{z}) \tag{B.5}$$

$$\theta_1=\Theta_1(\frac{1}{k}\tilde{z})+\frac{1}{k}\tilde{\theta}_1(x,\frac{1}{k}\tilde{z}),\quad \theta_2=\Theta_2(\frac{1}{k}\tilde{z})+\frac{1}{k}\tilde{\theta}_2(x,\frac{1}{k}\tilde{z}) \tag{B.6}$$

which are similar with the relations (3.52)-(3.56), the difference being made by the absence of the perturbation exponential form, which will be introduced later.

In the following computations, the capital letters denote the solutions of the basic flow system of equations, defined with respect, only, to the $\tilde{z}/k$ direction and the letters with

superscript "tilde" are the perturbations, defined with respect to the x and $\tilde{z}/k$ directions. Hence, the equations are given by:

$$Re\left(\frac{\partial U_1}{\partial t}+\frac{1}{k}\frac{\partial \tilde{u}_1}{\partial t}+U_1\frac{\partial U_1}{\partial x}+\frac{1}{k}\tilde{u}_1\frac{\partial U_1}{\partial x}+\frac{1}{k}U_1\frac{\partial \tilde{u}_1}{\partial x}+\frac{1}{k^2}\tilde{u}_1\frac{\partial \tilde{u}_1}{\partial x}+\frac{1}{k}\tilde{w}_1\frac{\partial U_1}{\partial z}+\frac{1}{k}\tilde{w}_1\frac{\partial \tilde{u}_1}{\partial z}\right)=$$

$$=-\frac{\partial P_1}{\partial x}-\frac{1}{k}\frac{\partial \tilde{p}_1}{\partial x}+\frac{1}{k}\frac{\partial^2 \tilde{u}_1}{\partial x^2}+\frac{1}{k}\frac{\partial^2 \tilde{u}_1}{\partial z^2}+\frac{\partial^2 \tilde{U}_1}{\partial x^2}+\frac{\partial^2 \tilde{U}_1}{\partial z^2} \tag{B.7}$$

$$\frac{1}{k}\frac{\partial \tilde{w}_1}{\partial t}+\frac{1}{k}U_1\frac{\partial \tilde{w}_1}{\partial x}+\frac{1}{k^2}\tilde{u}_1\frac{\partial \tilde{w}_1}{\partial x}+\frac{1}{k^2}\tilde{w}_1\frac{\partial \tilde{w}_1}{\partial z}=$$

$$\frac{1}{Re}\left(-\frac{\partial P_1}{\partial z}-\frac{1}{k}\frac{\partial \tilde{p}_1}{\partial z}+\frac{1}{k}\frac{\partial^2 \tilde{w}_1}{\partial x^2}+\frac{1}{k}\frac{\partial^2 \tilde{w}_1}{\partial z^2}\right)+\frac{Gr}{Re^2}\Theta_1+\frac{1}{k}\frac{Gr}{Re^2}\tilde{\theta}_1 \tag{B.8}$$

Moreover, we linearize the above equations taking into account that the solutions of the basic flow satisfy the equations. Thus, we keep only the terms of order $1/k$. Thus, we have:

$$Re\left(\frac{\partial \tilde{u}_1}{\partial t}+\tilde{u}_1\frac{\partial U_1}{\partial x}+U_1\frac{\partial \tilde{u}_1}{\partial x}+\tilde{w}_1\frac{\partial U_1}{\partial z}\right)=-\frac{\partial \tilde{p}_1}{\partial x}+\frac{\partial^2 \tilde{u}_1}{\partial x^2}+\frac{\partial^2 \tilde{u}_1}{\partial z^2} \tag{B.9}$$

$$\frac{\partial \tilde{w}_1}{\partial t}+U_1\frac{\partial \tilde{w}_1}{\partial x}=\frac{1}{Re}\left(-\frac{\partial \tilde{p}_1}{\partial z}+\frac{\partial^2 \tilde{w}_1}{\partial x^2}+\frac{\partial^2 \tilde{w}_1}{\partial z^2}\right)+\frac{Gr}{Re^2}\tilde{\theta}_1 \tag{B.10}$$

We assume that the perturbations have the exponential form introduced in relation (5.45) and after performing the computations we have:

$$Re\left(-ikc\tilde{u}_1+ik\tilde{u}_1U_1+\tilde{w}_1\frac{\partial U_1}{\partial z}\right)=-ik\tilde{p}_1-k^2\tilde{u}_1+\frac{\partial^2 \tilde{u}_1}{\partial z^2} \tag{B.11}$$

$$-ikc\tilde{w}_1+ikU_1\tilde{w}_1=\frac{1}{Re}\left(-\frac{\partial \tilde{p}_1}{\partial z}-k^2\tilde{w}_1+\frac{\partial^2 \tilde{w}_1}{\partial z^2}\right)+\frac{Gr}{Re^2}\tilde{\theta}_1 \tag{B.12}$$

Next, we express the perturbation from the equation (B.11) and performing a derivative with respect to the z direction, we plug-in the result into the equation (B.12). Thus, we obtain:

$$ik(U_1-c)\frac{\partial \tilde{u}_1}{\partial z}+k^2(U_1-c)\tilde{w}_1+\tilde{w}_1\frac{\partial^2 U_1}{\partial z^2}=$$

$$\frac{1}{Re}\left(\frac{\partial^3 \tilde{u}_1}{\partial z^3}-k^2\frac{\partial \tilde{u}_1}{\partial z}+ik^3\tilde{w}_1-ik\frac{\partial^2 \tilde{w}_1}{\partial z^2}\right)-ik\frac{Gr}{Re^2}\tilde{\theta}_1. \tag{B.13}$$

Nevertheless, we recall that the basic flow solutions and the perturbations are functions of the new introduced direction $\tilde{z}$, although the partial derivatives from the equation (B.15) are with respect to the old z direction. Hence, we apply the following transformation:

$$\frac{df}{dz}=\frac{df}{d\tilde{z}}\cdot\frac{d\tilde{z}}{dz} \tag{B.14}$$

where $d\tilde{z}/dz=k$. Thus, we obtain the following relations:

$$ik^2(U_1-c)\frac{\partial \tilde{u}_1}{\partial \tilde{z}}+k^2(U_1-c)\tilde{w}_1+k^2\tilde{w}_1\frac{\partial^2 U_1}{\partial \tilde{z}^2}=$$
$$\frac{1}{Re}\left(k^3\frac{\partial^3\tilde{u}_1}{\partial\tilde{z}^3}-k^3\frac{\partial\tilde{u}_1}{\partial\tilde{z}}+ik^3\tilde{w}_1-ik^3\frac{\partial^2\tilde{w}_1}{\partial\tilde{z}^2}\right)-ik\frac{Gr}{Re^2}\tilde{\theta}_1. \tag{B.15}$$

Further, we follow the technique applied in section 3.2 and taking into account relation (B.14), we introduce the stream function for each fluid, defined by:

$$\tilde{u}_j=k\frac{\partial\phi_j}{\partial\tilde{z}},\quad \tilde{w}_j=-ik\tilde{\phi}_j,\quad j=\overline{1,2}. \tag{B.16}$$

For the simplicity, we drop the "tilde" symbol for the z direction. We plug-in the above relation into equation (B.15) and we obtain the *Orr-Sommerfeld* equation in the short wave limit:

$$ik^3(U_1-c)\phi_1^{''}-ik^3(U_1-c)\phi_1-ik^3\tilde{\phi}_1\frac{\partial^2U_1}{\partial z^2}+ik\frac{Gr}{Re^2}\tilde{\theta}_1=$$
$$\frac{1}{Re}\left(k^4\phi_1^{iv}-k^4\phi_1^{''}+k^4\phi_1-k^4\phi_1^{''}\right). \tag{B.17}$$

The above relation is similar with the Orr-Sommerfeld equation (3.57), introduced in chapter 4:

$$k^4\left(\phi_1^{(iv)}-2\phi_1^{''}+\phi_1\right)=ik^3Re(U_1-c)(\phi_1^{''}-\phi_1)-ik^3Re\phi_1\frac{\partial^2U_1}{\partial z^2}+ik\frac{Gr}{Re}\tilde{\theta}_1 \tag{B.18}$$

Similarly, using the same technique as the one presented in this appendix, we derive the other equations and conditions in the short wave limit.

Appendix C

Linearization technique in the temperature dependent viscosity case

We consider, for simplicity, the non-dimensional tangential stress condition. Thus, we have:

$$\mu_2(\theta_2)\left[\left(\frac{\partial u_2}{\partial z}+\frac{\partial w_2}{\partial x}\right)-4h_x\frac{\partial u_2}{\partial x}\right]-\mu_1(\theta_1)\left[\left(\frac{\partial u_1}{\partial z}+\frac{\partial w_1}{\partial x}\right)-4h_x\frac{\partial u_1}{\partial x}\right]=0 \qquad \text{(C.1)}$$

Further, we perturb the solutions of the basic flow system of equations with small perturbations, as follows:

$$u_j=U_j+\epsilon\tilde{u}_j,\quad w_j=\epsilon\tilde{w}_j,\quad \theta_j=\Theta_j+\epsilon\tilde{\theta}_j,\quad h=\epsilon\tilde{h}. \qquad \text{(C.2)}$$

We plug-in the above relations into the equation C.1 and we obtain:

$$\mu_2(\Theta_2+\epsilon\tilde{\theta}_2)\left[\left(\frac{\partial U_2}{\partial z}+\epsilon\frac{\partial\tilde{u}_2}{\partial z}+\epsilon\frac{\partial\tilde{w}_2}{\partial x}\right)-4\epsilon\tilde{h}_x\left(\frac{\partial U_2}{\partial x}+\epsilon\frac{\partial\tilde{u}_2}{\partial x}\right)\right]-$$

$$-\mu_1(\Theta_1+\epsilon\tilde{\theta}_1)\left[\left(\frac{\partial U_1}{\partial z}+\epsilon\frac{\partial\tilde{u}_1}{\partial z}+\epsilon\frac{\partial\tilde{w}_1}{\partial x}\right)-4\epsilon\tilde{h}_x\left(\frac{\partial U_1}{\partial x}+\epsilon\frac{\partial\tilde{u}_1}{\partial x}\right)\right]=0 \qquad \text{(C.3)}$$

Further, we make the following artifice by adding and substracting in front of each square paranthesis the terms $\mu_1(\Theta_1)$ and $\mu_2(\Theta_2)$. Thus, we have:

$$\Big(\mu_2(\Theta_2)+\mu_2(\Theta_2+\epsilon\tilde{\theta}_2)-\mu_2(\Theta_2)\Big)\left[\left(\frac{\partial U_2}{\partial z}+\epsilon\frac{\partial\tilde{u}_2}{\partial z}+\epsilon\frac{\partial\tilde{w}_2}{\partial x}\right)-4\epsilon\tilde{h}_x\left(\frac{\partial U_2}{\partial x}+\epsilon\frac{\partial\tilde{u}_2}{\partial x}\right)\right]-$$

$$-\Big(\mu_1(\Theta_1)+\mu_1(\Theta_1+\epsilon\tilde{\theta}_1)-\mu_1(\Theta_1)\Big)\left[\left(\frac{\partial U_1}{\partial z}+\epsilon\frac{\partial\tilde{u}_1}{\partial z}+\epsilon\frac{\partial\tilde{w}_1}{\partial x}\right)-4\epsilon\tilde{h}_x\left(\frac{\partial U_1}{\partial x}+\epsilon\frac{\partial\tilde{u}_1}{\partial x}\right)\right]=0 \qquad \text{(C.4)}$$

We denote with μ_j^* the term $\mu_j(\Theta_j + \epsilon\tilde{\theta}_j) - \mu_j(\Theta_j)$ for $j = \overline{1,2}$ and we have:

$$\mu_2(\Theta_2)\left[\left(\frac{\partial U_2}{\partial z} + \epsilon\frac{\partial \tilde{u}_2}{\partial z} + \epsilon\frac{\partial \tilde{w}_2}{\partial x}\right) - 4\epsilon\tilde{h}_x\left(\frac{\partial U_2}{\partial x} + \epsilon\frac{\partial \tilde{u}_2}{\partial x}\right)\right] +$$
$$\mu_2^*\left[\left(\frac{\partial U_2}{\partial z} + \epsilon\frac{\partial \tilde{u}_2}{\partial z} + \epsilon\frac{\partial \tilde{w}_2}{\partial x}\right) - 4\epsilon\tilde{h}_x\left(\frac{\partial U_2}{\partial x} + \epsilon\frac{\partial \tilde{u}_2}{\partial x}\right)\right] -$$
$$-\mu_1(\Theta_1)\left[\left(\frac{\partial U_1}{\partial z} + \epsilon\frac{\partial \tilde{u}_1}{\partial z} + \epsilon\frac{\partial \tilde{w}_1}{\partial x}\right) - 4\epsilon\tilde{h}_x\left(\frac{\partial U_1}{\partial x} + \epsilon\frac{\partial \tilde{u}_1}{\partial x}\right)\right] -$$
$$-\mu_1^*\left[\left(\frac{\partial U_1}{\partial z} + \epsilon\frac{\partial \tilde{u}_1}{\partial z} + \epsilon\frac{\partial \tilde{w}_1}{\partial x}\right) - 4\epsilon\tilde{h}_x\left(\frac{\partial U_1}{\partial x} + \epsilon\frac{\partial \tilde{u}_1}{\partial x}\right)\right] = 0. \tag{C.5}$$

Nevertheless, due to the fact that we perturb the basic solutions with *small* perturbations, we can expand the terms μ_1^* and μ_2^* in Taylor series and we take into consideration only first two terms of the expansions. Thus, we obtain:

$$\mu_j^* = \mu_j(\Theta_j + \epsilon\tilde{\theta}_j) - \mu_j(\Theta_j) = \mu_j(\Theta_j) + \epsilon\tilde{\theta}_j\mu_j^{'}(\Theta_j)\frac{\partial\Theta_j}{\partial z} - \mu_j(\Theta_j) = \epsilon\tilde{\theta}_j\mu_j^{'}(\Theta_j)\frac{\partial\Theta_j}{\partial z}. \tag{C.6}$$

with $j = \overline{1,2}$.

Hence, the equation C.5 has the following new form:

$$\mu_2(\Theta_2)\left[\left(\frac{\partial U_2}{\partial z} + \epsilon\frac{\partial \tilde{u}_2}{\partial z} + \epsilon\frac{\partial \tilde{w}_2}{\partial x}\right) - 4\epsilon\tilde{h}_x\left(\frac{\partial U_2}{\partial x} + \epsilon\frac{\partial \tilde{u}_2}{\partial x}\right)\right] +$$
$$+\epsilon\tilde{\theta}_2\mu_2^{'}(\Theta_2)\frac{\partial\Theta_2}{\partial z}\left[\left(\frac{\partial U_2}{\partial z} + \epsilon\frac{\partial \tilde{u}_2}{\partial z} + \epsilon\frac{\partial \tilde{w}_2}{\partial x}\right) - 4\epsilon\tilde{h}_x\left(\frac{\partial U_2}{\partial x} + \epsilon\frac{\partial \tilde{u}_2}{\partial x}\right)\right] -$$
$$-\mu_1(\Theta_1)\left[\left(\frac{\partial U_1}{\partial z} + \epsilon\frac{\partial \tilde{u}_1}{\partial z} + \epsilon\frac{\partial \tilde{w}_1}{\partial x}\right) - 4\epsilon\tilde{h}_x\left(\frac{\partial U_1}{\partial x} + \epsilon\frac{\partial \tilde{u}_1}{\partial x}\right)\right] -$$
$$-\epsilon\tilde{\theta}_1\mu_1^{'}(\Theta_j)\frac{\partial\Theta_1}{\partial z}\left[\left(\frac{\partial U_1}{\partial z} + \epsilon\frac{\partial \tilde{u}_1}{\partial z} + \epsilon\frac{\partial \tilde{w}_1}{\partial x}\right) - 4\epsilon\tilde{h}_x\left(\frac{\partial U_1}{\partial x} + \epsilon\frac{\partial \tilde{u}_1}{\partial x}\right)\right] = 0. \tag{C.7}$$

We perform the computations and due to the fact that the solutions of the basic flow satisfy the equation C.1 and we focus on the linear perturbation terms, we keep only the terms of order ϵ. Thus, we have:

$$\mu_2(\Theta_2)\left[\left(\epsilon\frac{\partial \tilde{u}_2}{\partial z} + \epsilon\frac{\partial \tilde{w}_2}{\partial x}\right) - 4\epsilon\tilde{h}_x\frac{\partial U_2}{\partial x}\right] + \epsilon\tilde{\theta}_2\mu_2^{'}(\Theta_2)\frac{\partial\Theta_2}{\partial z}\frac{\partial U_2}{\partial z} -$$
$$-\mu_1(\Theta_1)\left[\left(\epsilon\frac{\partial \tilde{u}_1}{\partial z} + \epsilon\frac{\partial \tilde{w}_1}{\partial x}\right) - 4\epsilon\tilde{h}_x\frac{\partial U_1}{\partial x}\right] - \epsilon\tilde{\theta}_1\mu_1^{'}(\Theta_1)\frac{\partial\Theta_1}{\partial z}\frac{\partial U_1}{\partial z} = 0. \tag{C.8}$$

Moreover, we recall that the basic flow velocities are functions only of the z direction, thus, in the above relation, the terms containing the basic flow velocities derivative according with x direction vanish:

$$\mu_2(\Theta_2)\left(\frac{\partial \tilde{u}_2}{\partial z} + \frac{\partial \tilde{w}_2}{\partial x}\right) + \tilde{\theta}_2\mu_2^{'}(\Theta_2)\frac{\partial\Theta_2}{\partial z}\frac{\partial U_2}{\partial z} -$$

$$-\mu_1(\Theta_1)\left(\frac{\partial \tilde{u}_1}{\partial z}+\frac{\partial \tilde{w}_1}{\partial x}\right)-\tilde{\theta}_1\mu_1^{'}(\Theta_1)\frac{\partial \Theta_1}{\partial z}\frac{\partial U_1}{\partial z}=0. \tag{C.9}$$

Further, we assume that the perturbations have the exponential form introduced in relation (5.45) and after we define the stream function, we obtain the relation for the tangential stress, formula (5.56) from the chapter 5:

$$\mu_2(\Theta_2)(\phi_2^{''}+k^2\phi_2)+\mu_2^{'}(\Theta_2)\tilde{\theta}_2\frac{\partial \Theta_2}{\partial z}\frac{\partial U_2}{\partial z}=\mu_1(\Theta_1)(\phi_1^{''}+k^2\phi_1)+\mu_1^{'}(\Theta_1)\tilde{\theta}_1\frac{\partial \Theta_1}{\partial z}\frac{\partial U_1}{\partial z} \tag{C.10}$$

All the other equations and conditions which model the temperature dependent viscosity case are computed using the same technique as the one presented in this appendix.

Appendix D

Analytical computations: Base flow, Long Wave and Short Wave Limit

The files presented in this chapter are:

1. Constants_of_the_BASIC_FLOW.nb - contains the computed forms of the constants which determine the basic flow profiles (velocity and temperature) for both fluids.

2. Results_of_the_LONG_WAVES_Analysis.nb - presents the analytically computed eigenvalues c_0 and c_1 in the long wave limit (see section 3.3).

3. Results_of_the_SHORT_WAVES_Analysis.nb - presents the analytically computed eigenvalues c_0 and c_1 in the short wave limit for both cases discussed in section 3.4.

In the computations, we used the following notations:

$$\alpha 1 = \frac{Gr1}{Re1}, \quad \alpha 2 = \frac{\rho Gr1\beta}{\mu Re1},$$

$$\beta 1 = \frac{1}{Re1Pr1}, \quad \beta 2 = \frac{\alpha}{Re1Pr1}, \tag{D.1}$$

where $Gr1, Re1, Pr1$ and $We1$ are the non-dimensional numbers introduced in section 2.2, relation (2.20) and $Tc0, Tc1, Th0$ and $Th1$ are the given basic temperature constants introduced in section 3.1.

References

[1] C. S. Yih, "Instability due to viscous stratifications", J. Fluid Mech. **27**, (1967) 337

[2] A. P. Hooper, "Long wave instability at the interface between two viscous fluids: thin layer effects", Phys. Fluids **28** (1985) 1613

[3] A. P. Hooper and W. G. C. Boyd, "Shear-flow instability at the interface between two viscous fluids", J. Fluid Mech. **128** (1983) 507

[4] Y. Renardy, "The thin layer effect and interfacial stability in a two layer Couette flow with similar liquids", Phys. Fluids **30** (1987) 1627

[5] S. G. Yiantsios and B. G. Higgins, "Linear stability of plane Poiseuille flow of two superposed fluids", Phys. Fluids **31** (1988) 3225

[6] D. D. Joseph, M. Renardy and Y. Renardy, "Instability of the flow of two immiscible liquids with different viscosities in a pipe", J. Fluid Mech. **141** (1984) 309

[7] A. P. Hooper and R. Grimshaw, "Nonlinear instability at the interface between two viscous fluids", Phys. Fluids **28** (1985) 37

[8] F. Charru and J. Fabre, "Long waves at the interface between two viscous fluids", Phys. Fluids **6** (1994) 1223

[9] P. J. Blennerhassett and F. T. Smith, "Short-scale waves on wind-driven water (cat's paws)", Proc. R. Soc. London A **410** (1987) 1

[10] F. Charru, P. Luchini and P. Ern, "Instability of a nearly inextensible thin layer in a shear flow", Eur J. Mech.B/Fluids **22**, (2003) 39

[11] S. Madruga, C. Perez-Garcia and G. Lebon, "Convective instabilities in two superposed horizontal liquid layers heated laterally", Phys. Review E **68**, (2003) 041607

[12] Y. Renardy and D. D. Joseph, "Couette flow of two fluids between concentric cylinders", J. Fluid Mech. **150** (1985) 381

[13] M. C. Potter and E. Graber, "Stability of plane Poiseuille flow with heat tranfer", Phys. Fluids **15** (1972) 387

[14] H. Herwig and P. Schäfer, "Influence of variable properties on the stability of two-dimensional boundary layers", J. Fluid Mech. **243** (1992) 1

[15] D. P. Wall and S. K. Wilson, "The linear stability of channel flow of fluid with temperature dependent viscosity", J. Fluid Mech. **323** (1996) 107

[16] L. A. B. Pilkington, "The float glass process", Proc. Royal Soc. London A **314** (1969) 1

[17] O. S. Narayanaswamy, "A one-dimensional model of stretching float glass", J. Amer. Cer. Soc. **60** (1977) 1

[18] O. S. Narayanaswamy, "Computer simulation of float glass stretching", J. Amer. Cer. Soc. **64** (1981) 666

[19] M. Prieto, J. Diaz, E. Egusquiza, "Analysis of the fluid-dynamic and thermal behaviour of a tin bath in float glass manufacturing", Int. J. Thermal Sciences **41** (2002) 348

[20] J. Sander, "Dynamic equations and turbulent clossures in geophysics", Cont. Mech. Thermodyn., **10** (1998) 28

[21] P. Thunis and R. Bornstein, "Hierarchy of mesoscale flow assumptions and equations", JAS, **53** (1996) 397

[22] A. A. Mohamad and R. Viskanta, "Combined surface shear and buoyancy-driven convection in a shallow cavity", Fundamentals of natural convection, AIAA/ASME Thermophysics and Heat Trans. Conf., Seattle, Washington, **140** (1990) 1

[23] A. A. Mohamad, "Natural convection in a differentially heated enclosure filled with a low Prandtl parameter fluid, unsteady analysis", 3rd Int. Conf. Single Crystal Growth, Strength Problems and Heat Mass Trans., Obninsk, Russia, **2** (2000) 350

[24] M. K. Moallemi and K. S. Jang, "Prandtl number effects on laminar mixed convection heat transfer in a lid-driven cavity", Int. J. Heat Mass Transfer, **35** (1992) 1881

[25] A. A. Mohamad and R. Viskanta, "Laminar flow and heat transfer in Rayleigh-Benard convection with shear", Phys. Fluids A, **4** (1992) 2131

[26] P. J. Blennerhassett, "On the generation of waves by wind", Philos. Trans. R. Soc. London A **298** (1980) 43

[27] M. K. Smith and S. H. Davis, "The instability of sheared liquid layers", J. Fluid Mech. **121** (1982) 187

[28] D. A. S. Rees and I. Pop, "A note on free convection along a vertical wavy surface in a porous medium", J. Heat Transfer **116** (1994) 505

[29] S. A. Orszag, "Accurate solution of the Orr-Sommerfeld stability equation", J. Fluid Mech. **50** (1971) 689

[30] C. I. Gheorghiu and I. S. Pop, "A modified Chebyshev-Tau method for a hydrodynamic stability problem", Approximation and Optimization. Proceedings of the International Conference on Approximation and Optimization (Romania) - ICAOR, Cluj-Napoca, July 29 - August 1, **2** (1996) 119

[31] Ch. Cabos, "A preconditioning of the tau operator for ordinary differential equations", ZAMM **74** (1994) 521

[32] J. Shen, "Efficient spectral-Galerkin method II. Direct solvers of second and fourth order equations by using Chebyshev polynomials", SIAM J. Sci.Stat.Comput. **16** (1995) 74

[33] S. V. Malik and A. P. Hooper, "Linear Stability and Energy Growth of Viscosity Stratified Flows", Phys. Fluids (scheduled to appear in Vol.17, January 2005).

[34] W. Heinrichs, "A stabilized treatment of the biharmonic operator with spectral methods", SIAM J. Sci.Stat.Comput. **12** (1991) 1162

[35] M. J. South and A. P. Hooper, "Linear growth in two fluid plane Poiseuille flow", J. Fluid Mech. **381** (1999) 121

[36] D. A. Goussis and A. J. Pearlstein, "Removal of infinite eigenvalues in the generalized matrix eigenvalue problem", J. Comp. Phys. **84** (1989) 242

[37] S. S. Motsa and P. Sibanda, "On the stability of thermally stratified channel flow with a compliant boundary", Int. J. Heat and Mass Trans. **46** (2003) 939

[38] J. J. Dongarra, B. Straughan, D. W. Walker, "Chebyshev-Tau/QZ Algorithm Methods for Calculating Spectra of Hydrodynamic Stability Problems", J. Applied Num. Math., **22** (1996) 399

[39] P. J. Schmid and D. S. Henningson, "Stability and Transition in Shear Flows", Springer-Verlag New York (2001)

[40] J. V. Wehausen and E. V. Laitone, "Handbuch der Physik IX - Surface Waves", Springer-Verlag (1960)

[41] R. Narayanan, "Interfacial fluid dynamics and transport processes", Springer-Verlag Berlin (2003)

[42] E. Guyon, J. P. Hulin, L. Petit and C. Mitescu, "Physical hydrodynamics", Oxford University Press (2001)

[43] S. P. Haigh, "Non-symmetric Holmboe waves", PhD Thesis, University of British Columbia (1995)

[44] R. Zeytounian, "Asymptotic modeling of Atmospheric Flows", Springer-Verlag New York (1990) 142

[45] G. E. Collins, "The Orr-Sommerfeld Equation: Classical and Modern Techniques", PhD Thesis, University of Santa Barbara (2002)

[46] B. Gebhart, Y. Jaluria, R. L. Mahajan and B. Sammakia, "Buoyancy-induced flows and transport", Springer-Verlag Berlin (1988)

[47] C. Canuto, M. Y. Hussaini, A. Quarteroni and T. A. Zhang, "Spectral methods in fluid dynamics", Springer-Verlag New York (1988)

[48] L. N. Trefethen, "Spectral methods in MATLAB", SIAM Philadelphia (2000))

[49] http://www.esat.kuleuven.ac.be/ pollefey/tutorial/node74.html

[50] http://kluge.in-chemnitz.de/documents/fractal/node13.html

[51] http://www.math.vt.edu/people/renardym/class_home/nova/bifs/node49.html

[52] http://www.glassonweb.com/articles/article/233/

[53] http://ajzonca.tripod.com/glassprocess.html

[54] http://www.britglass.co.uk/files/documents/Float%20Process.pdf

[55] http://www.pilkington.com/pilkington/Corporate/education/float+process/default.htm

[56] http://www.pfg.co.za/home.asp?pid=13

[57] http://yarchive.net/metal/float_glass.html

[58] http://stommel.tamu.edu/~baum/paleo/ocean/node4.html